A functional characterization of Pib2: a key TORC1 regulator in *S. cerevisiae*

by

Kayla Kay Troutman

B.S., Moravian College, 2018

Submitted to the Graduate Faculty of the

School of Medicine in partial fulfillment

of the requirements for the degree of

Doctor of Philosophy

University of Pittsburgh

2022

UNIVERSITY OF PITTSBURGH

SCHOOL OF MEDICINE

This dissertation was presented

by

Kayla Kay Troutman

It was defended on

November 10, 2022

and approved by

Alexander Sorkin, Richard Beatty Mellon Professor and Chair, Department of Cell Biology

Jeffrey L. Brodsky, Avinoff Professor of Biological Sciences, Department of Biological Sciences

Gerald R. V. Hammond, Associate Professor, Department of Cell Biology

Allyson F. O'Donnell, Assistant Professor, Department of Biological Sciences

Dissertation Director: Marijn G. J. Ford, Associate Professor, Department of Cell Biology

A functional characterization of Pib2: a key TORC1 regulator in *S. cerevisiae*

Kayla Kay Troutman, PhD

University of Pittsburgh, 2022

Cell growth and survival are dependent on the ability of cells to respond to their environment and the nutrients that are available to them. The target of rapamycin complex 1 (TORC1) is a highly conserved kinase that is critical for nutrient sensing and the control of cell growth. Dysregulation of TORC1 signaling, including both hyper- and hypo-activity, has been implicated in a variety of diseases; thus, understanding how TORC1 is regulated is crucial. In *Saccharomyces cerevisiae*, TORC1 subcellular localization and cellular nutrient availability are key for its activity. TORC1 localizes to both vacuolar and endosomal membranes, where distinct TORC1 signaling occurs. Nutrient availability is signaled to TORC1 by the combined actions of several signaling pathways and proteins. One notable regulator, Phosphatidylinositol 3-phosphate-binding protein 2 (Pib2), is necessary for TORC1 reactivation after starvation or pharmacological inhibition. Interestingly, Pib2 can both hinder and facilitate TORC1 activity, however, the regulatory mechanisms remain poorly understood. Through a systematic mutagenesis and functional dissection of conserved regions and domains within *S. cerevisiae* Pib2, we have identified regions and key residues involved in TORC1 regulation and Pib2 localization. We use rapamycin exposure assays and live-cell confocal imaging to show that two Pib2 regions, helical region E and the tail motif, are vital for TORC1 reactivation, whereas the N-terminal regions A and B have TORC1 inhibitory functions. Furthermore, we show that while the Pib2 PI3P-binding FYVE domain is critical for vacuolar localization, it is unexpectedly not required for recovery from rapamycin induced growth arrest. Using chimeric Pib2 targeting constructs, we show that

endosomal Pib2 is not sufficient for TORC1 reactivation and cell growth following rapamycin exposure. Here we have demonstrated that Pib2 plays a unique role as a dual modulator of TORC1 activity in *S. cerevisiae*, and that each of the conserved Pib2 regions differentially contribute to TORC1 regulation. These findings highlight key factors that could be manipulated to control cell growth and could provide insight into TORC1 regulation mechanisms in other eukaryotes.

Table of Contents

List of Tables

List of Figures

Preface

I first want to thank my advisor, Marijn Ford. Marijn, thank you for being an incredible mentor and for all of your scientific guidance, patience, and support. I could not have asked for a better mentor to help navigate graduate school, especially through the unique circumstances of the last few years. I would like to thank the Ford Lab members, Natasha and Bryan, for being wonderful lab mates and creating a great work environment. I would also like to thank my thesis committee, Sasha Sorkin, Ally O'Donnell, Gerry Hammond, and Jeff Brodsky. Thank you for your time, scientific advice, and support at our scheduled meetings and at numerous retreats. Lastly, I would like to thank my friends and family. Thank you for encouraging me, listening to me vent, and being supportive at every step along the way.

This work was supported by the University of Pittsburgh School of Medicine Cell Biology Teaching Fellowship and funding from the NIH grants GM120102 and GM139546 to Marijn and the Interinstitutional Program in Cell Biology and Molecular Biology T32 training grant GM133353 to me.

List of Abbreviations

ADP: adenosine diphosphate

AMP: adenosine monophosphate

AMPK: AMP-activated protein kinase

ATP: adenosine triphosphate

CDK: cyclin-dependent kinase

CLS: chronological lifespan

Cryo-EM: cryogenic electron microscopy

EAPF: ER-associated apoptosis-involved protein containing PH and FYVE domains

EGO: exit from rapamycin-induced growth arrest

ER: endoplasmic reticulum

FKBP: FK506-binding protein

FRB: FKBP-rapamycin binding domain

FYVE: Fab1, YOTB, Vac1, and EEA1

GAP: GTPase-activating proteins

GCN2: general control nonderepressible 2

GEF: guanine nucleotide exchange factor

GDP: guanosine diphosphate

GTP: guanosine triphosphate

ITC: isothermal titration calorimetry

LAPF: lysosome-associated apoptosis-inducing protein contain PH and FYVE domains

LMP: lysosomal membrane permeabilization

MSA: multiple sequence alignment

NA: numerical aperture

PE: phosphatidylethanolamine

PH: pleckstrin homology domain

PIB2: phosphatidylinositol 3-phosphate-binding protein 2

PI3K: phosphoinositide 3-kinse

PI3P: phosphatidylinositol 3-phosphate

$PI(3,5)P_2$: phosphatidylinositol 3,5-bisphosphate

PKA: protein kinase A

PTM: post-translational modification

PX: phox homology domain

RLS: replicative lifespan

ROI: region of interest

SC: synthetic complete

SD: synthetic defined

SEC-MALS: size exclusion chromatography coupled to multiangle light scattering

Snf1: sucrose non-fermenting 1

SNX-BAR: sorting nexin – Bin/Amphiphysin/Rvs domain

TOR: target of rapamycin

TORC1: target of rapamycin complex 1

TOROID: TORC1 organized in inhibited domains

TSC: tuberous sclerosis complex

yEGFP: yeast enhanced green fluorescent protein

YPD: yeast extract, peptone, dextrose

3’ UTR: 3’ untranslated region

5’ UTR: 5’ untranslated region

1.0 Introduction

1.1 Cell Growth

Cell survival is dependent on the meticulous coordination of cellular growth and degradation processes. Cells need to be able to recognize when conditions are right for cell growth and proliferation and manage intracellular processes appropriately to promote cell biomass and volume increases which support progression through the cell cycle.[1] In times of nutrient limitation, cells need to be able to redirect the utilization of available resources to survive. Furthermore, cells need to be able to recognize when cellular damage is beyond repair to initiate cell death. Many cell processes work together to direct these activities and they are all closely regulated to ensure that aberrant activity does not occur. As a result, mutations or perturbations that result in an inability to appropriately regulate these processes can lead to various diseases.

1.1.1 Nutrient and Energy Sensing

Nutrient sensing and integration are essential for cellular growth and survival. Fundamental nutrient integrating mechanisms include the TORC1, AMPK, and GCN2 pathways. These pathways are conserved from yeast through humans and play central roles in controlling cell growth in eukaryotes through sensing energy, glucose, amino acids, and, in multicellular organisms, growth factors and hormones.[2] The ability of cells to recognize and respond to these stimuli enables them to grow and proliferate.

1.1.1.1 TORC1 Pathway

The target of rapamycin complex 1 (TORC1) plays a vital role in controlling cell growth and autophagy. TORC1 signaling is a fundamental nutrient sensing pathway, and its dysregulation can disrupt the delicate balance between growth and degradation required to maintain cellular homeostasis. Dysregulation of TORC1 signaling has been implicated in a variety of diseases such as cancer, diabetes, and neurodegeneration.[3] TORC1 is also considered a pro-aging pathway; and its inhibition, typically through rapamycin treatment or caloric restriction, has shown to be promising in extending lifespan in a variety of eukaryotes.[4]

The mechanisms of TORC1 signaling are highly conserved throughout eukarya. In yeast, TORC1 consists of two copies of each of four components: the serine/threonine kinase Tor1 (or Tor2), Kog1, Lst8 and Tco89 (Figure 1.1A).[5–7] These correspond to mTOR, Raptor, and mLst8, respectively, in higher eukaryotes.[8–10] Tco89 can inhibit TORC1 via an interaction with the small regulatory GTPase Gtr1 in its GDP-bound form[11] and does not have a mammalian counterpart. The Tor kinases, as ethe name suggests, are sensitive to rapamycin exposure. Kog1 (kontroller of growth)/Raptor help with substrate recruitment.[8,12–15] Lst8/mLst8 (lethal with Sec13 protein 8) associates with the kinase domain of Tor1/mTOR to promote kinase activity.[9,14] In yeast, Lst8 is involved in the regulation of transcription factors Gln3 and Rtg1-Rtg3, which are involved in synthesis of alpha-ketoglutarate, glutamate, and glutamine.[16,17]

Nutrient sensing and integration are key aspects of TORC1 regulation. Amino acids and glucose presence are important regulators of TORC1 in both yeast and mammals. In yeast, leucine and glutamine are key amino acids sensed by the TORC1 regulatory machinery.[11,17] In mammals, glutamine, leucine, and arginine play important roles.[18] In mammals, an additional layer of control exists through growth factor signaling. mTORC1 is activated by growth factors and insulin via

downstream signaling from their respective receptors through the tuberous sclerosis complex (TSC) and Rheb GTPase.[19–23] The cellular nutrient status is directed to TORC1 via several upstream regulatory proteins outlined in (Figure 1.1B).

Active TORC1 promotes anabolic processes and inhibits catabolic processes. TORC1 has many downstream targets, which when phosphorylated promote cell growth and ribosome biogenesis and inhibit lysosome biogenesis and autophagy (Figure 1.1C).[24–28] One major downstream effector of yeast TORC1 is Sch9 (mammalian S6K1).[26,29] Sch9/S6K1 are members of the AGC protein kinase family (homologous to protein kinases A, G, and C).[26,30] (See Pearce et al., 2010 for AGC protein review).[30] Phosphorylation of Sch9/S6K1 by TORC1 helps to promote cell growth through promoting ribosome biogenesis and protein synthesis.[30–33] TORC1 inhibits autophagic processes through the phosphorylation of autophagy components Atg1, Atg13 (part of the Atg1 kinase complex), and Vps27 (Atg13 and ULK1 in mammals).[27,28,34–37] TORC1 activity also fluctuates throughout the cell cycle to regulate phase transition in combination with other proteins.[38]

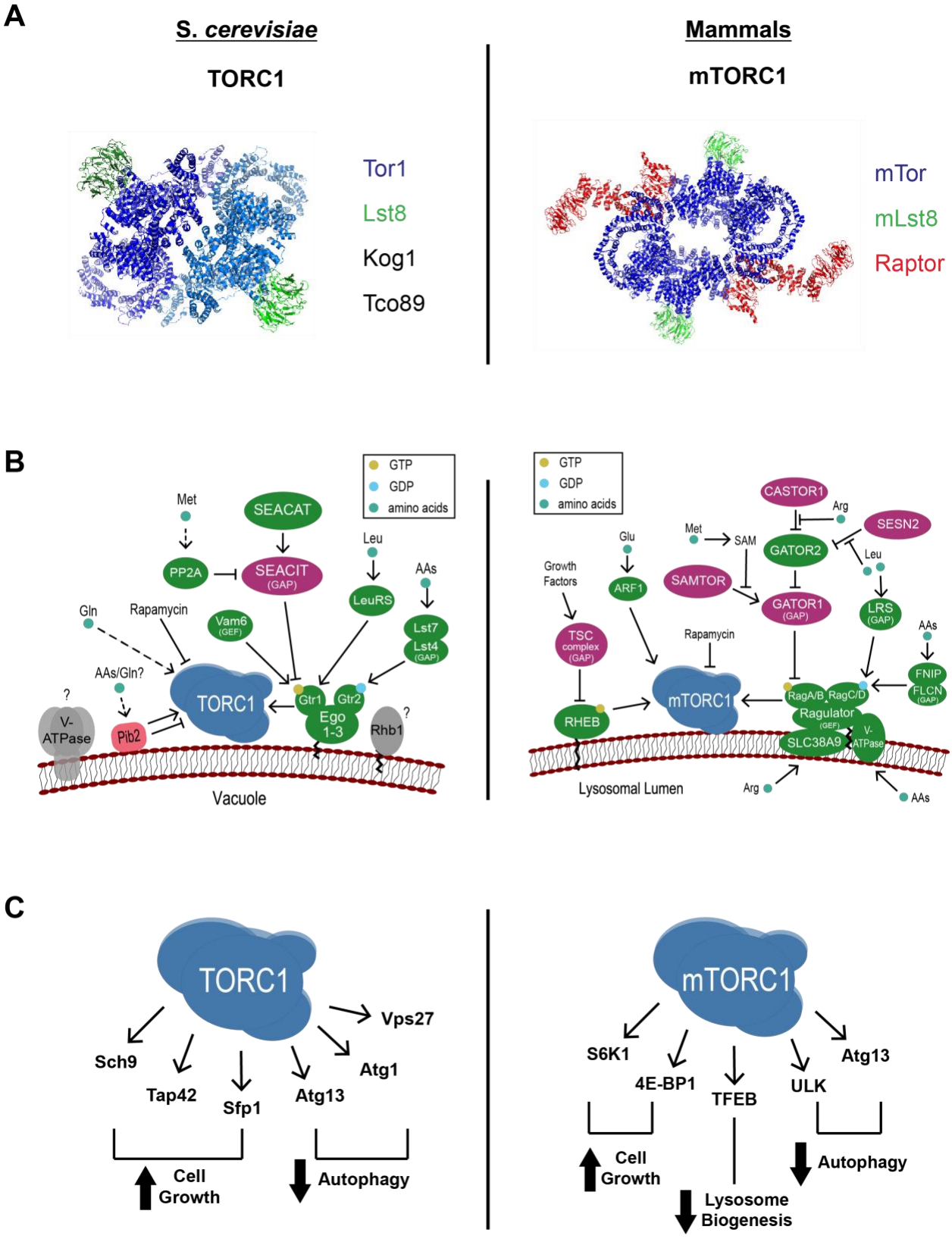
A
S. cerevisiae
TORC1
Tor1
Lst8
Kog1
Tco89
Mammals
mTORC1
mTor
mLst8
Raptor
B
GTP
GDP
amino acids
Met
SEACAT
PP2A
SEACIT
(GAP)
Leu
LeuRS
AAs
Lst7
Lst4
(GAP)
Gln
Rapamycin
Vam6
(GEF)
AAs/Gln?
TORC1
Gtr1
Gtr2
Ego
1-3
Rhb1
V-
ATPase
Pib2
Vacuole
CASTOR1
Arg
SESN2
Glu
Met
SAM
GATOR2
Leu
Growth
Factors
ARF1
SAMTOR
GATOR1
(GAP)
LRS
(GAP)
TSC
complex
(GAP)
Rapamycin
AAs
FNIP
FLCN
(GAP)
RHEB
mTORC1
RagA/B
RagC/D
Ragulator
(GEF)
SLC38A9
V-
ATPase
Lysosomal Lumen
Arg
AAs
C
TORC1
Sch9
Tap42
Sfp1
Atg13
Atg1
Vps27
Cell
Growth
Autophagy
mTORC1
S6K1
4E-BP1
TFEB
ULK
Atg13
Cell
Growth
Lysosome
Biogenesis
Autophagy

Figure 1.1 Yeast and Mammalian TORC1 A) Ribbon models derived from the cryo-EM structures of yeast (PDB: 5FVM)[39] and mammlian TORC1 (PDB: 5H64).[40] B) Comparison of yeast and mammalian TORC1 regulatory proteins. Proteins in green promote TORC1 activity whereas proteins in magenta inhibit TORC1 activity. C) Comparison of yeast and mammalian TORC1 effectors.

1.1.1.2 AMPK/Snf1 Pathway

The AMP-activated protein kinase (AMPK) pathway regulates cell growth and metabolism by monitoring intracellular ATP levels.[41] AMPK was initially discovered for its role in lipid metabolism and later linked to its yeast homolog Snf1.[42–45] Snf1 (sucrose nonfermenting 1) is named such due to a mutant's inability to use sucrose.[46] Under stressed conditions, AMPK/Snf1 works to inhibit anabolic processes and promote catabolic processes and ATP generation.[2] Dysregulation of this pathway is a contributing factor in metabolic diseases such as type II diabetes and cancer.[47]

AMPK/Snf1 is a serine/threonine kinase which is activated by increased AMP/ADP binding.[41] AMPK/Snf1 exists as a heterotrimer with 3 subunits: catalytic subunit α and regulatory subunits β and γ (Figure 1.2A). In mammals, there are several isoforms for each of these AMPK subunits and their expression and functional responses differ based on tissue type.[48] The subunit isoforms are as follows: α1, α2, β1, β2, γ1, γ2, and γ3.[48] In S. *cerevisiae*, the complex consists of the Snf1 catalytic subunit, one of three β subunits (Sip1, Sip2, and Gal83), and the γ subunit, Snf4.[49–53] Each of the β subunits have unique N-termini which result in different subcellular localization under glucose starvation conditions. Sip1 localizes to the vacuolar membrane, Sip2 remains cytoplasmic, and Gal83 localizes to the nucleus.[54–56] The γ subunit contains adenosine binding Bateman domains where AMP/ADP can bind.[57,58]

The AMPK/Snf1 γ subunit binds AMP or ADP when ATP levels are low.[59] AMP/ADP binding results in a conformational change, which allows for phosphorylation and activation of AMPK/Snf1.[60–62] AMPK/Snf1 is regulated by upstream kinases and phosphatases (Figure 1.2B). Under starvation conditions and certain stressors, AMPK is phosphorylated by LKB1, TAK1, or CaMKKβ.[63–70] The main upstream kinases of Snf1 in yeast include Sak1, Tos3, and Elm1.[71–74] AMP/ADP binding also protects AMPK/Snf1 from dephosphorylation.[60,61,75,76] In yeast the Reg1-Glc7 protein phosphatase targets Snf1 for dephosphorylation.[77–80] The mammalian AMPK phosphatases include PP2A, PP2C, and PPM1E.[47,76,81,82] Mammalian AMPK also has additional methods of regulation. Following phosphorylation, AMPK can then be further activated by an allosteric change caused by AMP binding; this does not occur with Snf1 in yeast.[44,45,60,75,83,84] Mammalian AMPK is also regulated by hormones and cytokines.[2,48] In the brain, insulin, leptin, and ghrelin have been shown to regulate food intake via AMPK signaling.[2,85–90]

AMPK and Snf1 have numerous downstream targets that affect processes such as glucose and lipid metabolism, cell growth, autophagy, cell polarity, and transcriptional control.[41,90] AMPK phosphorylates and inactivates enzymes involved in fatty acid and sterol synthesis.[42,91,92] Active AMPK/Snf1 alter glucose uptake and transcription of metabolic genes in response to carbon stress to promote ATP production.[2,41] Under nutrient restrictive conditions, AMPK/Snf1 can inhibit cell growth via inhibition of TORC1 (Figure 1.2C). In mammals, AMPK phosphorylates TSC2 and the Raptor subunit of the mTORC1 complex to inhibit TORC1 activity.[19,93] In yeast lacking TSC2, Snf1 phosphorylates the Kog1 subunit of the TORC1 complex to inhibit its activity.[94] Conversely, Kog1 has also been shown to regulate Snf1 to promote the transcriptional response necessary for adaptation to nutrient limitation.[95]

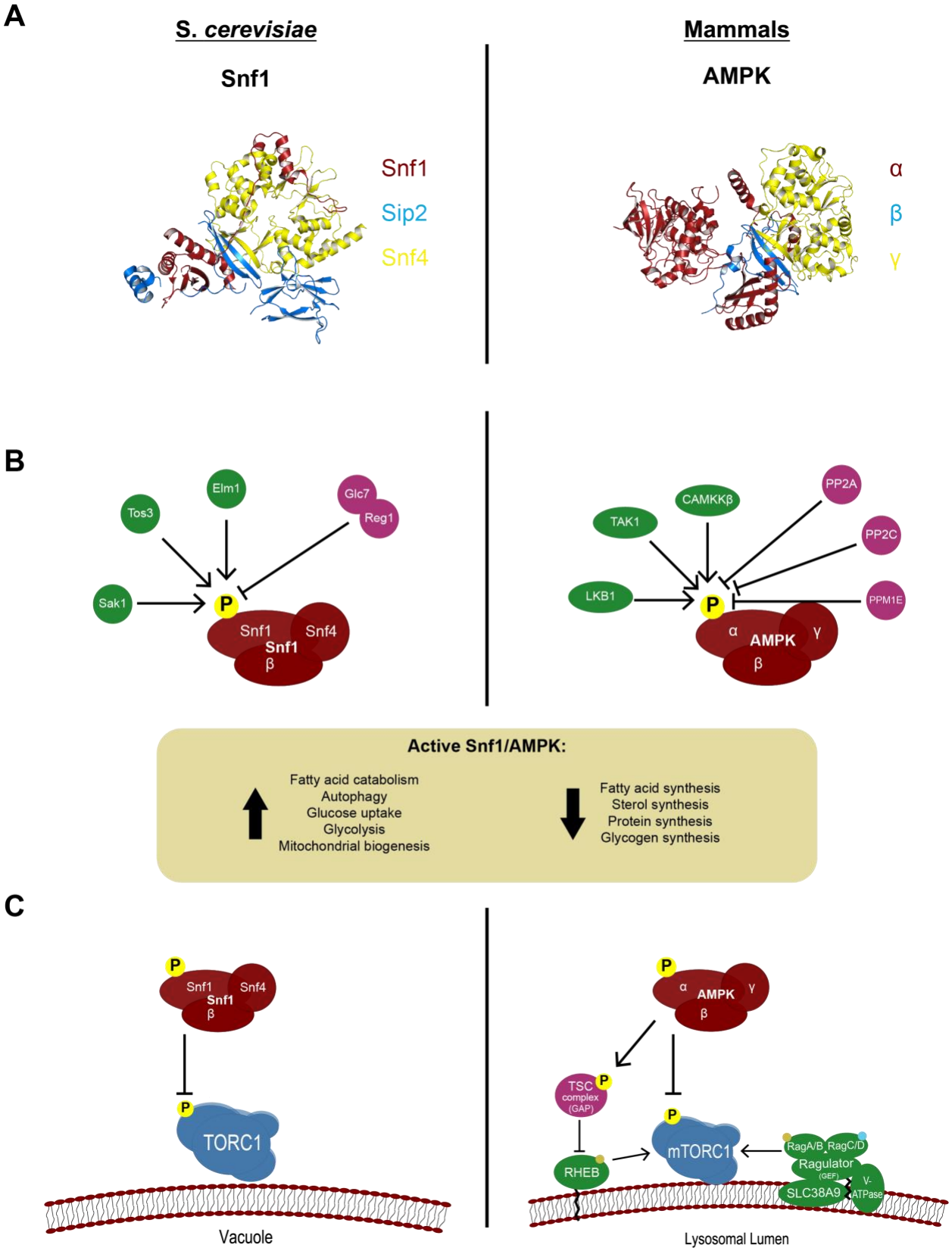
A
S. cerevisiae
Snf1
Snf1
Sip2
Snf4
Mammals
AMPK
α
β
γ
B
Elm1
Tos3
Glc7
Reg1
Sak1
P
Snf1
Snf4
Snf1
β
PP2A
CAMKKβ
TAK1
PP2C
LKB1
PPM1E
P
α
AMPK
γ
β
Active Snf1/AMPK:
Fatty acid catabolism
Autophagy
Glucose uptake
Glycolysis
Mitochondrial biogenesis
Fatty acid synthesis
Sterol synthesis
Protein synthesis
Glycogen synthesis
C
P
Snf1
Snf4
Snf1
β
P
TORC1
Vacuole
P
α
AMPK
γ
β
TSC
complex
(GAP)
P
RHEB
P
mTORC1
RagA/B
RagC/D
Ragulator
(GEF)
SLC38A9
V-
ATPase
Lysosomal Lumen

Figure 1.2 Yeast and Mammalian Snf1/AMPK A) Ribbon models derived from the crystal structures of yeast Snf1 (PDB: 2QLV)[96] and mammlian AMPK (PDB: 4CFH).[97] B) Comparison of yeast and mammalian Snf1/AMPK regulatory proteins. Green proteins are Snf1/AMPK activating kinases and magenta proteins are phosphatases. An overview of processes up- or down-regulated by active Snf1/AMPK are indicated in the yellow box. C) Crosstalk between Snf1/AMPK and TORC1 singaling.

1.1.1.3 GCN2 Pathway

The GCN2 (general control non-derepressible 2) pathway senses intracellular amino acid levels. In both yeast and mammals, GCN2 monitors amino acid levels by sensing uncharged tRNAs and responds by limiting further translation and upregulating autophagy and biosynthetic pathways.[98] Gcn2 is a serine/threonine kinase (Figure 1.3A). When an uncharged tRNA binds to Gcn2, this prompts autophosphorylation and homodimerization of Gcn2 resulting in activation.[99,100] Full activation of Gcn2 is also dependent on Gcn1 and Gcn20, which complex with Gcn2 on ribosomes.[101,102]

The primary target of Gcn2 is eIF2α (eukaryotic initiation factor-2α).[103] In nutrient replete conditions, eIF2α functions to promote protein translation (Figure 1.3B).[104] When eIF2α is phosphorylated by Gcn2 under amino acid starvation, it results in inhibition of general protein translation.[103,105–108] In contrast, the transcription factor Gcn4, in yeast, is derepressed and upon accumulation this transcription factor promotes expression of genes involved in amino acid biosynthesis.[103,105,106] This differing regulation is mediated at upstream open reading frames (uORFs) in the 5' UTR of the GCN2 mRNA.[105,109] ATF4, the mammalian ortholog of GCN4, is similarly regulated by uORFs.[110] ATF4 induces expression of genes which regulate apoptosis, autophagy, and amino acid biosynthesis and transport.[111–115] It has recently been shown in yeast

that this translational response is further fine-tuned by Gcn2 phosphorylation of eIF2β and Gcn20.[116]

Like AMPK, GCN2 also displays crosstalk with the TORC1/mTORC1 pathway (Figure 1.3C). In yeast, GCN2 has been shown to act upstream and downstream of TORC1.[117,118] TORC1 can downregulate Gcn2 activity in the presence of abundant nutrients.[117,119] Conversely, TORC1 has also been shown to be a target of the Gcn2 kinase; Gcn2 phosphorylates the Kog1 subunit and downregulates TORC1 activity in yeast.[118] Gcn2 has been shown to be upregulated in response to rapamycin exposure in both yeast and mammals.[117,119,120] In mammals, GCN2 has been described to act upstream of mTORC1.[120,121] GCN2 signaling has also been shown to play a role in an organism's feeding behaviors through its activity in neurons, similar to AMPK. GCN2 directs animals to consume lower amounts of foods that are lacking in essential amino acids through mediating GABA signaling in dopaminergic neurons.[122–126]

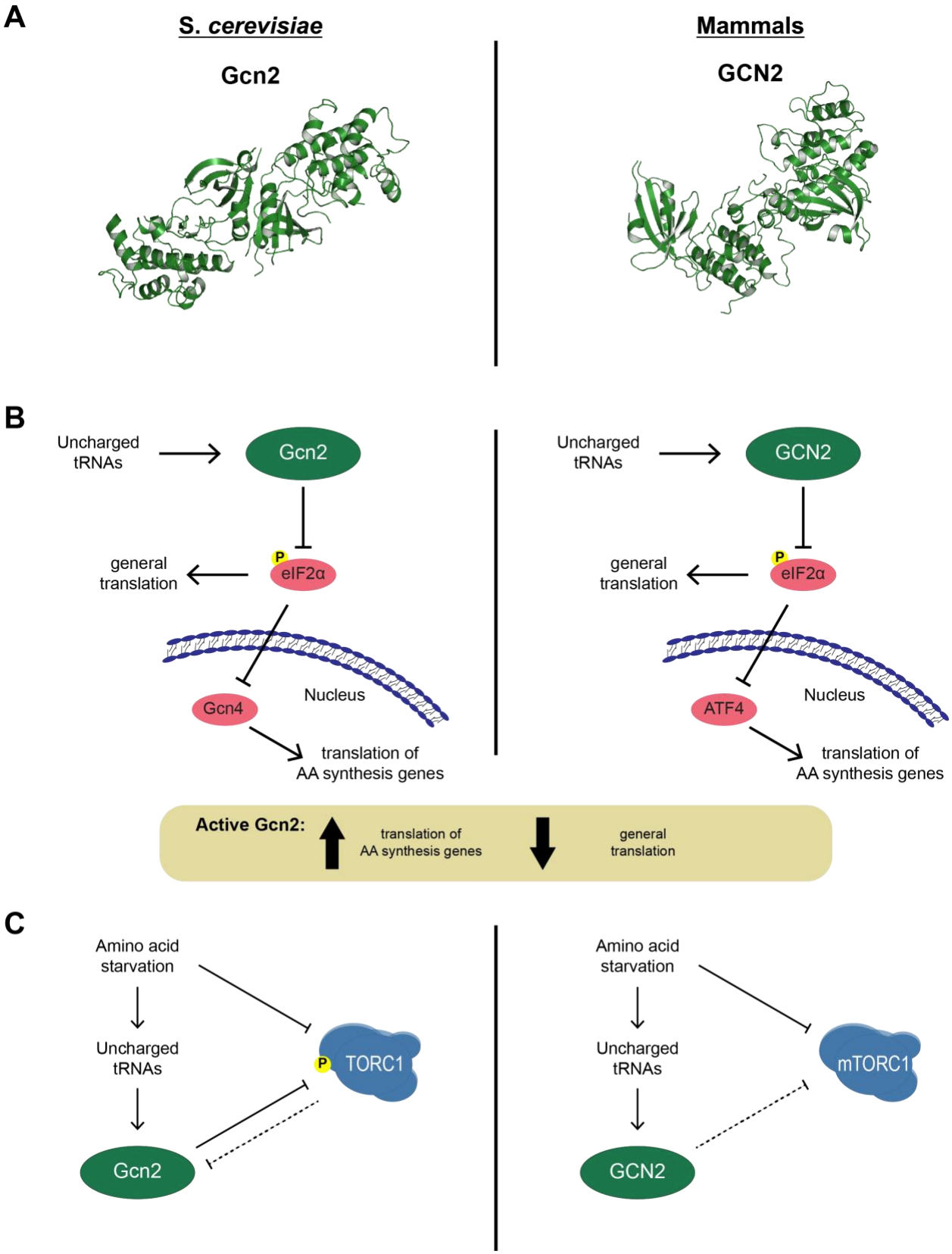
A
S. cerevisiae
Gcn2
Mammals
GCN2
B
Uncharged tRNAs
Gcn2
general translation
P
eIF2α
Nucleus
Gcn4
translation of AA synthesis genes
Uncharged tRNAs
GCN2
general translation
P
eIF2α
Nucleus
ATF4
translation of AA synthesis genes
Active Gcn2:
translation of AA synthesis genes
general translation
C
Amino acid starvation
Uncharged tRNAs
P
TORC1
Gcn2
Amino acid starvation
Uncharged tRNAs
mTORC1
GCN2

Figure 1.3 Yeast and Mammalian Gcn2 A) Ribbon models derived from the crystal structures of yeast Gcn2 (PDB: 1ZYC)[127] and mammlian GCN2 (PDB: 7QQ6).[128] B) Comparison of yeast and mammalian Gcn2 pathways. An overview of processes up- or down-regulated by active Gcn2 are indicated in the yellow box. C) Crosstalk between Gcn2 and TORC1 singaling.

1.1.2 Autophagy

Macroautophagy (hereafter "autophagy") is a cellular degradation process which removes damaged, unnecessary, or pathogenic cytosolic contents.[129] Autophagy is initiated under conditions of cellular stress but is also needed at low levels under normal conditions to recycle materials and maintain cellular homeostasis.[129] Under limited nutrients, cells use autophagy to recycle cellular materials to produce essential components and energy.[129] Autophagy is primarily regulated by the TORC1 and AMPK pathways.[129] Dysregulation of autophagy is implicated in several neurodegenerative diseases.[129]

Autophagy requires the formation of a double-membraned autophagosome which fuses with the vacuole or lysosome where degradation occurs.[129,130] The primary steps in autophagosome formation include induction, nucleation, and expansion, which are followed by fusion, and cargo degradation and recycling.[129] During the induction step, several autophagy proteins form a complex (Yeast: Atg1 complex and Vps34/PI3K complex; Mammals: ULK complex and Beclin1/PI3K complex) which then recruits other Atg proteins to construct the phagophore assembly site (PAS).[131–136] Further recruitment of proteins to the PAS occurs during the nucleation step. Activation of the PI3K complex results in PI3P accumulation,[137,138] which is necessary for the proper localization and recruitment of PAS proteins.[139] The third step of autophagosome formation is expansion of the phagophore. Expansion of the phagophore requires ubiquitin-like

conjugation systems which promote the enlargement of the phagophore; at this point the structure is called an autophagosome.[140–142] The ubiquitin-like conjugation systems promote lipidation of Atg8 (LC3 in mammals) with phosphatidylethanolamine (PE).[129,143–148] When the autophagosome closes, a portion of the Atg8/LC3-PE is retained on the inside of the autophagosome where it is degraded and what remains on the outer membrane is deconjugated.[130,143,144,149–151] Once the autophagosome has been formed it next fuses with the vacuole/lysosome allowing the autophagosomal cargo to be released into the vacuole/lysosome.[129] Lastly, the membrane is degraded by a lipase[152,153] and the cargo is degraded by vacuolar/lysosomal hydrolases and the macromolecules are released back into the cytosol to be reused.[153,154]

Autophagy is controlled by the nutrient and energy sensing signaling pathways TORC1 and AMPK. In yeast, TORC1 phosphorylates the key autophagy proteins Atg13, Atg1, and Atg14 resulting in inhibition of autophagy induction.[27,131,155] In mammals, mTORC1 phosphorylates ULK1 (the mammalian homolog of yeast Atg1) to inhibit autophagy.[34] The yeast Gcn2 kinase also promotes the transcription of ATG genes to promote autophagy under nutrient starvation conditions.[111] In the presence of glucose, PKA (protein kinase A) phosphorylates ATG proteins preventing autophagosome formation.[156] PKA is a well conserved protein that, like TORC1, responds to the cellular environment to regulate cell growth.[157] PKA also directly phosphorylates TORC1 in yeast, thus activating TORC1 and inhibiting autophagy.[129] In mammals, PKA inhibits autophagy through the activation of mTORC1 via AMPK.[129] Conversely, APMK promotes autophagy under low energy conditions by phosphorylating the raptor subunit of mTORC1 or the TSC complex.[129,158] AMPK is also able to directly promote autophagy through phosphorylation of ULK1.[34]

1.1.3 Cell Cycle

The cell cycle is a carefully managed process that controls cell growth and division. The cell cycle consists of two growth phases, G_1 and G_2, a nuclear DNA synthesis phase (S), and the mitosis/cytokinesis phase (M). Additionally, there is a G_0 phase, which is characterized by cellular senescence. These phases are outlined in Figure 1.4. During the growth phases the cell prepares for DNA synthesis (G_1) and mitosis (G_2).[159] The S phase is the point of nuclear DNA replication.[159] Finally, during M phase, the cell undergoes chromosome segregation and cell division by mitosis and cytokinesis, respectively.[160]

Progression of the cell cycle from one phase to the next relies on cyclins, cyclin-dependent kinases (CDKs), and cell cycle checkpoints. Cyclins are a family of proteins that activate CDKs to control cell cycle progression.[159,161,162] CDKs are serine/threonine kinases and require cyclin binding for activation.[159,161,162] Gene expression of many cyclins oscillate during the cell cycle such that they activate specific CDKs only at certain stages.[163] CDK activity can also be further modulated by phosphorylations or interactions with other binding partners.[160,164] CDKs, along with other regulatory proteins, act at cell cycle checkpoints, which are evaluation points where the cell assesses damages or abnormalities before progressing to the next stage of the cycle. When abnormalities are detected, the cell cycle is slowed or stopped until the issues can be resolved, or the cell decides to abort the cell cycle and enter quiescence or senescence, or induce apoptosis.[160,165] The main checkpoints are DNA damage, DNA replication stress, and spindle assembly checkpoints (Figure 1.4).[160,165] Depending on the extent of the damage sensed at these checkpoints, the cell can choose to re-enter the cell cycle, permanently exit the cell cycle, or induce apoptosis.[160,165] A failure to recognize damages at these checkpoints and correct them, or

permanently exit the cell cycle, can lead to inappropriate cellular proliferation and diseases, such as cancer.[160]

Cell growth processes are vital for progression through the cell division cycle and resulting proliferation. During the cell cycle, cells exhibit oscillations in volume.[166–168] These oscillations are a result of the fine-tuned control of anabolic and catabolic processes. In budding yeast, TORC1 and PKA activity fluctuations have been shown to regulate the cell cycle through numerous mechanisms.[38] Together, TORC1 and PKA in yeast have been shown to regulate ribosome biogenesis,[26,31,169–172] as well as cyclin abundance and certain cell cycle phase transitions.[173–185] The fluctuations in TORC1 and PKA activity during the cell cycle are partly mediated by upstream, nutrient-sensing regulators.[38]

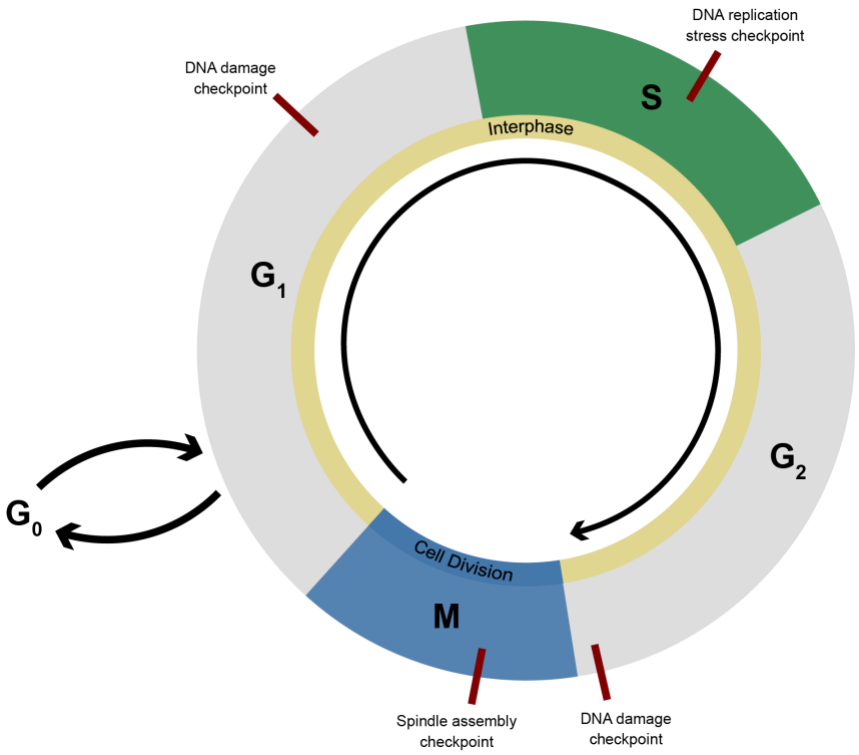

Figure 1.4 The Cell Cycle Overview of cell cycle phases. Growth phases are indicated by G1 and G2. The synthesis phase is indicated by S. Mitosis and cytokinesis are combined and indicated by M. Cell cycle checkpoints are marked by dark red lines. G0 is the stage of cellular senescence or quiescence.

1.2 Yeast as a Model Organism

Saccharomyces cerevisiae is a species of ascomycete yeast which is commonly used in baking and brewing. *S. cerevisiae* divide by budding and can survive as both haploid and diploid cells. Yeast possess many important traits of a model organism. They have a relatively short doubling time under optimal growth conditions and a fully sequenced genome. There are many well-established methods and protocols for easy genetic manipulation of yeast which simplifies gene deletions and the introduction of mutations. It is also easy to change the growth environment of yeast cells which allows for facile study of how nutrients and the external environment affects their growth. Unlike *ex vivo* cells or *in vitro* cell lines, yeast provide a fully *in vivo* system to work in that does not depend on extraneous factors, like synthetic immobilization or addictive media components, for survival. Further, yeast share a significant amount of conservation with higher eukaryotes. There is also a large community of yeast researchers which provides a broad pool of data and resources like the yeast genome database (yeastgenome.org), the cell map (thecellmap.org), and the yeast RGB database (yeastRGB.org). These resources provide compiled information on *S. cerevisiae* gene products, genetic interactions, and subcellular localization of fluorescently tagged proteins, respectively. Combined these qualities make yeast a great eukaryotic model organism and thus many key cellular processes, such as autophagy, have been discovered in yeast.[186]

1.2.1 Yeast Genetics

The *S. cerevisiae* genome, the first completely sequenced eukaryotic genome, contains approximately 6000 genes across 16 chromosomes.[187] Very few *S. cerevisiae* genes contain

introns, and yeast have limited intergenic DNA, which provides a very compact genome.[187] *S. cerevisiae* can survive as either haploid or diploid cells. Haploid cells exist as one of two mating types: A or α.[188] Yeast can be heterothallic or homothallic, where homothallic haploid yeast can switch mating types and fuse to form diploid cells.[188–191] Lab strains, however, contain mutations in the endonuclease that is required for mating type switching, allowing haploid cells of a single mating type to be propagated and maintained.[188] Many lab strains are also auxotrophs and cannot synthesize all the nutrients they need to survive on their own.[192] Auxotrophs can only grow if the appropriate nutrient is supplemented in the growth media or if the gene for the appropriate enzyme is reintroduced. These auxotrophies are a great tool for selection.

An attractive attribute of yeast as a model organism is the ease of genetic manipulation. Yeast cells can be transformed with plasmids to overexpress a gene or express gene mutants.[193,194] There are several methods for transforming yeast with plasmid DNA; the most efficient of these uses lithium acetate, a single-stranded carrier DNA, and polyethylene glycol.[193,194] The plasmids typically contain a selectable marker which reverts an auxotrophy of the parent strain allowing for simple selection of plasmid-containing cells. Several methods have also been developed to easily disrupt gene expression endogenously.[195–199] In the most commonly used of these methods, PCR products containing selectable markers, such as genes that complement amino acid auxotrophies or provide antibiotic resistance, along with the flanking sequences of the target gene are amplified and transformed into the yeast cells.[195–197] This allows for homologous recombination at the genomic locus and insertion of a selectable marker which enables easy selection of knock-out mutants.[195–197] A similar method can also be used for endogenous tagging of genes with fluorescent or other tags.[200]

These methods enabled the development of a yeast deletion collection. The yeast deletion collection is a key advantage to yeast as a model organism. The collection consists of more than twenty thousand mutant strains each of which carry a deletion of one non-essential yeast open reading frame.[201] One benefit of this deletion collection is that it has enabled genome-wide screens. Genome-wide screens have been used to identify proteins involved in specific biological functions, stress responses, and drug mechanisms of action.[201] Other phenotypic screens include screens for cell growth/fitness, mating, sporulation, membrane trafficking, and environmental stressors.[201] One notable use of the deletion collection has been the development of synthetic genetic arrays (SGA) as a high-throughput method to determine genetic interactions.[202] SGAs enable systematic development of double mutants which can uncover both positive and negative genetic interactions.[202,203] Using this method, a database for genetic interactions of *S. cerevisiae* genes, called The Cell Map, was generated.[203,204] Essential gene functions can be studied using other yeast mutant collections, such as, temperature sensitive collections and the DAmP (Decreased Abundance by mRNA Perturbation) collection.[205–207]

1.2.2 Conserved mechanisms

Yeast have been fundamental in the discovery of many key proteins and mechanisms that are conserved through humans. One of the most notable findings using yeast has been the identification of autophagy proteins. The first autophagy proteins were identified in yeast in the 1990s via a screen of a mutagenized proteinase-deficient yeast strain.[186] In this screen, autophagy deficient genes were identified based on vacuolar morphology variations. Cells that did not accumulate autophagic bodies in their vacuoles under starvation conditions were selected for further analysis.[186] This resulted in the discovery of the first autophagy gene, *APG*1, and further

screening using mutagenesis and vital dye staining highlighted many more autophagy genes that could be categorized into 15 complementation groups.[186] As more autophagy genes were discovered, a unified naming convention was determined, and autophagy related gene names were changed to Atg.[208]

Many other key proteins and processes were elucidated using yeast screens. The TOR kinases were initially discovered in yeast screens for rapamycin resistance.[209–212] Membrane trafficking pathways were also first characterized in yeast.[213] The secretory pathway was elucidated in yeast in the 1980s through a screen that isolated genes that are unable to secrete an extracellular enzyme.[214–216] Furthermore, yeast have shown to be vital in learning about the mechanisms of aging and neurodegenerative diseases. Two main types of aging can be observed in yeast, replicative and chronological, and many of the evolutionarily conserved cellular mechanisms of aging overlap between both yeast aging mechanisms.[217] The large amount of conservation between yeast and humans make yeast an ideal model organism for quickly studying cellular processes.

1.3 Regulation of yeast TORC1

TORC1 activity directs cell growth and autophagy. There are several elements that coordinate to regulate TORC1 signaling. First, subcellular localization of TORC1 is essential for its activity. TORC1 generally localizes to the vacuolar membrane; however, recent studies have shown that its localization may be more complex than previously thought.[28,218,219] Additionally, TORC1 activity is regulated by nutrient status and a variety of accessory factors. Activation of TORC1 is highly dependent on amino acid presence, particularly glutamine and leucine, as well

as key upstream regulatory proteins. TORC1 can be inactivated through nutrient starvation or the specific inhibitor rapamycin. This results in halted cell growth and increased autophagy. To recover from the stressors and resume cell growth, TORC1 reactivation is crucial.

1.3.1 Pharmacological Regulation

The yeast TOR proteins were identified by mutants' resistance to the macrolide rapamycin.[209] Rapamycin was discovered during a screen of antifungal agents from the bacteria *Streptomyces hygroscopicus*, found on Easter Island.[220] The mechanism of TOR regulation by rapamycin involves an interaction with the FKBP12 protein. Rapamycin binds to FKBP12 with a high affinity.[221] This complex can then bind to the FRB domain of the Tor proteins.[221] The interaction between FKBP-rapamycin and FRB is also a high affinity interaction and blocks the Tor kinase domain preventing TORC1 kinase activity.[221,222] Rapamycin inhibition of TORC1 has been shown to arrest cell growth in the G1 stage of the cell cycle in yeast.[173,209,222]

1.3.2 Regulatory Proteins

1.3.2.1 EGO Complex

TORC1 activity is regulated by a variety of upstream regulatory proteins. The most well studied of these is the Exit from rapamycin-induced GrOwth arrest (EGO) complex. The EGO complex consists of the proteins Ego1, Ego2, and Ego3 which anchor the GTPases Gtr1 and Gtr2 to the vacuole.[223,224] The nucleotide binding status of the Gtr GTPases is key for their activity and activation of TORC1. For the EGO complex to activate TORC1, Gtr1 needs to be GTP bound, and Gtr2 needs to be GDP bound.[25,225,226] Several upstream GAPs and GEFs are responsible for this

regulation (Figure 1.1B).[11,227–229] These GAPs and GEFs interact with intracellular nutrients, like amino acids, and those interactions translate to the appropriate GAP/GEF activity to activate TORC1 in a nutrient replete environment or inhibit TORC1 during nutrient starvation.[11,227–229]

1.3.2.2 Pib2

Phosphatidylinositol 3-phosphate-binding protein 2 (Pib2) is a crucial protein that is a master regulator of TORC1. Pib2 was identified in screens for both rapamycin sensitivity[223,230] and rapamycin resistance.[231] As such, Pib2 has been determined to be both an activator and inhibitor of TORC1 activity.[231–233] Δ*pib2* cells grow similarly to control W303A cells in nutrient replete conditions but on rapamycin treatment and recovery they display altered vacuolar morphology[234] and exhibit a drastic growth defect.[231,233,234] These differences demonstrate that Pib2 plays different roles in TORC1 reactivation and steady state TORC1 activity. Further, Pib2 has been shown to interact with Tor1 and Kog1, as well as EGO complex components.[231,232,235–237] Pib2 also promotes TORC1 reactivation in response to both glutamine and leucine[234,237] and has been demonstrated as a glutamine sensor that requires a direct TORC1 interaction to promote TORC1 activity.[235,237,238] Recently, Pib2 has been implicated in regulating TORC1 activity oscillations during the cell cycle.[38]

Pib2 was named based on the presence of a C-terminal FYVE domain that is known to interact with PI3P.[239] Like TORC1, wild-type Pib2 localizes to the vacuolar membrane and occasional endosomal puncta.[28,240] The localization of Pib2 is dependent on PI3P and the kinase that generates it, Vps34.[240] Previous work has divided Pib2 into two functional regions: an inhibiting N-terminus and an activating C-terminus.[231,232] Multiple sequence alignments (MSAs) using sequences of Pib2 homologs from 15 ascomycete fungi identified seven conserved regions in Pib2: N-terminal regions A-D, a helical E region, and a C-terminal FYVE domain and tail motif

(Figure 1.5A, Appendix Figure 1). Previous alignments defined a smaller region E,[240] which we extended to include other well-conserved residues (298-418). The AlphaFold2 prediction of Pib2 structural elements[241] suggest this region has alpha-helical secondary structure, hence the name helical E region (helE) (Figure 1.5B). The low complexity N-terminus is not well conserved among species, with the exception of the small regions A-D.[240] Conversely the C-terminal FYVE domain and tail motif are universally conserved.[240] Pib2 has previously been shown to induce lysosomal membrane permeabilization (LMP) and cell death through increasing TORC1 activation in cells treated with ER stressors or calcineurin inhibitors.[240] In this context, both the FYVE domain and tail motif are necessary for the activation of TORC1 and promotion of LMP.[240]

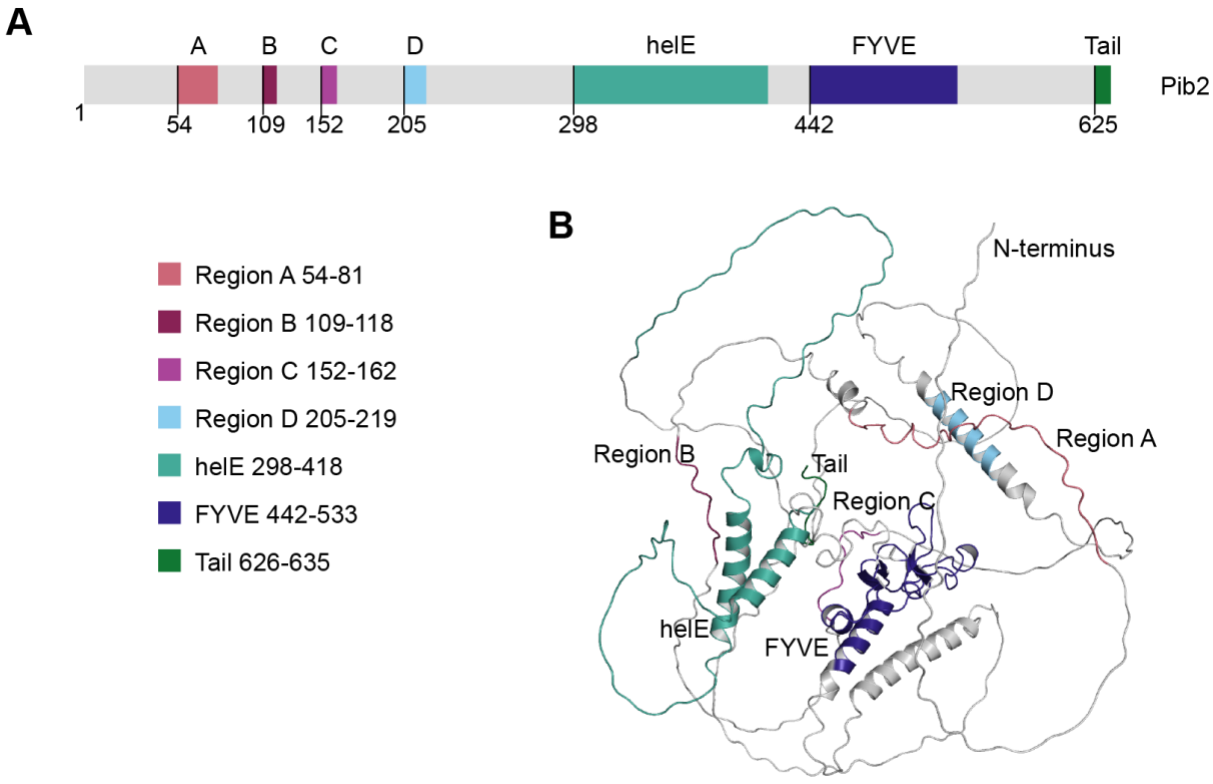

Figure 1.5 Pib2 Conserved Regions A) The primary structure of Pib2, highlighting its conserved regions. The starting residue number of each region is shown below the schematic. Deletion constructs were generated by replacing the

indicated regions with a short AGAGA linker. B) AlphaFold2 prediction of structural elements in Pib2 (PDB AF-P53191-F1-model_v1). Conserved regions are colored to match map in A.

1.3.3 Nutrient sensing

Nutrient integration is a key part of TORC1 regulation. In yeast, TORC1 integrates amino acids and glucose presence to promote cell growth under the appropriate conditions.[25] Two major amino acids that contribute to TORC1 activation are glutamine and leucine. Leucine acts through Gtr1 to promote an active EGO complex and thus TORC1 activity.[11,229] LeuRS has been demonstrated as a cytosolic leucine sensor that binds to Gtr1 to promote TORC1 activation.[229] Glutamine has been shown to activate TORC1 via Gtr-independent mechanisms. One of these TORC1 activation mechanisms involves glutamine interacting with Pib2.[237,238]

Quality nitrogen sources are important in nutrient sensing. Leucine and glutamine are important amino acids that stimulate sustained TORC1 activity in yeast. Leucine is an essential amino acid and is characterized as a branched chain amino acid. Branched chain amino acids, like leucine, isoleucine, and valine, have been shown to be important in regulating energy homeostasis and metabolism of glucose, lipids, and proteins.[242,243] The best nitrogen source for yeast cells is glutamine.[244–246] Glutamine plays an important role in nitrogen and carbon sensing and general cellular metabolism. Glutamine can be interconverted to α-ketoglutarate, an intermediate in the citric acid (TCA) cycle.[247,248] α-ketoglutarate can be further converted to other amino acids, including proline and arginine, or it can move through the TCA cycle.[248] Other TCA cycle intermediates, like oxaloacetate, can then be converted to other amino acids.[248] Glutamine also serves as a nitrogen donor and co-substrate for the synthesis of nucleotides.[248]

TORC1 also responds to the presence or absence of glucose. In the absence of glucose, the yeast AMPK, Snf1, inactivates TORC1.[249] Snf1 has been shown to phosphorylate Kog1 resulting in inhibition of TORC1 and translocation of vacuolar TORC1 to perivacuolar sites.[250] In that study, expression of a constitutively active EGO complex is not sufficient to rescue TORC1 inhibition via glucose starvation, implying that this inhibition mechanism is independent of the EGO complex.[250] TORC1 has also been shown to translocate and be inhibited in a Gtr/EGO-dependent manner.[251] Furthermore, TORC1 complexes have been shown to be inactivated by oligomerization under glucose starvation conditions.[218]

1.3.4 The role of lipids in TORC1 regulation

Vacuolar and endosomal lipid composition is an important factor in TORC1 regulation. The two key lipids are phosphatidylinositol 3-phosphate (PI3P) and phosphatidylinositol 3,5-bisphospahte ($PI(3,5)P_2$). Yeast strains lacking the phosphatidylinositol 3-phosphate kinase (PI3K), Vps34, show an absence of PI3P and $PI(3,5)P_2$ and are hypersensitive to rapamycin exposure.[252] TORC1 localization in both mammalian and yeast cells has been shown to be affected by $PI(3,5)P_2$ levels.[219,253] $PI(3,5)P_2$ is generated from PI3P by the yeast PIKFYVE kinase Fab1.[219,254] The localization of the TORC1 regulator, Pib2, has also shown to be dependent on Vps34 activity.[240]

1.3.5 The role of subcellular localization in TORC1 regulation

In yeast, TORC1 is found at the vacuolar membrane and occasionally in perivacuolar puncta.[28] These puncta are signaling endosomes where differential TORC1 signaling occurs.[28,255]

TORC1 regulatory proteins and effectors can also be found at one or both of these subcellular localizations.[28,219,255] Differences in TORC1 localization and/or the localization of TORC1 regulators and effectors has been shown to be an important aspect of TORC1 regulation and activity.

Under glucose starvation conditions, TORC1 has been observed to localize to perivacuolar puncta.[218,250,251] These puncta have been shown to be oligomerized TORC1 complexes arranged into a helical structure termed a TOROID (TORC1 organized in inhibited domain)[218]. The formation of TOROIDs is dependent on the nucleotide binding status of the EGO complex Gtr proteins.[218] This oligomerization of TORC1 dimers obscures the kinase active site resulting in TORC1 inactivation.[218] When glucose is reintroduced, TORC1 redistributes to the vacuolar membrane and activity resumes.[218]

Recently, two distinct pools of TORC1 have been described in yeast. The first is the well described vacuolar pool of TORC1, which has been shown to phosphorylate effectors which promote cell growth processes, such as Sch9.[26,28] It has also been demonstrated that vacuolar TORC1 phosphorylates the PIKFYVE kinase Fab1.[219,254] The second pool of TORC1 is that found at signaling endosomes.[219,255,256] TORC1 at signaling endosomes phosphorylates effectors which inhibit autophagy, including Atg13 and Vps27.[28] Differences in the TORC1 regulatory mechanisms at these different subcellular locations have yet to be elucidated.

1.3.6 Feedback mechanisms

Many positive and negative feedback mechanisms work to regulate TORC1 activity. Npr1 and Par32, which are downstream effectors of TORC1, in conjunction with ammonium metabolism form a feedback loop that regulates TORC1 activity.[257] TORC1 inactivation results in

Npr1 activation;[258,259] Npr1 then inhibits Par32 thus preventing TORC1 reactivation.[257,260] Npr1 has also been shown to regulate Pib2-dependent inhibition of TORC1.[261] Gcn2 has been demonstrated to be involved in feedback regulation of TORC1, where active TORC1 inhibits Gcn2 and active Gcn2 inhibits TORC1.[117,118] Another TORC1 effector, Sfp1, is a transcriptional activator that regulates ribosomal protein and ribosome biogenesis genes and regulates TORC1 phosphorylation of Sch9.[262] The yeast AMPK, Snf1, is also a negative regulator of TORC1. In nutrient starvation conditions, Snf1 phosphorylates the Kog1 subunit of TORC1 to inhibit its activity.[94,250] TORC1 localization is also impacted by a feedback loop involving the PIKFYVE kinase, Fab1.[219] TORC1 phosphorylates Fab1 at the vacuole.[219] This phosphorylation promotes translocation of Fab1 to signaling endosomes where it uses endosomal PI3P to generate PI(3,5)P_2, an important TORC1 regulating lipid.[219,253] This also results in TORC1 and the EGO complex shifting to signaling endosomes and thus altering TORC1 activity.[219] Autophagy proteins are also involved in TORC1 feedback loops.[263] For example, the TORC1 effector Atg1 phosphorylates upstream TORC1 regulatory proteins, particularly subunits of the SECAT complex (Figure 1.1B), to modulate TORC1 activity.[263]

1.4 Overview

Elucidating the mechanisms of cellular nutrient integration is essential in understanding fundamental cell growth processes. Here, I will address mechanisms by which the yeast protein Pib2 regulates TORC1 reactivation and cell growth following rapamycin exposure. Pib2 has been shown to be a glutamine sensor and both an activator and inhibitor of TORC1 activity. However, the mechanisms by which Pib2 regulates TORC1 activity remain unclear. Further, the impact of

endosomal versus vacuolar Pib2 activity has yet to be revealed. Here, I show that Pib2 N-terminal regions A and B demonstrate TORC1 inhibitory functions, and the Pib2 C-terminal regions are essential for appropriate Pib2 subcellular localization and TORC1 reactivation.

2.0 Conserved Pib2 regions contribute to Pib2 subcellular localization

Select text and figures have been pulled from the following publication and have been adapted for flow and the inclusion of additional data:

K.K. Troutman, N.V. Varlakhanova, B.A. Tornabene, R. Ramachandran, and M.G.J. Ford. Conserved Pib2 regions have distinct roles in TORC1 regulation at the vacuole. *J Cell Sci* (2022) https://doi.org/10.1242/jcs.259994

2.1 Introduction

The subcellular localization of TORC1, its regulators, and its effectors is imperative for TORC1 activity. The localization of these proteins is largely dependent on the lipid composition of vacuolar and endosomal membranes, where TORC1 and its regulators are predominantly found.[28,219,255] PI3P and PI(3,5)P_2 have shown to be key lipids necessary for the appropriate localization and regulation of TORC1.[219,240,252,253] The vacuolar localization of Pib2 has been shown to depend on PI3P and the Pib2 FYVE domain.[240]

In many proteins, including Pib2, lipid binding domains are critical for protein targeting and localization to cellular membranes. Lipid-binding FYVE domains are canonically known to bind PI3P and FYVE domain-containing proteins generally display endosomal localization.[264] FYVE domains are named based on the first letter of four proteins containing this domain including: Fab1, YOTB, Vac1, and EEA1.[265] FYVE domains contain conserved cysteine residues that are essential for zinc-coordination, which is necessary for FYVE domain binding to

PI3P.[264,266] These domains also contain lipid binding motifs: R+HHCRxCG and WxxD, where x is any amino acid.[264] Some FYVE domains are monomers and others dimerize, which has been shown to improve lipid-binding.[267,268] The dimerization interface is well demonstrated by the structure of the EEA1 FYVE domain, which shows the interaction of α-helices which are N-terminal to the FYVE domain itself.[268]

As FYVE domains are generally known to promote endosomal localization, and this is not the case with Pib2, we sought to determine how each of the Pib2 regions contribute to its subcellular localization. Here we show that both the Pib2 FYVE domain and helE region are essential for proper subcellular localization of Pib2.

2.2 Results

2.2.1 Conserved Pib2 regions differentially affect Pib2 subcellular localization

TORC1 localizes to the both the vacuolar and endosomal membranes where differential TORC1 signaling occurs.[11,28,251,269] As localization is likely an important aspect of the ability of Pib2 to reactivate TORC1, we sought to determine how the Pib2 regions contribute to its subcellular localization. To this end, we generated Pib2 region deletion constructs N-terminally tagged with yEGFP, as C-terminal tagging has been shown to interfere with Pib2 activity by disrupting the tail motif.[237] Expression of these constructs was confirmed by western blot (Figure 2.1A,B). We also confirmed, using genomically yEGFP-tagged *PIB2*, that this tag does not interfere with the ability of Pib2 to activate TORC1 and promote cell growth under these conditions (Figure 2.1C).

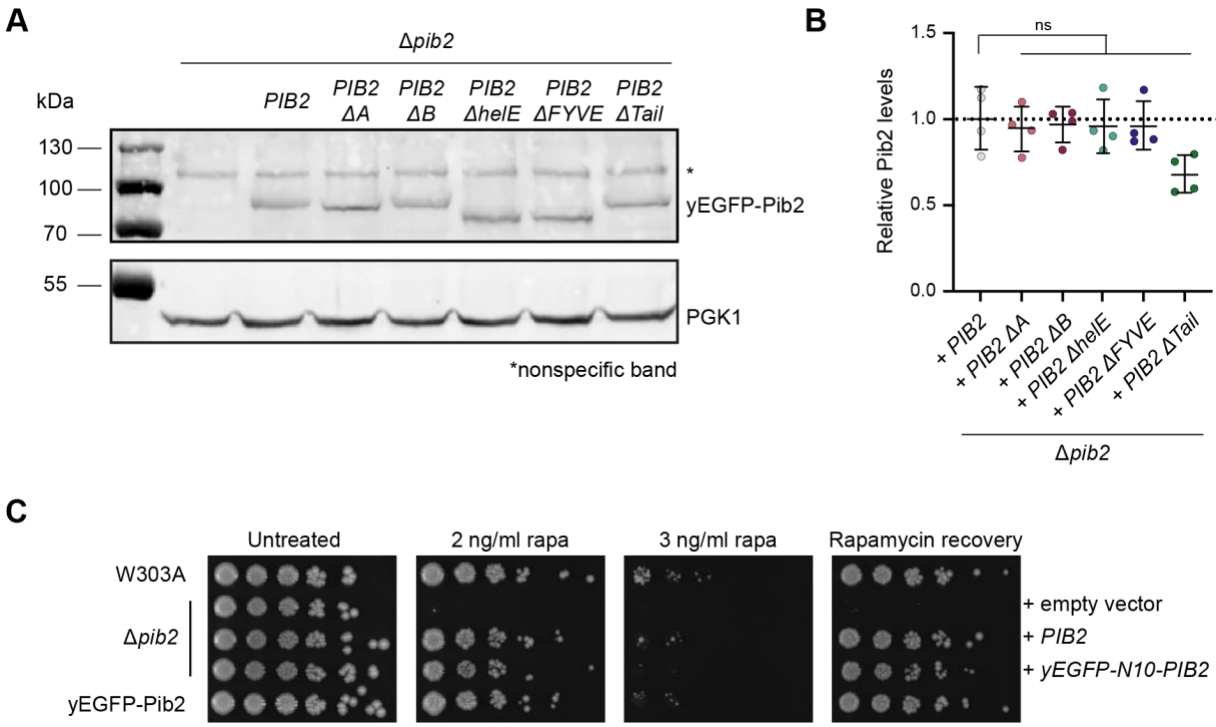

Figure 2.1 yEGFP-tagged Pib2 A) Representative western blot for relative protein expression levels of select yEGFP-Pib2 constructs. B) Quantification (mean ± s.d.) of the blots in A (n=4). Values were normalized to the corresponding Pgk1 loading control. Differences were evaluated by one-way ANOVA (F = 2.488, P = 0.1678). There were no significant differences from wild-type Pib2 expression levels as determined by Tukey post-hoc multiple comparisons test. C) Rapamycin exposure and recovery assays of an endogenously tagged yEGFP-Pib2 strain.

To assess localization of the yEGFP-tagged Pib2 deletion constructs, cells were imaged using confocal microscopy (Figure 2.2A,B). To visualize the vacuole, cells were stained with the lipophilic dye FM4-64, which is endocytosed by living cells and produces a uniform distribution on the vacuolar membrane.[270] Use of a vital dye for vacuolar visualization as opposed to a fluorescently tagged protein is beneficial as it does not require additional cell resources to generate the fluorescent tag. To quantify the vacuolar localization of the Pib2 constructs the ratio of vacuolar to cytosolic yEGFP signal was determined. First, a region within the image lacking cells was chosen to determine the mean background fluorescence. A vacuolar and a cytosolic region of

interest (ROI) of equal size were then determined for each cell. FM4-64 fluorescence was used to determine the location of the vacuolar membrane ROI. The mean GFP fluorescence within each ROI was determined and then the mean background fluorescence value was subtracted from each. The localization was then expressed as a ratio of vacuolar to cytosolic yEGFP signal, such that a number > 1 shows vacuolar enrichment and a number < 1 shows vacuolar exclusion. A minimum of 100 total cells from three experiments were counted for each construct. Outliers were identified using a ROUT outliers test (Q=0.1%) and data were further assessed by one-way ANOVA with Tukey multiple comparisons.

Wild-type Pib2 localized primarily to the vacuolar membrane with occasional perivacuolar puncta (Figure 2.2A,C). This vacuolar localization phenotype was consistent for most of the Pib2 deletion constructs. However, we observed that deletion of the FYVE domain resulted in a mixed phenotype, with some vacuolar localization and a large cytosolic component (Figure 2.2A,B), as previously described.[237] We also observed a similar phenotype with the ΔhelE construct (Figure 2.2A,B), suggesting that both the FYVE and helE domains might act as a potentially redundant dual vacuolar recruitment mechanism.

To further assess the subcellular localization of Pib2, we expressed yEGFP-Pib2 in a Δ*pib2* Δ*vps4* strain. Vps4 is an ATPase that is essential for endosomal morphology and endosome to vacuole transport.[271,272] The vacuolar protein sorting (Vps) genes are divided into phenotypic classes based on vacuolar morphology defects caused by their deletion.[273,274] Vps4 is a Class E mutant; these mutants have enlarged prevacuolar endosomal structures termed Class E compartments.[271,272,274] Using this deletion strain, we observe that the perivacuolar Pib2 puncta correspond to endosomal structures as evidenced by the presence of Pib2 on the Class E

compartments (Figure 2.2D). Vacuolar localization was not affected. These results agree with previous studies showing that Pib2 localizes to signaling endosomes.[255]

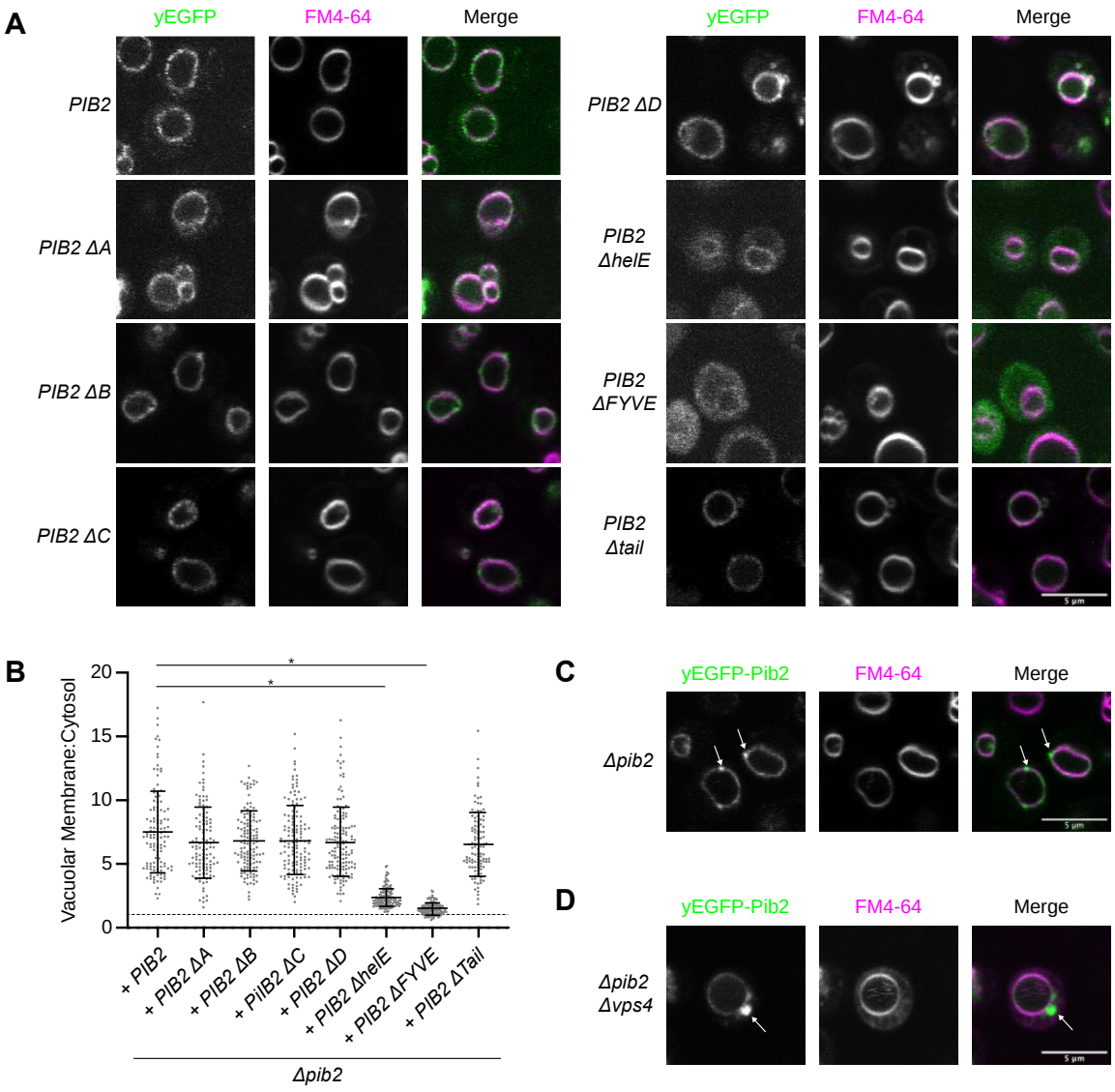

Figure 2.2 Localization of Pib2 deletion constructs A) Localization of Δ*pib2* cells expressing the indicated N-terminally yEGFP-tagged Pib2 constructs. For vacuolar visualization, cells were stained with FM4-64 prior to imaging. Representative fields of view are shown. B) Quantification (means ± s.d.) of the data presented in A. Vacuolar localization is determined as the ratio of vacuolar yEGFP signal to cytosolic yEGFP signal. Following a ROUT outlier analysis (Q=0.1%), a one-way ANOVA was conducted to determine differences in vacuolar localization ($F=121.6$, $P<0.0001$). Constructs significantly different from the localization of Pib2, as assessed by Tukey post-hoc

multiple comparisons test, are indicated (*P<0.0001). A total of 117-143 cells were quantified for each construct. C) yEGFP-Pib2 expressed in a Δ*pib2* strain with perivacuolar puncta (arrows). D) yEGFP-Pib2 expressed in Δ*pib2*Δv*ps4* cells showing Pib2 localization to the Class E compartment (arrow). Images are representative of 3 experiments.

2.2.2 Pib2 vacuolar localization is dependent on its helE and FYVE domains

The vacuolar localization of Pib2 has been shown to depend on PI3P and Vps34.[240] PI3P binding motifs within FYVE domains include WxxD and R+HHCRxCG (where x is any amino acid).[264,275] As these are both conserved across Pib2 FYVE domains (Appendix Figure 1A), we generated two mutants, one for each of these motifs: Pib2 W449A, D452A (Pib2 WD) and Pib2 R470A, H472A, H473A (Pib2 RHH). Both mutants showed compromised localization and were primarily cytosolic (Figure 2.3). Mutation of highly conserved residues in the helE region, 325RQI327→AAA (Pib2 RQI), 330PKK332→AAA (Pib2 PKK), 333PLY335→AAA (Pib2 PLY) and 339VLR341→AAA (Pib2 VLR), did not influence vacuolar localization (Figure 2.3). Simultaneous deletion of both the helE region and FYVE domain resulted in a primarily cytosolic phenotype as expected (Figure 2.3).

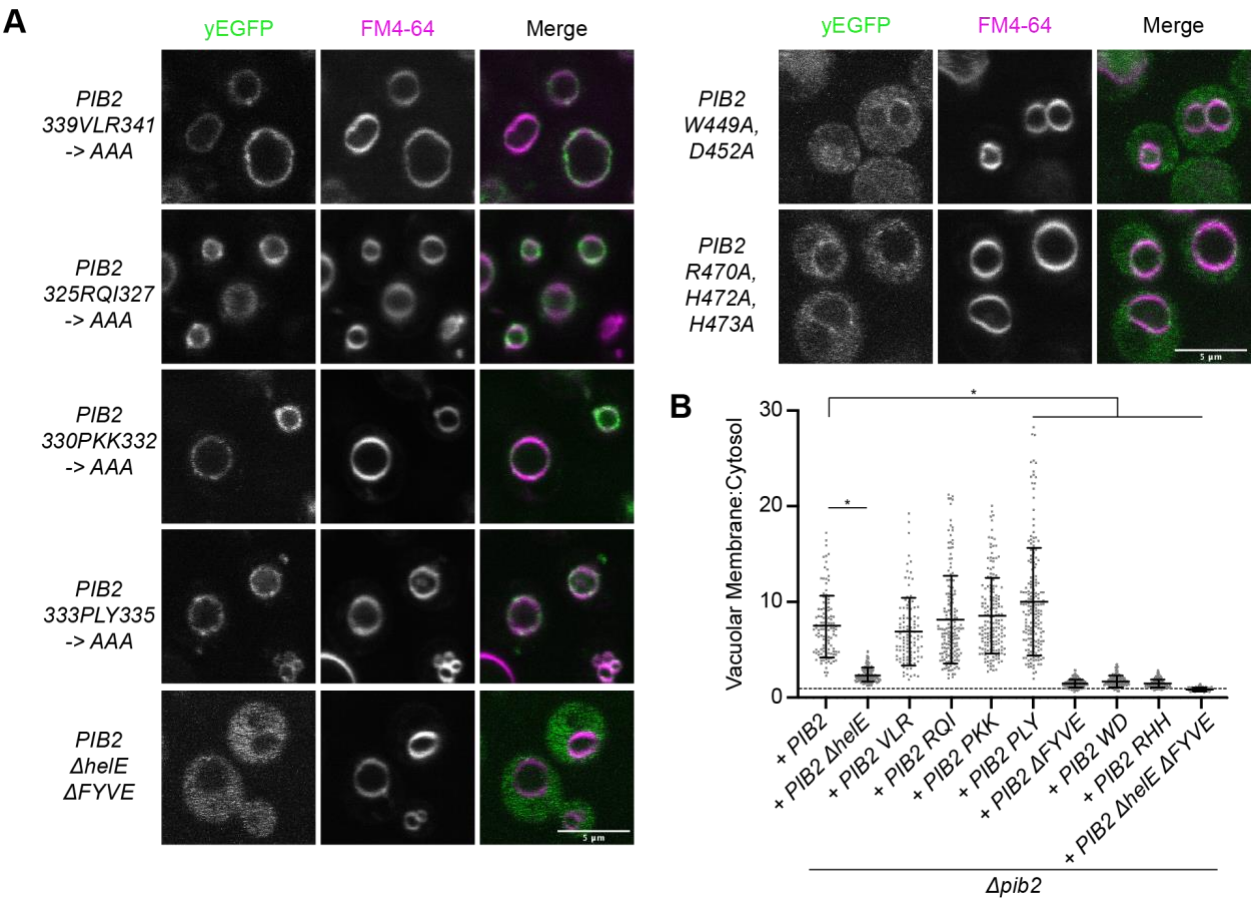

Figure 2.3 Localization of Pib2 helE and FYVE mutants A) Localization of the indicated yEGFP-Pib2 mutants expressed in Δ*pib2* cells. Vacuoles were strained with FM4-64. B) Quantification (mean ± s.d.) of the data. Data for Pib2, Pib2 ΔhelE, and Pib2 ΔFYVE were the same as in **Figure 2.2**. Following a ROUT outlier analysis (Q=0.1%), a one-way ANOVA was conducted to determine differences in vacuolar localization (F=180.9, P<0.0001). Constructs significantly different from WT Pib2, as assessed by Tukey post-hoc multiple comparisons test, are indicated (*P<0.0001). A total of 107-181 cells were quantified for each construct.

2.2.3 The Pib2 FYVE domain demonstrates a weak affinity for PI3P

As the FYVE domain alone was not sufficient to direct Pib2 localization to the vacuole, we investigated the ability of the Pib2 FYVE domain to bind to PI3P using isothermal titration calorimetry (ITC). ITC senses heat changes that are associated with binding interactions to enable

the determination of binding thermodynamics.[276] Unlike other methods, ITC is label-free which minimizes artifacts.[276] We expressed and purified Pib2 442-625, which included the start of the FYVE domain to the beginning of the tail motif. We also purified Pib2 419-625, which starts 23 residues before the core of the FYVE domain. While the AlphaFold2 Pib2 model does not show any structural elements here, some canonical FYVE domains include an α-helix immediately before the FYVE core, that is involved in dimerization. ITC with Pib2 442-625 showed a weak binding interaction with the PI3P headgroup, inositol 1,3 bisphosphate, with a mean K_D = 212 μM, as well as the short chain lipid, PI3P diC4 (mean K_D = 736 μM) (Figure 2.4A, Table 2.1). A mutant version of this construct, Pib2 442-625 RHH, did not bind to the lipid headgroup, as expected (Table 2.1). ITC with Pib2 419-625 also showed a low affinity interaction with the PI3P headgroup (K_D > 290 μM (Table 2.1). To validate the assay, we purified two EEA1 FYVE domain constructs, EEA1 1287-1411 and 1347-1411. The boundaries of these constructs were defined using the PDB structures 1JOC[268] and 1HYI,[277] respectively. The shorter EEA1 FYVE construct, 1347-1411, showed a weak binding affinity (K_D > 300 μM) that was difficult to fit (Table 2.1). The longer EEA1 FYVE construct, EEA1 1287-1411, showed a higher affinity for the PI3P headgroup (K_D ~95.8 μM) (Table 2.1). Although not necessarily representative of lipid binding affinity in the membrane, these affinities are comparable to previously published values, which demonstrate micromolar affinities of the purified EEA1 FYVE domain for the PI3P headgroup.[266] Furthermore, we used PIP strips to assess FYVE domain binding to various lipids. Using 5 μg/ml of purified protein, we detected an interaction of EEA1 1287-1411 with PI3P (Figure 2.4B). However, there was no PI3P interaction with Pib2 419-625 at that concentration (Figure 2.4B). When the protein concentrations were increased to 25 μg/ml, we observed an interaction between Pib2 419-625 and

PI3P, but not EEA1 1347-1411 (Figure 2.4C). Combined, this supports the lower affinity for PI3P of the Pib2 FYVE domain compared to EEA1 1287-1411.

Table 2.1: ITC Data

Construct	Cell Concentration (μM)	Syringe Concentration (mM)	K_D (M) ± error of the fit
Ins(1,3)P2			
His_6-S cer. PIB2 442-625	75	2	51.3E-6 ± 126E-6
His_6-S cer. PIB2 442-625	100	4	87.3E-6 ± 48.4E-6
His_6-S cer. PIB2 442-625	150	4	178E-6 ± 69.4E-6
His_6-S cer. PIB2 442-625	150	4	224E-6 ± 91.7E-6
His_6-S cer. PIB2 442-625	150	4	520E-6 ± 355E-6
His_6-S cer. PIB2 442-625 R470A, H472A, H473A	100	4	No binding
His_6-S cer. PIB2 419-625	200	3	293E-6 ± 402E-6
His_6-EEA1 1347-1411	200	3	310E-6 ± 2.02E-3
His_6-EEA1 1287-1411	200	3	95.8E-6 ± 53.1E-6
DiC4 PI3P			
His_6-S cer. PIB2 442-625	150	2	145E-6 ± 271E-6
His_6-S cer. PIB2 442-625	150	2	1.03E-3 ± 8.57E-3
His_6-S cer. PIB2 442-625	150	2	87.2E-6 ± 35E-6
His_6-S cer. PIB2 442-625	150	2	1.55E-3 ± 23.4E-3
His_6-S cer. PIB2 442-625	150	2	881E-6 ± 4.32E-3
His_6-S cer. PIB2 442-625	153	3	725E-6 ± 809E-6

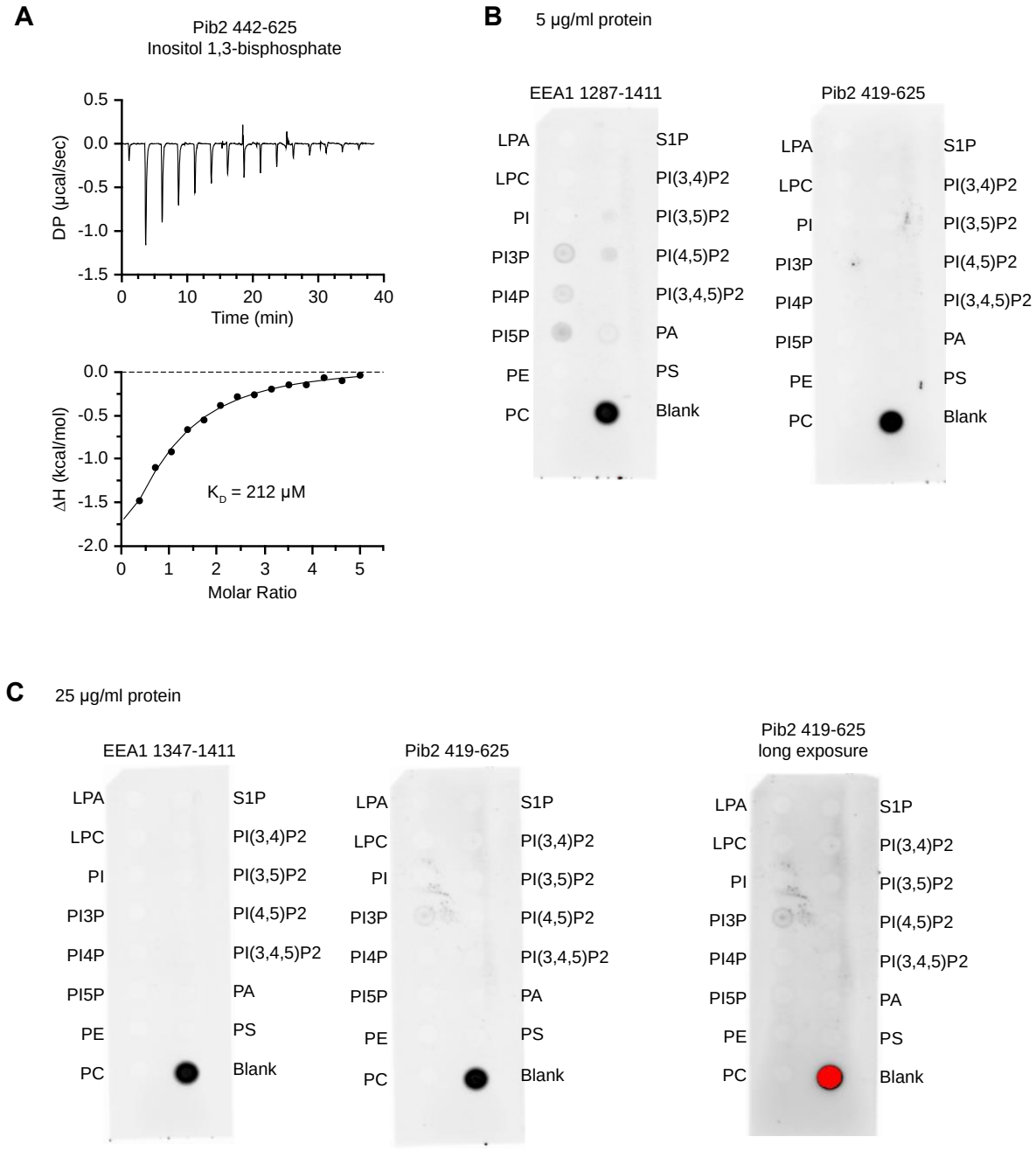

Figure 2.4 The Pib2 FYVE domain weakly binds PI3P A) Binding of inositol 1,3 bisphosphate to *S. cerevisiae* Pib2 442-625 as determined by ITC. The upper panel is a representative thermogram (DP – differential power) and the lower panel is a representative normalized binding isotherm obtained by integration of the peaks shown in the thermogram. The fit is obtained from a single-site binding model (smooth line). The mean determined K_D value is shown on the isotherm. B) Binding of 5 µg/ml of the indicated purified proteins to lipids on a PIP strip. Protein binding

determined by anti-His antibody. C) Binding of 25 µg/ml of the indicated purified proteins to lipids on a PIP strip. Note the overexposed image of the Pib2 419-625 PIP strip that shows weak PI3P binding.

Although many FYVE domains are monomeric, some are known to dimerize to facilitate PI3P binding.[267] We therefore used size exclusion chromatography coupled with multi-angle light scattering (SEC-MALS) to determine the oligomeric state of the purified FYVE domains. SEC-MALS separates the sample by hydrodynamic size using size-exclusion chromatography then, the sample is passed through a MALS detector which uses Rayleigh scattering of light to determine the mass of particles in solution.[278,279] Pib2 419-625 and Pib2 442-625 were predominantly monomeric (Figure 2.5A,B). As these constructs included predicted low complexity sequence downstream of the FYVE domain, we expressed and purified a smaller construct, Pib2 437-542. This was again predominately monomeric (Figure 2.5B). We also assessed the oligomeric state of the two EEA1 constructs. The crystal structure of EEA1 1287-1411 is a dimer,[268] where, in addition to the contacts between the core of the FYVE, there are significant interactions between the N-terminal α-helices (Figure 2.5C). Accordingly, this construct was largely dimeric, as assessed by SEC-MALS (Figure 2.5C). By contrast, and consistent with existing NMR models,[277] EEA1 1347-1411, which lacks the N-terminal α-helix, was largely monomeric (Figure 2.5C). The AlphaFold2 model of Pib2 lacks an α-helix before the FYVE domain (Figure 2.5D) and is, accordingly, monomeric with a PI3P binding affinity consistent with monomeric EEA1 1347-1411. As the binding affinities of the Pib2 constructs were relatively weak, it further supports that both the helE and FYVE domain are needed for appropriate subcellular localization of Pib2.

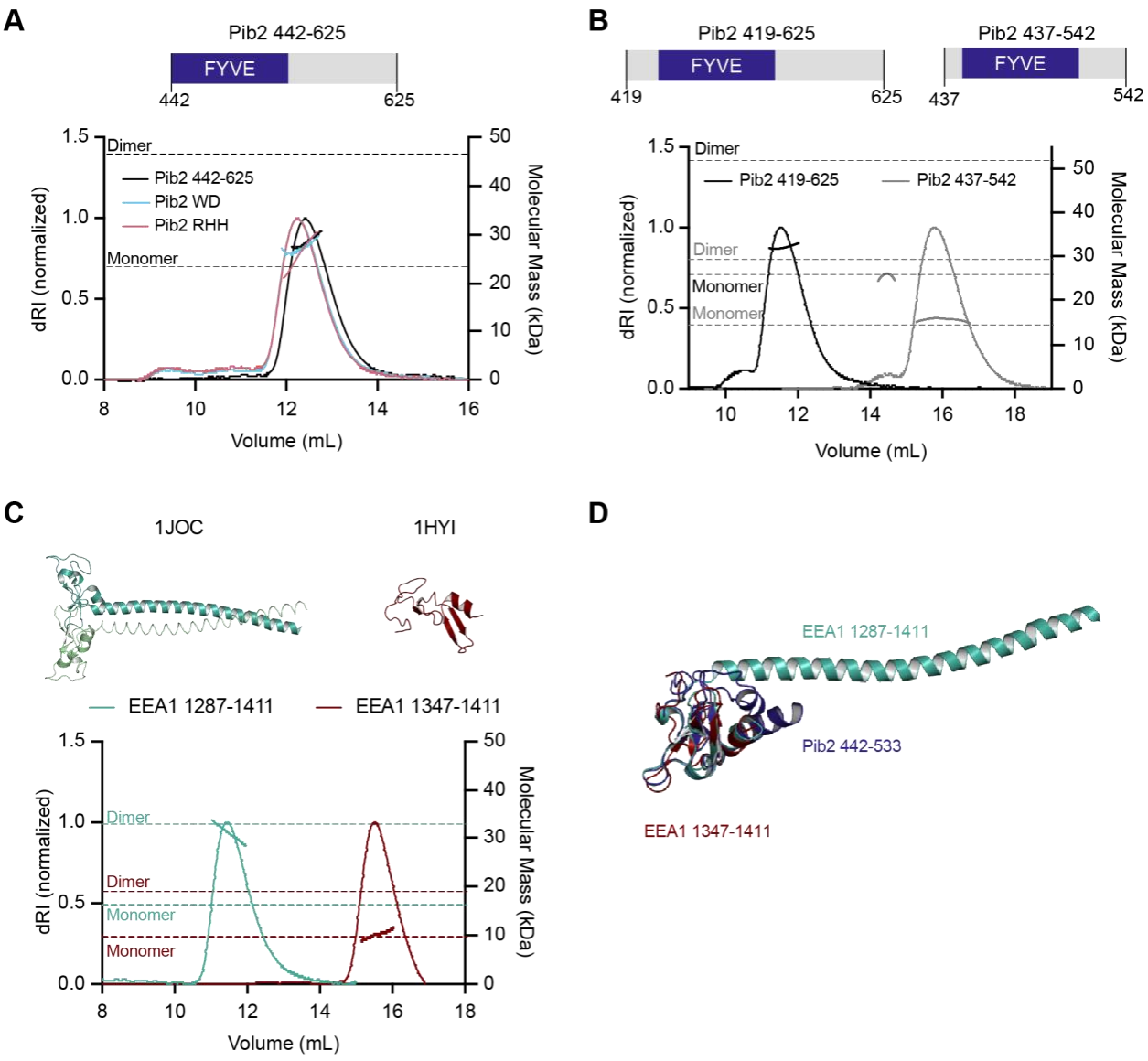

Figure 2.5 The Pib2 FYVE domain is monomeric

A) Determination of the molar mass of Pib2 442-625 and indicated mutants by SEC-MALS. The theoretical molecular masses of monomers and dimers are shown as dotted lines. B) Determination of the molar mass of Pib2 419-625 and Pib2 437-542. C) Determination of the molar mass of two EEA1 FYVE constructs. Boundaries determined from existig structures: EEA1 1287-1411 (PDB: 1JOC) and EEA1 1347-1411 (PDB: 1HYI). D) Aligned FYVE domains comparing the structures of EEA1 1287-1411 and EEA1 1347-1411 to the AlphaFold2 predicted structures of the Pib2 FYVE domain (residues 442-533). Alignment rendered in PyMOL.

2.3 Discussion

Subcellular localization has been shown to be an important aspect of TORC1 regulation and activity.[28,218] As we show here, the Pib2 helE region and FYVE domain are essential for Pib2 localization at the vacuolar membrane (Figure 2.2, Figure 2.3).[240] FYVE domains are most notably known as PI3P-binding domains and typically display endosomal localization.[264] As that is not the case with Pib2, it is possible that the Pib2 FYVE domain may favor other interactions to help direct it to the vacuole. Indeed, our measurements indicate low affinities for both the headgroup and a soluble PI3P. As these purified Pib2 FYVE constructs are predominately monomeric, regulation of assembly into a dimeric form may also be required to facilitate interaction with its preferred ligand. We show here that the FYVE domain alone is not sufficient for Pib2 vacuolar localization. Our data showed that while the Pib2 ΔFYVE construct had a mostly cytosolic cellular distribution, as previously described,[237] it did still have some enrichment at the vacuolar membrane likely due to the presence of the helE region (Figure 2.2A,B; Figure 2.3). As the Pib2 helE region is a TORC1 interaction site,[231,232] TORC1 and PI3P, via the FYVE domain, may act as a dual recruitment mechanism to maintain Pib2 localization at the vacuole. It is possible that these two weak recruitment mechanisms, via the helE region and FYVE domain, might provide an additional layer of regulation, where changes in local Pib2 concentrations influence PI3P binding, potentially through dimerization of the FYVE domain. Future studies are needed to further elucidate the mechanism of vacuolar recruitment of Pib2.

Pib2 is also found at signaling endosomes, although the mechanisms and dynamics of this were not studied here. It is possible that changes in vacuolar and endosomal localization of Pib2 is another aspect by which Pib2 regulates TORC1 activity. However, our preliminary observations show that rapamycin exposure does not seem to influence the subcellular localization of Pib2 (data

not shown). Future studies are needed to determine the dynamics that regulate vacuolar versus endosomal localization of Pib2.

3.0 Pib2 regulation of TORC1 activity

Select text and figures have been pulled from the following publication and have been adapted for flow and the inclusion of additional data:

K.K. Troutman, N.V. Varlakhanova, B.A. Tornabene, R. Ramachandran, and M.G.J. Ford. Conserved Pib2 regions have distinct roles in TORC1 regulation at the vacuole. *J Cell Sci* (2022) https://doi.org/10.1242/jcs.259994

3.1 Introduction

Pib2 is a master regulator of TORC1 signaling in yeast.[280] Pib2 is unique in that it was identified in screens for both rapamycin sensitivity[223,230] and rapamycin resistance.[231] Interestingly, Pib2 has two opposing functions in its regulation of TORC1: an inhibitory effect mediated by its N-terminal regions, and an activation effect mediated by its C-terminal domains.[231,232] It has been demonstrated that Pib2 interacts with Tor1 and Kog1, as well as EGO complex components.[231,232,235–237] Pib2 is essential for reactivation of TORC1 following rapamycin exposure and in response to glutamine and leucine following nitrogen starvation.[234] Recently, Pib2 has been implicated as a glutamine sensor which directly interacts with TORC1, in a glutamine-dependent manner, to promote TORC1 activity.[235,237,238] However, the molecular mechanisms of Pib2's regulatory interactions remain poorly understood. Here we demonstrate that conserved regions A and B within the Pib2 N-terminus are responsible for the inhibitory effect on

TORC1 reactivation following rapamycin exposure, whereas the C-terminal alpha-helical E region and tail motif are essential for TORC1 reactivation.

To demonstrate how each of the conserved Pib2 regions differentially contribute to the regulation of TORC1 activity we used rapamycin exposure assays. Using Δ*pib2* cells and plasmid-expressed Pib2 region deletion constructs, we performed two types of rapamycin growth assays. We assessed growth of cells in the presence of a low concentration of rapamycin (2 and 3 ng/ml) and on nutrient-rich plates following a 4-hour exposure to a high (200 ng/ml) concentration of rapamycin. These two approaches assay growth in an ongoing stress state and recovery from the stressor, respectively. In selecting these rapamycin concentrations, we considered previous works as well as our own titration experiments. For growth on rapamycin plates, we used a range of rapamycin concentrations from 2-5 ng/ml and found that above 3 ng/ml rapamycin, little growth is seen. Thus, 2 ng/ml and 3 ng/ml rapamycin YPD plates were determined to be the best for highlighting Pib2 growth phenotypes. For our rapamycin recovery assay, we used 200 ng/ml for 4 hours. While some previous studies have treated cells over the course of days, as opposed to hours, it is worth noting that during a longer time frame, there is more concern over the appearance of suppressors that could muddle the results. Ultimately, the chosen rapamycin concentrations have shown to be sublethal doses which help to maximally emphasize the Pib2 mutant phenotypes.

3.2 Results

3.2.1 Conserved Pib2 regions differentially regulate TORC1 reactivation

To elucidate the TORC1 regulatory functions of Pib2, we assessed cell growth in rapamycin exposure assays using deletion constructs for each of the seven conserved Pib2 regions (Figure 1.5A). Δ*pib2* cells expressing Pib2 ΔhelE and Pib2 ΔTail constructs did not grow on rapamycin-containing plates (Figure 3.1A) and were unable to recover from rapamycin treatment (Figure 3.1B). Unexpectedly, expression of the Pib2 construct lacking its FYVE domain (Pib2 ΔFYVE) was able to mediate growth on rapamycin-containing plates and recovery from exposure to rapamycin, although at a much slower rate than isogenic wild-type (W303A) cells or Δ*pib2* cells expressing wild-type Pib2 (Figure 3.1A,B). In contrast, deletion of Pib2 regions A or B resulted in enhanced growth in both rapamycin exposure assays (Figure 3.1A,B). Deletion of Pib2 regions C or D did not influence cell growth on rapamycin plates nor the ability to recover following rapamycin exposure (Figure 3.1A,B). These results suggested that the N-terminal regions A and B were key for the inhibitory function of Pib2, whereas the C-terminal helE region and tail motif were essential for TORC1 reactivation. Although previous studies used more extensive region deletions, our results support these observations, showing that the Pib2 N-terminal regions have an inhibitory function, and the C-terminal regions are needed for TORC1 reactivation.[231,232]

As a control, the growth of the Pib2 deletion constructs did not differ on YPD plates without rapamycin exposure (Figure 3.1A). Further, as the rapamycin assays used plasmid-based expression of Pib2, we generated genomic strains of *PIB2* ΔA, *PIB2* ΔB, and *PIB2* ΔhelE, as well as wild-type *PIB2*, where the only source of *PIB2* is its native genomic context, to demonstrate that plasmid expression was representative of endogenous expression. Using these genomically-

modified strains, we repeated the rapamycin growth assays and observed that the genomic *PIB2* region deletion mutants showed the same growth patterns as the plasmid-expressed deletion constructs (Figure 3.1C).

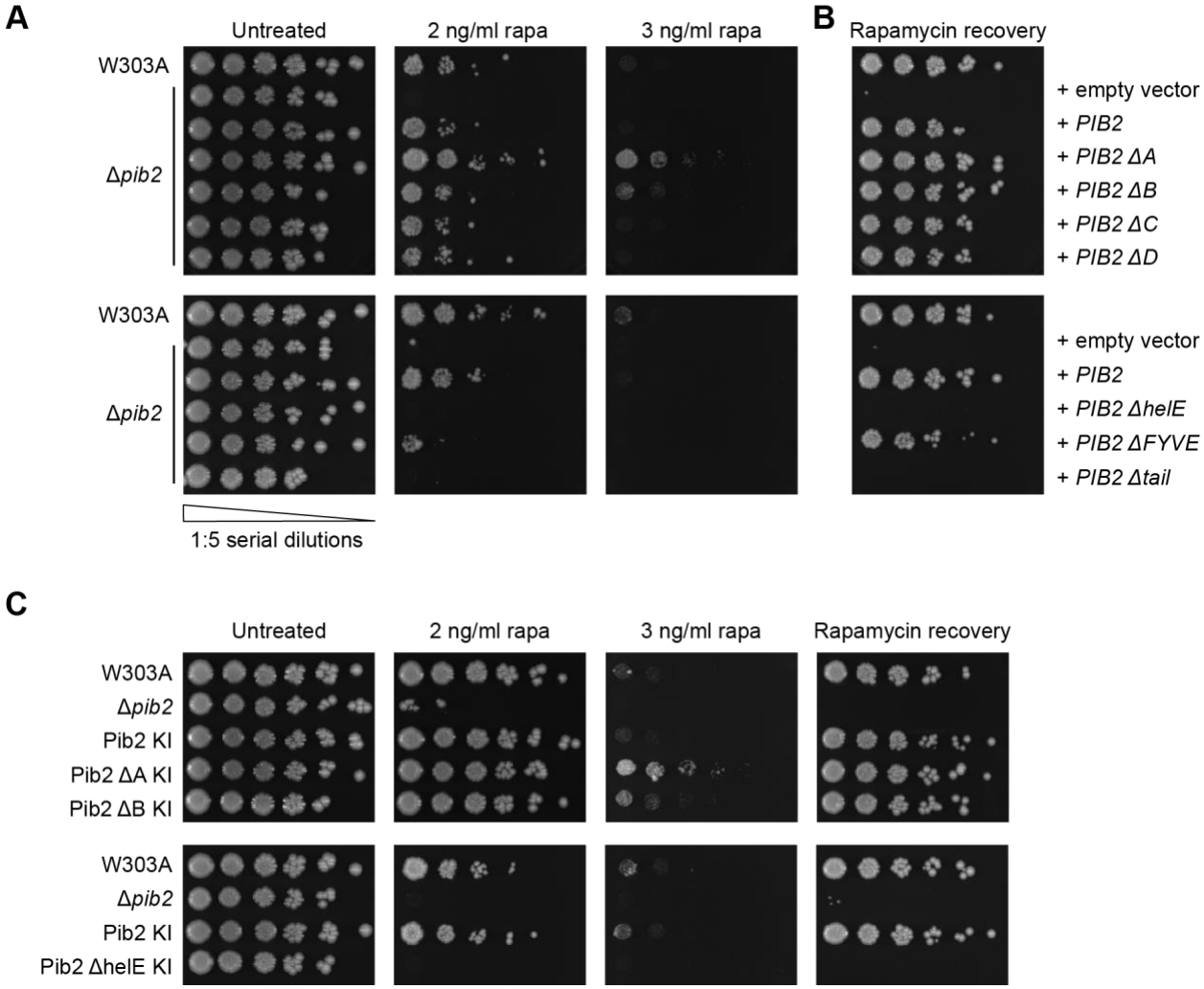

Figure 3.1 TORC1 reactivation is differentially regulated by conserved Pib2 regions

A) Rapamycin exposure assay assessing growth of W303A and Δ*pib2* cells expressing the indicated constructs on YPD or YPD supplemented with the indicated low concentration of rapamycin (rapa). The left-most spots correspond to 2 µl of a OD_{600}=0.5 culture, followed by 2 µl of sequential 1:5 diliutions. B) Rapamycin recovery assay assessing growth of W303A and Δ*pib2* expressing the indicated constructs on YPD following rapamycin exposure. Exponentially growing cells were treated with 200 ng/ml rapamycin in YPD at 30°C for 4 h. After washing, cells were plated on YPD and incubated at 30°C for 3 days. Cells were plated as in A. Images are representative of three

experiments. C) Rapamycin exposure and recovery assays of endogenous Pib2 deletion strains performed as described in A and B.

To ensure that the differences in rapamycin recovery were not due to changes in protein expression levels, we used Pib2 region deletion constructs tagged at the N-terminus with yEGFP and western blotting to confirm that these mutants are expressed at equal levels under logarithmic phase growth conditions (Figure 2.1A,B). Furthermore, we used GFP-Atg8 to assess the induction of autophagy in response to both rapamycin exposure and nutrient starvation.[281,282] No differences were observed between W303A and Δ*pib2* cells in either condition (Figure 3.2A,B).[234] Additionally, without these stressors, no differences in autophagy induction were observed at steady state in Δ*pib2* cells compared to W303A, thus Pib2 does not influence the repressive function of TORC1 on autophagy (Figure 3.2A,B).[234] Cells were confirmed to be viable following 4 hours of 200 ng/ml rapamycin exposure and a 48 hour recovery period by staining with FM4-64 and subsequent imaging showing that the dye is endocytosed by both W303A and Δ*pib2* cells (Figure 3.2C).

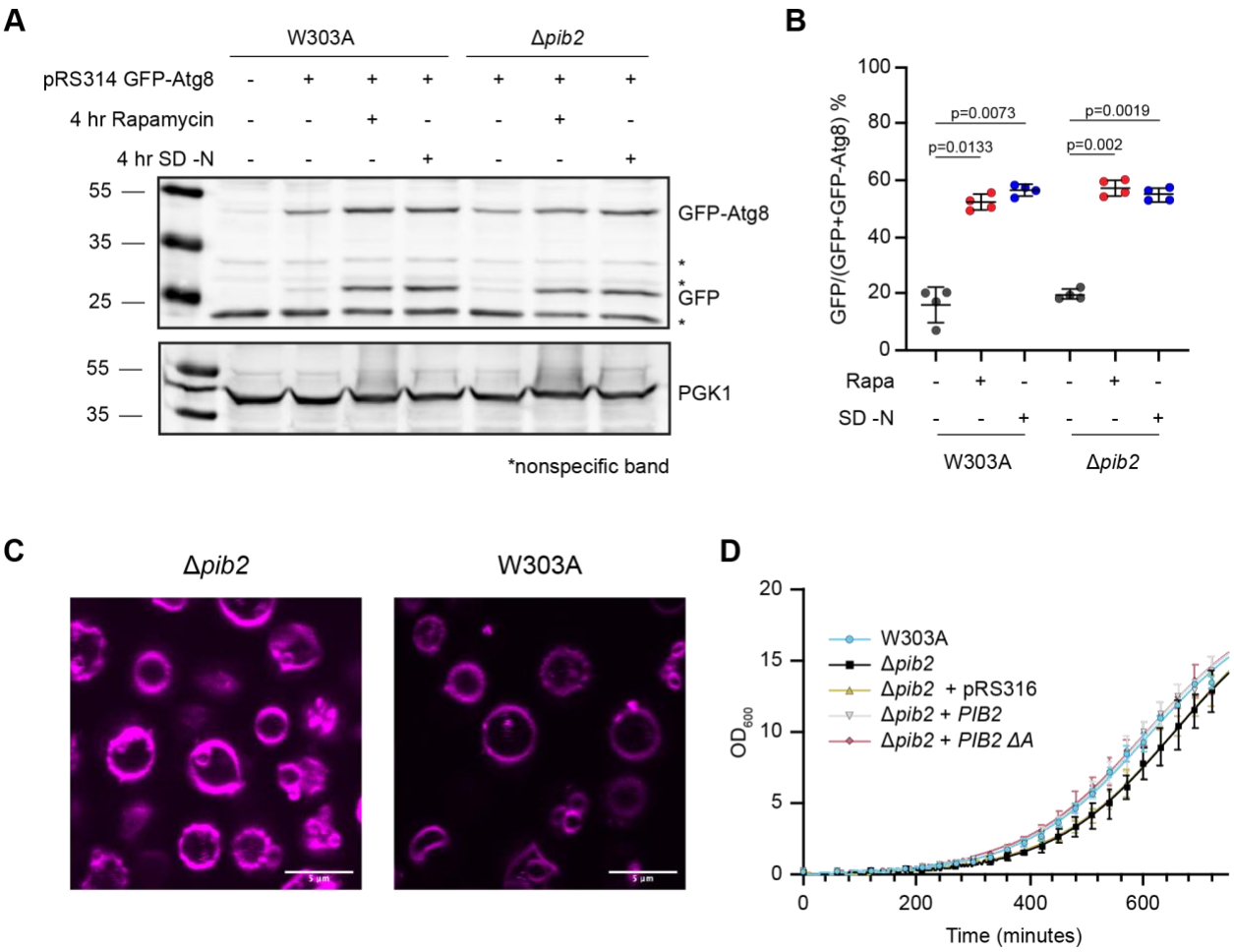

Figure 3.2 Δ*pib2* Controls A) Representative western blot assessing induction of autophagy. W303A or Δ*pib2* cells expressing GFP-Atg8 were treated with rapamycin or nitrogen starved for 4 hours. GFP-Atg8 and free GFP were detected using an anti-GFP antibody. B) Quantification (mean±s.d.) of the blots in A (n=4). Differences in the ratios of free GFP to total GFP for each condition were ealuated by one-way ANOVA ($F = 117.3$, $P < 0.0001$). Significant differences between untreated and treated cells as determined by Tukey post-hoc multiple comparison tests are denoted. No significant differences were observed in comparing W303A and Δ*pib2* cells**.** C) Representative images of cells stained with FM4-64 following rapamycin exposure. Cells were treated with 200 ng/ml rapamycin for 4 hours, washed, and allowed to recover for 48 hours. At 48 hours, cells were stained with FM4-64 for 1 hour and imaged. D) 12-hour growth curve of select yeast strains expressing the indicated Pib2 constructs.

3.2.2 N-terminal Pib2 regions A and B display a TORC1 inhibitory function

Previous studies have demonstrated a TORC1 inhibitory function for Pib2 as it pertains to TORC1 reactivation following rapamycin exposure.[231] Studies using large truncations of its N-terminal region, residues 1-50 or 1-164, have shown that in the absence of the N-terminus, Pib2 is better able to reactivate TORC1 and promote cell growth.[231,237] In our rapamycin assays (Figure 3.1 A,B), we demonstrated that Regions A (residues 54-81) and B (residues 109-118) were central to the Pib2 inhibitory function. As the Pib2 ΔA construct showed enhanced growth in the rapamycin exposure assays, we sought to determine whether the increased growth rate and TORC1 activity is specific to TORC1 reactivation. For this, we assessed growth of select Pib2 constructs in liquid culture. In nutrient replete growth conditions (YPD), we found that the Pib2 ΔA construct grew at the same rate as wild-type Pib2 (Figure 3.2D). This suggests the difference in growth rates between wild-type Pib2 and Pib2 ΔA, as observed in rapamycin exposure assays, is specific to TORC1 reactivation.

To further uncover the inhibitory mechanism of Pib2 we used our MSAs to select highly conserved residues within regions A and B that might be involved in TORC1 inhibition. Region A contains a series of conserved lysine residues, lysines 59-61, and a series of conserved serines, S73, S76, S77, and S79 (Figure 3.3A). We mutated the serine residues to alanines to generate a mutant denoted Pib2 4SA. In rapamycin exposure assays Pib2 4SA grew at a similar rate to wild-type Pib2 and maintained vacuolar localization (Figure 3.3B,D,E). As the lysine residues would be susceptible to post-translational modifications (PTMs) we generated a triple lysine 59-61 to alanine mutant, denoted Pib2 KA. Pib2 KA grew on rapamycin-containing plates and recovered from rapamycin exposure at a similar rate to the Pib2 ΔA construct, and this mutation did not affect Pib2 subcellular localization (Figure 3.3B,D,E). Further, as the positive charge of these lysine

residues could form part of a binding interface and result in interactions with negatively charged residues in a binding partner, we also mutated these residues to arginine (Pib2 KR) to maintain a positive charge or glutamate (Pib2 KE) for a charge reversal. Pib2 KE grew at a similar rate to the Pib2 ΔA and Pib2 KA mutants (Figure 3.3C). The Pib2 KR mutant, however, grew at a similar rate to wild-type Pib2 (Figure 3.3C). As mutation from lysine to either alanine or glutamate residues had a similar effect, and the lysine to arginine mutant had no effect, on cell growth, we propose that the positive charge of the lysine residues in this region are key to its TORC1 inhibitory function.

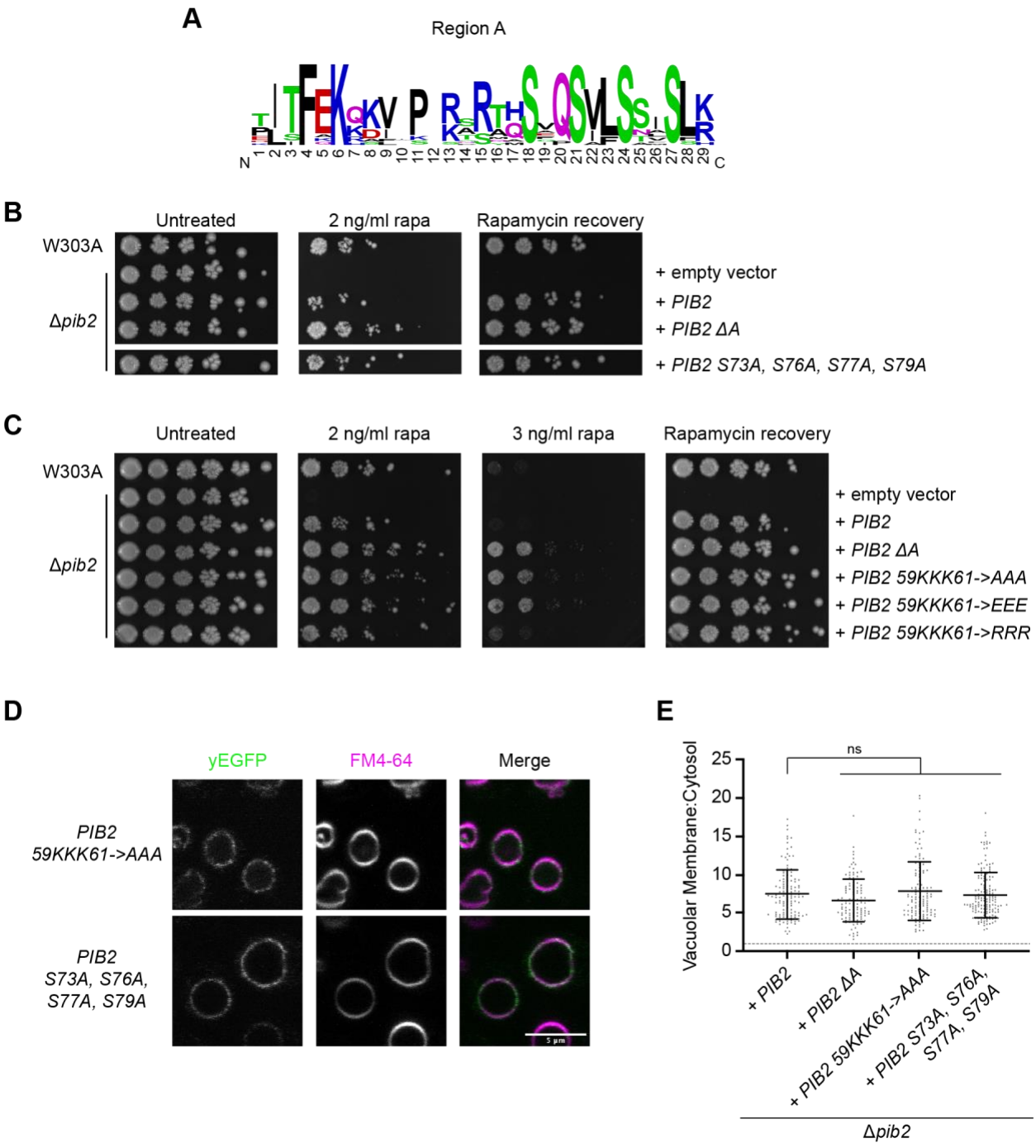

Figure 3.3 Pib2 Region A mutants A) Sequence logs illustrating the residues conserved in Pib2 region A (15 ascomycete fungi sequences used for alignment). Residue label size is proportional to conservation. B-C) Rapamycin exposure and recovery assays of Δ*pib2* cells expressing the indicated constructs. These were performed as in **Figure 3.1** and images are representative of three experiments. D) Vacuolar localization of indicated yEGFP-Pib2 mutant constructs. Vacuoles were stained with FM4-64. E) Quantification (means±s.d.) of the data presented in D. Data for

Pib2 and Pib2 ΔA are the same as in **Figure 2.2**. Following a ROUT outlier analysis (Q=0.1%), a one-way ANOVA was conducted to determine differences in vacuolar localization (F=2.703, P=0.0449). There were no significant differences from wild-type Pib2 localization as determined by Tukey post-hoc multiple comparisons test. A total of 117-151 cells was quantified for each construct.

In region B, we identified conserved serine residues S113 and S118 (Figure 3.4A). Bioinformatic analyses of the Pib2 sequence showed that S113 is a predicted phosphorylation site.[283] We therefore assessed phospho-dead and phosphomimetic mutants for growth on rapamycin plates and recovery from rapamycin exposure. The phospho-dead mutant, Pib2 S113A, S118A (Pib2 SA), showed reduced growth compared to wild-type Pib2 but did maintain vacuolar localization (Figure 3.4B,E,F). However, the phosphomimetic mutant, Pib2 S113E, S118E (Pib2 SE), grew better than wild-type Pib2 in these rapamycin exposure assays (Figure 3.4B). This is most notable on the 2 ng/ml rapamycin plate, as the effects diminished with increased rapamycin concentration (Figure 3.4B). This suggests that phosphorylation at one or both of these sites may be involved in the TORC1 inhibitory mechanism of Pib2.

Region B also has a series of conserved glutamine residues, Q109, Q110, and Q112, and a proline, P114. We mutated these residues to alanines to generate two additional Region B mutants denoted Pib2 QA and Pib2 PA, respectively. In rapamycin assays, Pib2 QA grew at a rate similar to wild-type Pib2, whereas Pib2 PA grew slightly faster than wild-type Pib2 (Figure 3.4C,D). The increased growth rate of Pib2 PA is most noticeable on the 3 ng/ml rapamycin plate (Figure 3.4D). Both mutants maintained vacuolar localization (Figure 3.4E,F).

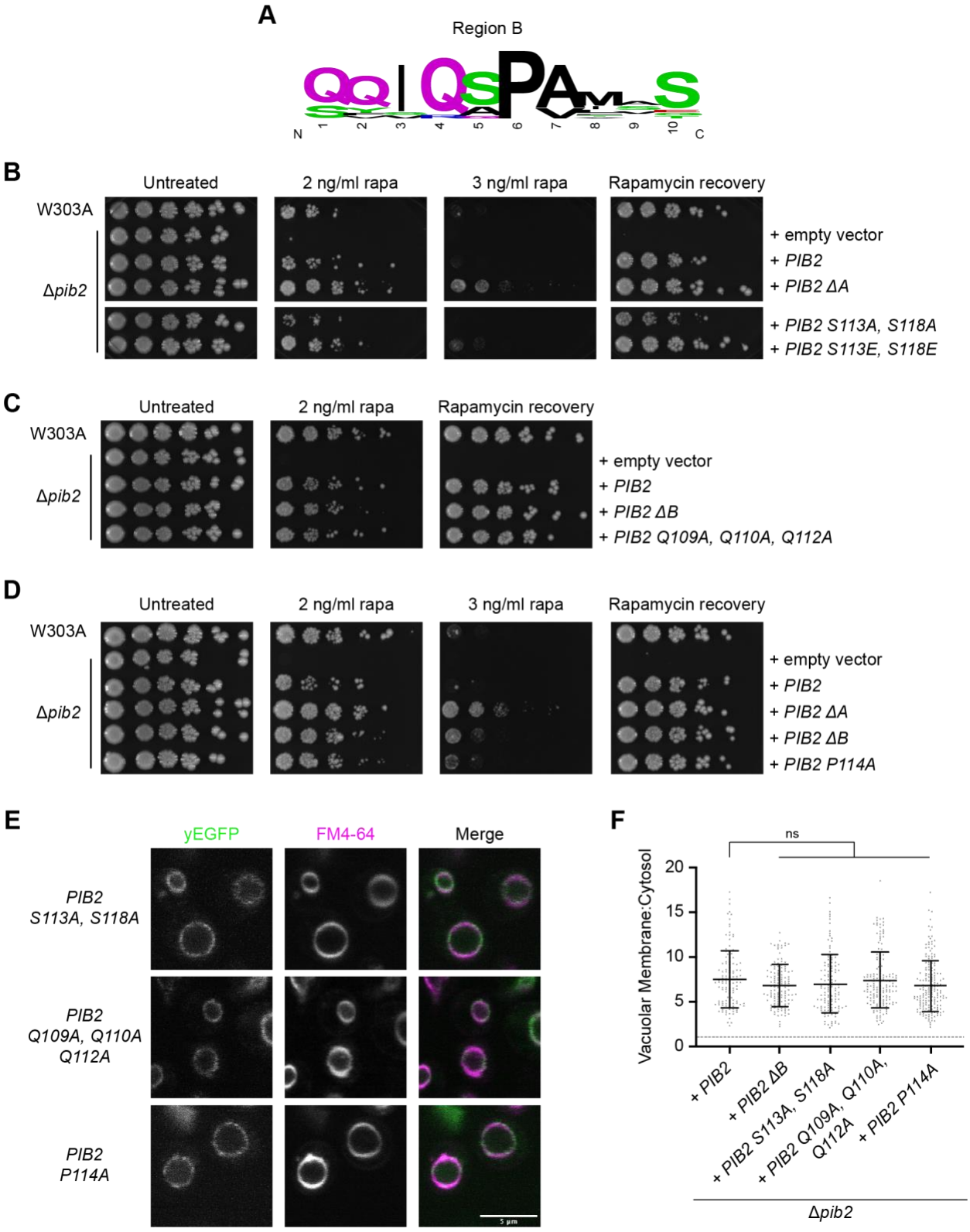

Figure 3.4 Pib2 Region B mutants A) Sequence logos illustrating the residues conserved in Pib2 region B (15 ascomycete fungi sequences used for alignment). Residue label size is proportional to conservation. B-D) Rapmaycin

exposure and recovery assays of Δ*pib2* cells expressing the indicated constructs. These were performed as in **Figure 3.1**. E) Vacuolar localization of indicated yEGFP-Pib2 mutant constructs. Vacuoles were stained with FM4-64. F) Quantification (mean±s.d.) of the data presented in E. Data for Pib2 and Pib2 ΔB are the same as in **Figure 2.2**. Following a ROUT outlier analysis (Q=0.1%), a one-way ANOVA was conducted to determine differences in vacuolar localization (F=1.874, P=0.1132). There were no significant differences from wild-type Pib2 localization as determined by Tukey post-hoc multiple comparisons test. A total of 122-183 cells was quantified for each construct.

A potential model of TORC1 inhibition by Pib2 could involve intramolecular interactions. To determine whether regions A and B work together to inhibit TORC1 activity, we generated 2 combinatorial deletion mutants and 4 combinatorial mutants of key region A and B residues. These included: Pib2 ΔA ΔB (Δ54-81, Δ109-118), Pib2 ΔA-B (Δ54-118), Pib2 KA/SA, Pib2 KA/SE, Pib2 KE/SA, and Pib2 KE/SE. Each of these mutants showed improved growth over wild-type cells in both rapamycin exposure assays (Figure 3.5A). As the lysine mutations in region A were able to override the activity of the region B serine mutations, this suggests region A is dominant to region B in this mechanism.

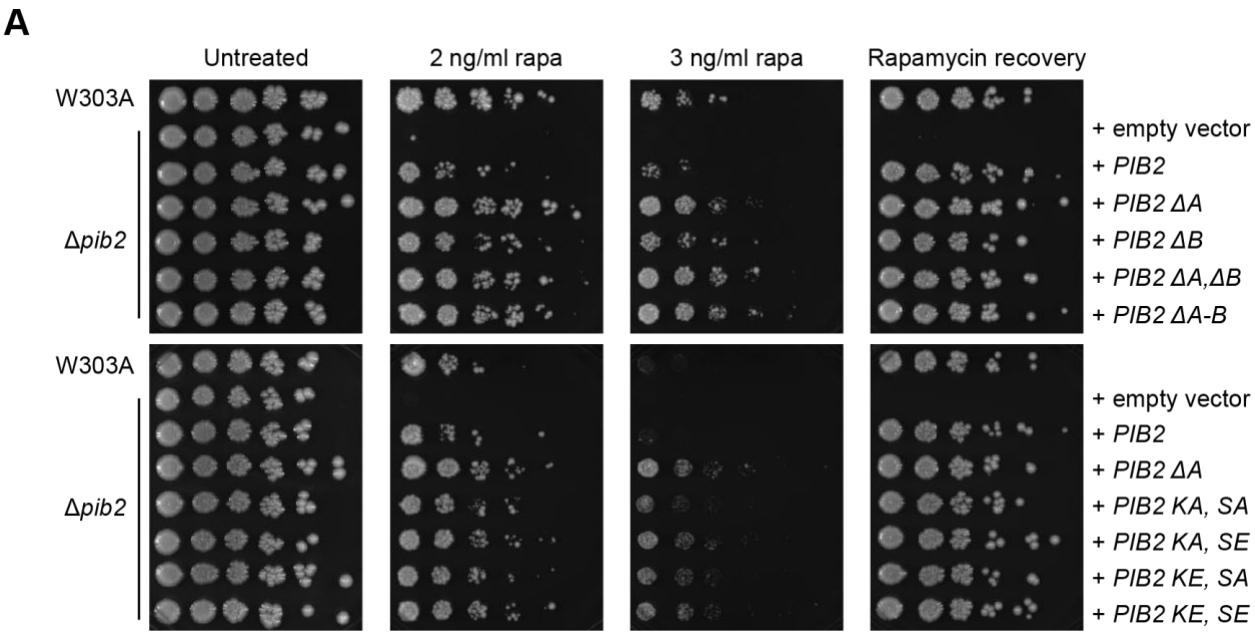

Figure 3.5 Pib2 Region A is dominant to Region B A) Rapamycin exposure and recovery assays of Δ*pib2* cells expressing the indicated constructs. These were perfomed as in **Figure 3.1**. Images are representative of three experiments.

3.2.3 Pib2 C-terminal regions are essential for TORC1 reactivation following rapamycin exposure

Previous studies have shown that truncation of the Pib2 C-terminal tail, and larger C-terminal portions, impedes the reactivation of TORC1 following rapamycin exposure.[231,237] As shown in Figure 3.1, the helE and tail motif were essential for TORC1 reactivation under rapamycin exposure conditions. The FYVE domain also influenced TORC1 reactivation, although less so than the other two domains. To determine what aspects of these conserved regions might be key for TORC1 reactivation, we generated point mutations of highly conserved residues within the helE region and FYVE domain to assess their effects on TORC1 activation. The helE region mutants Pib2 VLR and PLY were not able to mediate growth on rapamycin plates and Δ*pib2* cells

expressing these did not recover from rapamycin exposure, similar to what was found for the helE region deletion construct (Figure 3.6A). Two other helE mutants, Pib2 RQI and PKK, were able to mediate growth on and recovery from rapamycin though at a slower rate than W303A cells or Δ*pib2* cells expressing wild-type Pib2 (Figure 3.6A). As shown above, unlike the helE region deletion construct, these mutants localized predominately to the vacuole, resembling WT Pib2 localization (Figure 2.3A,B). The helE region of Pib2 is a putative Kog1 binding region,[231,232] thus it is possible that these residues might be required for that interaction.

Another highly conserved residue in the Pib2 helE region is P337; thus, we generated two additional helE mutants, Pib2 P337A and Pib2 P337S, to assess their growth in Δ*pib2* cells. A previous study identified Pib2 P337S as a temperature sensitive mutant in Δ*gtr1*Δ*ego1* cells.[237] When expressed in Δ*gtr1*Δ*ego1* cells, these cells show reduced growth and TORC1 activity at 37°C compared to expression of wild-type Pib2 and growth at 30°C.[237] Further, Pib2 P337S displayed a decreased Tor1 interaction at 37°C, leading the authors to the hypothesis that this proline residue is important in the Pib2-TORC1 interaction necessary for TORC1 activation.[237] In our rapamycin growth assays, both Pib2 P337A and Pib2 P337S displayed slightly slower growth than wild-type Pib2 even when grown at 30°C (Figure 3.6B). These mutants maintained vacuolar localization (data not shown), which supports the possibility that these residues have some involvement in the activating interactions that occur with the TORC1 complex.

We also assessed growth of the PI3P binding motif mutations within the Pib2 FYVE domain, Pib2 WD and Pib2 RHH. In addition to their altered localization described above (Figure 2.3A,B), these mutants phenocopied deletion of the FYVE domain in that they mediated recovery at a slower rate than seen in Δ*pib2* cells expressing wild-type Pib2 (Figure 3.6C).

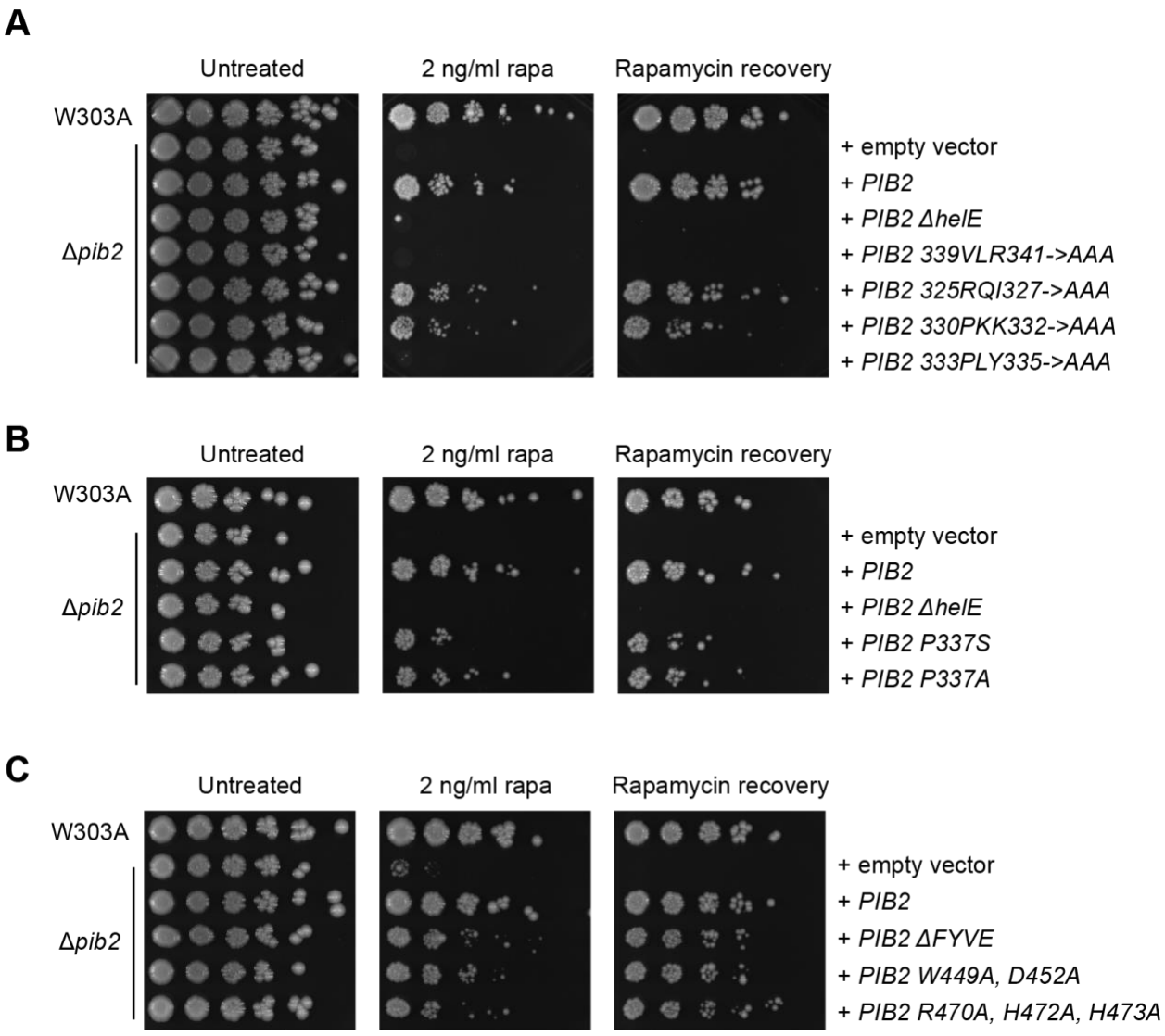

Figure 3.6 The Pib2 helE region and FYVE domain are essential for TORC1 reactivation A-B) Rapamycin exposure and recovery assays of Δ*pib2* cells expressing the indicated Pib2 helE region mutants. These were performed as in **Figure 3.1**. C) Rapamycin exposure and recovery assays of Δ*pib2* cells expressing the indicated Pib2 FYVE domain mutants. These were performed as in **Figure 3.1**. Images are representative of three experiments.

3.2.4 N- and C-terminal interactions

To determine whether the Pib2 inhibitory regions interact with Pib2 C-terminal activation regions we generated compound deletion mutations. To assess the growth of these constructs, we

assessed rapamycin recovery after 2 hours of exposure to 200 ng/ml of rapamycin. Deletion of region A in combination with one of the C-terminal activation regions (helical E, FYVE, or tail) enabled mild recovery following rapamycin exposure compared to deletion of the C-terminal regions alone (Figure 3.7A). Two additional combination mutants combined an N-terminal deletion or mutant, with a C-terminal mutant or deletion, respectively. These mutants were Pib2 KA ΔhelE and Pib2 ΔA VLR. As with the other mutants, both enabled mild recovery from rapamycin exposure at a similar rate, much slower than wild-type Pib2 (Figure 3.7B). Although these mutants displayed a less robust recovery, this indicates that the N- and C-terminal mechanisms for Pib2-mediated inhibition and activation of TORC1 might be separable, as also implicated in a previous study.[231]

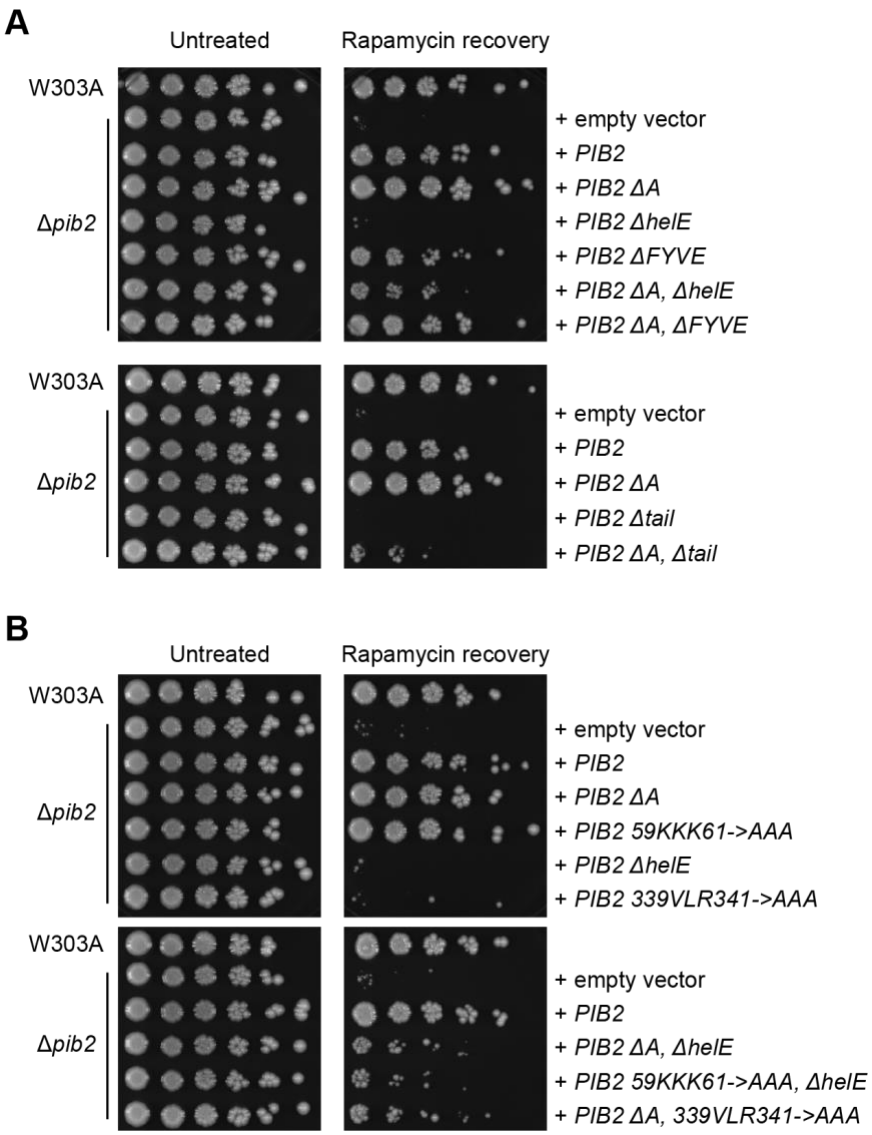

Figure 3.7 Are the N- and C- terminal functions separable? A-B) Rapamycin recovery assays of Δ*pib2* cells expressing the indicated constructs. These assays were performed as in **Figure 3.1**, except rapamycin treatment was 2 hours. Images are representative of three experiments.

3.2.5 Pib2 and the Gtrs

The Gtr-dependent pathway of TORC1 regulation relies on nutrient sensing by upstream GAPs and GEFs to control TORC1 activation through the EGO complex. Whether Pib2 activation

of TORC1 is a Gtr-dependent or Gtr-independent mechanism has attracted considerable discussion. Simultaneous deletion of Pib2 and EGO subunits results in synthetic lethality.[240] Further, Pib2 has been shown to interact with EGO subunits and both Pib2 and EGO are required for TORC1 activation by amino acids.[234,236,240] However, some studies have described a parallel, Gtr-independent activation pathway via glutamine.[235,237,238] As such, we expressed the Pib2 ΔA construct in a Δ*gtr1*Δ*gtr2* strain to determine if this could reduce the rapamycin sensitivity of the Δ*gtr1*Δ*gtr2* strain. As noted above, Pib2 ΔA expression in Δ*pib2* cells increases their rapamycin resistance. In the Δ*gtr1*Δ*gtr2* strain however, Pib2 ΔA was unable to rescue the rapamycin sensitivity of the strain, as it did not allow for growth on rapamycin plates or recovery from rapamycin exposure (Figure 3.8A).

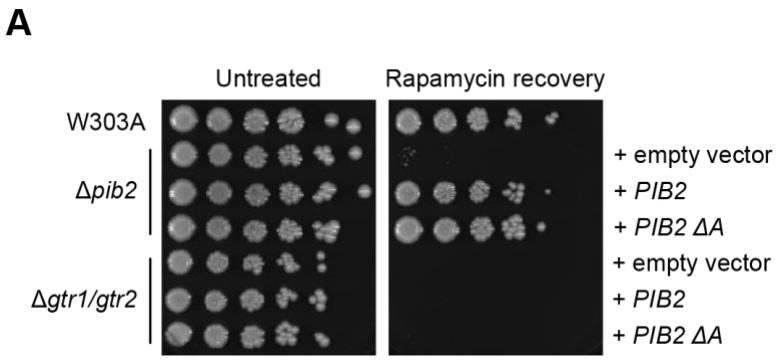

Figure 3.8 Pib2 ΔA expression does not rescue rapamycin sensitivity of Δ*gtr1*Δ*gtr2* cells A) Rapamycin exposure and recovery assays of Δ*pib2* or Δ*gtr1*Δ*gtr2* cells expressing Pib2 ΔA. Assays performed as in **Figure 3.1**, except in rapmycin recovery cells were treated with rapamycin for 2 hours.

3.3 Discussion

Pib2 C-terminal regions have been shown to be essential for TORC1 reactivation. Deletion mutants of the tail motif or Kog1 binding domains (found within the conserved helE region) exhibit

increased rapamycin sensitivity.[231,232] We demonstrated here that helE specific VLR and PLY sequences, and the tail motif were required for the ability of Pib2 to mediate growth on rapamycin-containing plates and recovery following rapamycin exposure (Figure 3.1, Figure 3.6A). The mechanism through which the tail motif acts in TORC1 reactivation is unclear. However, several hyperactive tail mutations were recently reported, and it was proposed that the tail directly interacts with TORC1 to promote its activation.[238]

Pib2 interaction with TORC1 components, Kog1 and Tor1, have previously been demonstrated by western blotting and yeast two-hybrid experiments.[231,232,235,237] The helE region has been identified as a putative binding region for these interactions.[231,232] As confocal imaging of our Pib2 ΔhelE mutant showed, this region is partially responsible for Pib2 localization at the vacuole (Figure 2.2B). However, the helE mutants Pib2 PLY and Pib2 VLR demonstrated that these residues were essential for TORC1 reactivation following rapamycin exposure, even though they have no effect on vacuolar localization (Figure 2.3, Figure 3.6A). It has recently been reported that some of these residues, particularly R341, may be essential for glutamine induced TORC1 activation,[238] which could be a part of the TORC1 activation mechanism. However, further experiments are needed to define how Pib2 interacts with TORC1 components or other TORC1 regulators. One potential model is that these residues are crucial for the interaction between Pib2 and TORC1 components needed for TORC1 reactivation. We were unable to reliably detect an interaction between Pib2 and Kog1 using yeast two-hybrid experiments, so potential effects of the helE mutations on this interaction could not be confirmed.

Previous studies have shown that truncations of the Pib2 N-terminus result in increased resistance to rapamycin exposure,[231,237] suggesting these regions have inhibitory effects on TORC1 reactivation. One study implicated Pib2 residues 1-50 in its inhibitory function.[237] Our results,

however, showed that regions A (residues 54-81) and B (residues 109-118) are required for this inhibitory role. We did not investigate the inhibitory role of residues 1-50, however, it is possible this discrepancy may be due to interactions between these residues and regions A and B or other intramolecular interactions. Deletion of regions C and D had no effect on TORC1 reactivation with the readouts used here. Pib2 MSAs showed fewer conserved residues in these regions compared to regions A and B so they might not be vital for this function (Appendix Figure 1A). Alternatively, regions C and D could play a role in LMP[240] or another Pib2 function that is yet to be discovered. Mutation of conserved residues within regions A and B highlighted a series of lysine and serine residues involved in the inhibitory mechanism. Based on our results and bioinformatic PTM predictions, the positive charge of the lysine residues and the phosphorylation status of the serine residues are likely part of this mechanism. Other groups have reported phosphorylation of Pib2 by the TORC1 downstream kinase Npr1[259,261] and there are several predicted phosphorylation sites within the Pib2 N-terminus which could affect its function (Appendix Figure 1A). One candidate kinase includes Cdk1, which has previously been shown to phosphorylate Pib2 at S113.[284] As the AlphaFold2 prediction shows, these N-terminal regions are found in low complexity sequence, which not only makes them more accessible and susceptible to PTMs but also protein-interactions which could play a role in TORC1 regulation. Further studies are needed to elucidate this inhibitory mechanism.

4.0 Pib2 subcellular localization effects on TORC1 activity

Select text and figures have been pulled from the following publication and have been adapted for flow and the inclusion of additional data:

K.K. Troutman, N.V. Varlakhanova, B.A. Tornabene, R. Ramachandran, and M.G.J. Ford. Conserved Pib2 regions have distinct roles in TORC1 regulation at the vacuole. *J Cell Sci* (2022) https://doi.org/10.1242/jcs.259994

4.1 Introduction

Protein localization plays a significant role in its function, and the proper subcellular localization of proteins is vital for the appropriate regulation of cellular processes. There are several localization signals that a protein can have. The subcellular distribution of an individual protein is then dependent on which signals it contains, the strength of those signals, and protein concentration.[285] Some examples of protein localization signals include targeting sequences, such as nuclear localization sequences, post-translational modifications (PTMs), lipid modifications, protein binding domains, and lipid binding domains, such as the FYVE domain previously discussed.[285] These signals can also be used as tools to artificially modulate protein localization.

TORC1 and Pib2 localize to vacuolar and endosomal membranes.[28,240] As described above, proper localization of Pib2 is dependent on its FYVE domain and helE region (Figure 2.2). The localization of TORC1 is vital for its activity. It has been shown that TORC1 activity at the vacuole promotes protein synthesis and cell growth via phosphorylation of Sch9,[26,28] whereas endosomal

TORC1 activity inhibits autophagy through phosphorylation of Atg13 and Vps27.[28] However, the role of specific TORC1 regulators at these subcellular locations is unclear.

As Pib2 is found at both the vacuolar membrane and endosomes, we set out to investigate how cellular localization of Pib2 affects TORC1 reactivation. Here, we use endosomal and vacuolar targeting constructs to identify the role of Pib2 at these subcellular localizations. Using these chimeric constructs, we show that endosomal Pib2 is not sufficient for TORC1 reactivation and cell growth. Furthermore, we show that vacuolar localization of Pib2 is essential for cell growth and recovery following rapamycin exposure. We previously demonstrated that Pib2 does not influence the repressive function of TORC1 on autophagy[234] (Figure 3.2A,B) and thus the effects on autophagy were not assessed.

4.2 Results

4.2.1 Generation and validation of targeting constructs

To assess the role of Pib2 at different subcellular locations, we generated several chimeric Pib2 constructs targeted to either the vacuole or the endosome. These constructs consisted of a targeting protein linked to Pib2 via a yEGFP bridge (Figure 4.1A). Prior to TORC1 activity assays, localization of each construct was confirmed by confocal microscopy. Furthermore, we quantified total GFP fluorescence in cells expressing these constructs to confirm that all targeting constructs were expressed at similar levels (Figure 4.1B). This method was used due to concerns over differential western blotting transfer efficiencies of proteins of significantly different sizes. All constructs showed comparable fluorescence intensities (Figure 4.1B). As a control, we expressed

yEGFP alone, using a stronger promoter (*VPS1*). As expected, we observed elevated fluorescence from yEGFP alone compared to the constructs using *PIB2* and *MVP1* promoters (Figure 4.1B).

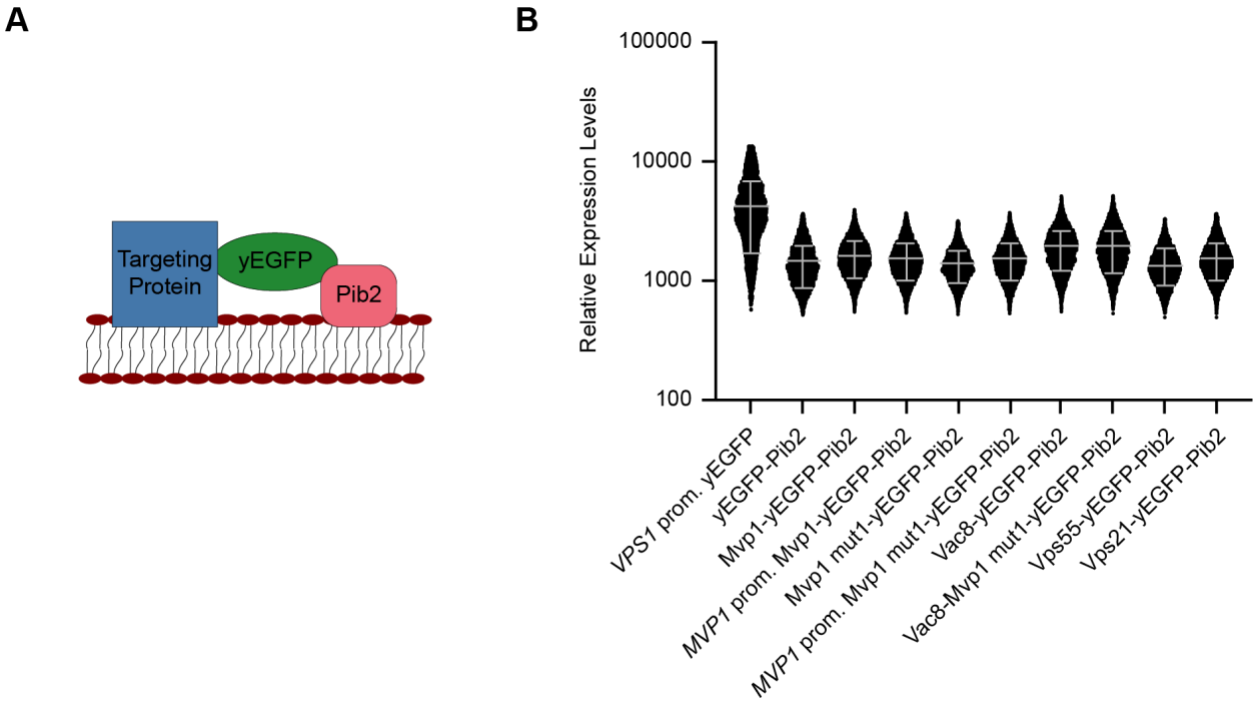

Figure 4.1 Pib2 vacuolar and endosomal targeting constructs A) Schematic of chimeric Pib2 vacuolar and endosomal targeting constructs. Each construct consists of the targeting protein and yEGFP fused to the N-terminus of Pib2. B) Quantification (mean±s.d.) of protein expression of targeting constructs based on total GFP fluorescence detected in individual cells normalized to cell area. 6102-9463 cells were quantified in each case. All constructs have a *PIB2* promoter unless otherwise specified.

4.2.2 First generation targeting constructs

Our initial targeting constructs utilized the yeast proteins Vac8 and Mvp1. To target Pib2 specifically to the vacuole we used Vac8, which is localized to the vacuole through N-terminal lipid modifications (myristoylation and palmitoylation)[286] and has been shown to interact with the TORC1 component Tco89.[287] To target Pib2 specifically to endosomes we used the yeast SNX-

BAR (sorting nexin family - Bin/Amphiphysin/RVS), Mvp1, which uses its PX and BAR domains to specifically bind endosomal membranes, which are enriched in PI3P.[288] The Vac8-yEGFP-Pib2 construct localized to the vacuolar membrane with scarce endosomal puncta (Figure 4.2A,B). In contrast, the Mvp1-yEGFP-Pib2 construct localized primarily to endosomal puncta with minimal vacuolar localization (Figure 4.2A,B).

Using these targeting constructs, we used rapamycin exposure assays to determine the ability of Pib2 to reactivate TORC1 and promote cell growth from these different subcellular localizations. In response to these rapamycin exposure assays, Δ*pib2* cells containing Vac8-yEGFP-Pib2 were able to mediate growth on rapamycin-containing plates and recovery from rapamycin exposure, as expected (Figure 4.2C). Growth of Δ*pib2* cells containing Mvp1-yEGFP-Pib2, however, was significantly compromised in response to rapamycin exposure (Figure 4.2C). Since Pib2 has been suggested to be a glutamine sensor,[235,237,238] we additionally assessed cell growth after nutrient starvation and stimulation with glutamine using phosphorylation of Rps6 at S232/S233 as a readout of TORC1 activity.[289] We demonstrated that the endosomal Mvp1-yEGFP-Pib2 construct is deficient in reactivating TORC1 signaling following nitrogen starvation and glutamine stimulation compared to the vacuolar Vac8-yEGFP-Pib2 construct and wild-type Pib2 (Figure 4.2D,E). Glutamine is a preferred nitrogen source in yeast and has been shown to result in both a rapid, transient activation of TORC1 and a sustained TORC1 activation that is independent of the Gtrs.[244] The Vac8-yEGFP-Pib2 construct was slower to respond to glutamine than wild-type Pib2, exhibiting sustained TORC1 activity, as determined from phosphorylation of Rps6 at 30 minutes, but not the rapid activation seen at 5 minutes (Figure 4.2D,E). Rps6 is an indirect effector of TORC1, it is phosphorylated by the direct TORC1 substrate Ypk3.[172,289] As only vacuolar

localization of Pib2 resulted in Rps6 phosphorylation, this might suggest that Ypk3 is a substrate of vacuolar TORC1.

Further, we generated an Mvp1 mutant targeting construct, which will be referred to as Mvp1 mut1. We have previously shown that this mutation results in cytosolic localization of Mvp1 as it is PI3P-binding-deficient.[288] This mutation allowed for the regions and domains of Pib2 to direct the localization of the construct and resulted in a subcellular distribution much closer to that of wild-type Pib2 (Figure 4.2A,B). However, this construct was still unable to promote rapamycin recovery (Figure 4.2C).

Since both Mvp1 and Mvp1 mut1 are known to multimerize (tetramer and dimer, respectively),[288] we reasoned that this may preclude Pib2 from mediating reactivation of TORC1. The cells used for these experiments contain endogenous Mvp1, which is able to multimerize with both wild-type Mvp1 and Mvp1 mut1,[288] which could confound Pib2 function in these experiments. As such, we generated an additional Mvp1 chimeric construct: Vac8-Mvp1 mut1-yEGFP-Pib2. We reasoned that the addition of a vacuole targeted protein could override the targeting of Mvp1 and allow us to assess the functionality of Pib2 in these constructs. Vac8-Mvp1 mut1-yEGFP-Pib2 showed a similar distribution to wild-type Pib2 with a largely vacuolar distribution and occasional puncta (Figure 4.2A,B). Vac8-Mvp1 mut1-yEGFP-Pib2 was able to support rapamycin growth and recovery, however at a slower rate than that observed in W303A cells or Δ*pib2* cells expressing wild-type Pib2 (Figure 4.2C). This reduced growth rate might be due to the influence of endogenous Mvp1, however since relocalization of Pib2 to the vacuole promotes partial recovery, Pib2 activity is not compromised in this construct.

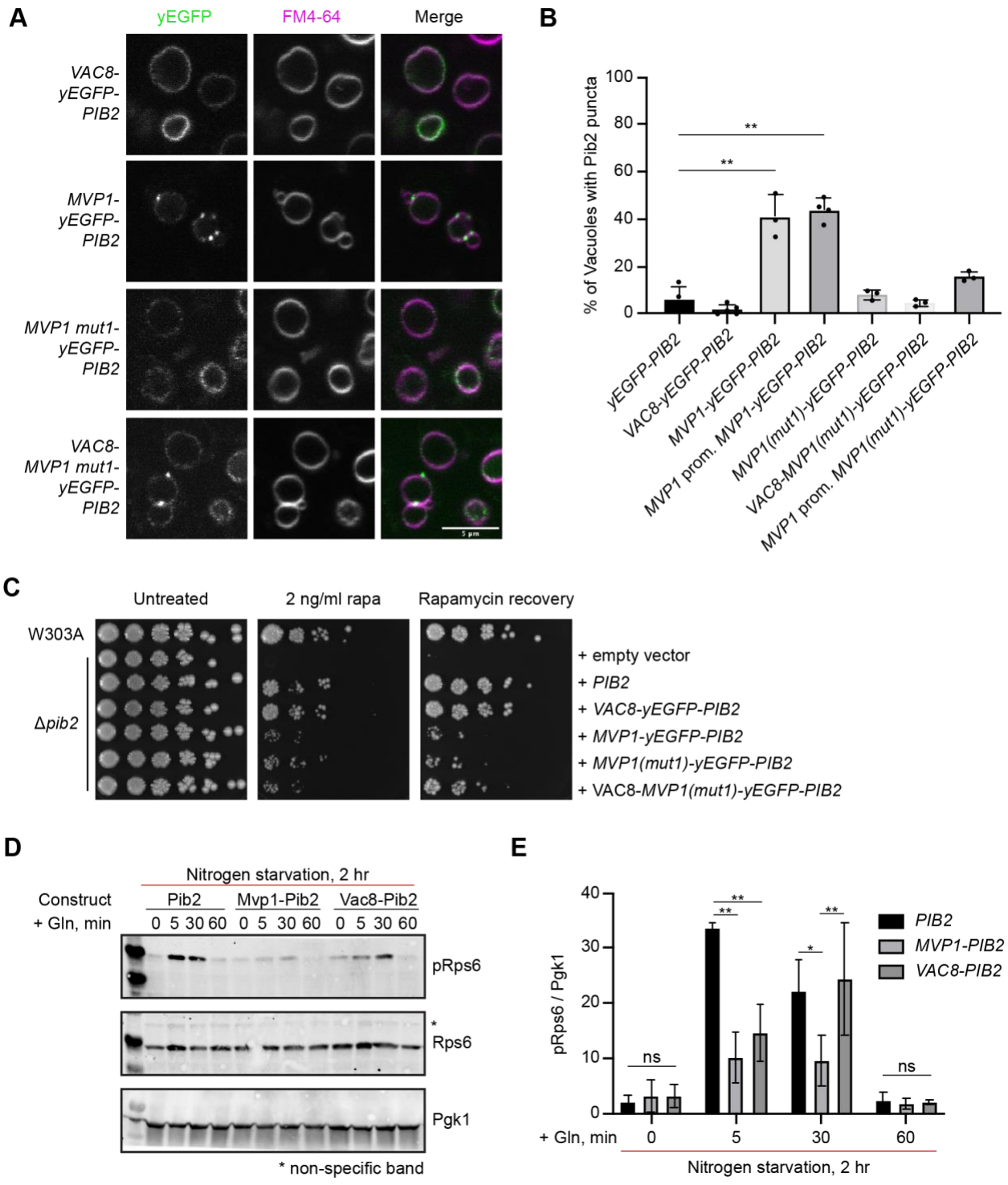

Figure 4.2 First generation targeting constructs A) Localization of the indicated targeting constructs. Vacuoles were stained with FM4-64. B) Quantification (mean±s.d.), from z-stack images, of the percentage of vacuoles containing Pib2 puncta in Δ*pib2* cells expressing the indicated constructs. Differences were assessed by one-way ANOVA ($F=56.70$, $P < 0.0001$). Significant differences from yEGFP-Pib2 as determined by Tukey post-hoc multiple

comparisons are noted (**p<0.0001). C) Rapamycin exposure and recovery assays of Δ*pib2* cells expressing the indicated targeting constructs. These were performed as in **Figure 3.1**. D) Representative western blot from a glutamine response assay (n=4). Cells were nitrogen starved for 2 hr in SD -N. For stimulation, cells were treated with SD -N supplemented with 3 mM glutamine and incubated for indicated times prior to lysis. TORC1 activation was assessed by phosphorylation of Rps6 under the indicated conditions. Total Rps6 and Pgk1 are shown as loading controls. E) Quantification of D (mean±s.d.; n=4). Values were normalized to the corresponding Pgk1 loading control. Differences were assessed by two-way ANOVA (P<0.0001). Differences between constructs at each time point as determined by Tukey post-hoc multiple comparisons are indicated (*P=0.0007, ** P<0.0001).

4.2.3 Second generation targeting constructs

To address the concerns and functionality of Pib2 associated with the endosomal Mvp1 constructs, we generated two additional constructs to assess localized TORC1 reactivation: Vps55-yEGFP-Pib2, and Vps21-yEGFP-Pib2. Vps21 (vacuolar protein sorting 21) is involved in transporting proteins to the vacuole[290] and is localized to endosomes by a C-terminal lipidation.[291] Although Vps21 itself is endosomal, fusions to its C-terminus affect the lipidation required for its membrane association and were therefore deliberate to determine the effects on Pib2 localization of a nonfunctional protein. Accordingly, as previously observed, Vps21-yEGFP is cytosolic (Figure 4.3A).[292] By contrast, like wild-type Pib2, Vps21-yEGFP-Pib2 localized to the vacuole with few perivacuolar puncta (Figure 4.3B,C). Hence, Pib2 can direct localization of this chimeric construct. Vps55, an integral membrane protein involved in endosome to vacuole trafficking localizes at endosomes (Figure 4.3A).[293–295] Based on a topology analysis of Leptin receptor gene related protein and Leptin receptor overlapping transcript-like 1 (LEPROT and LEPROTL1; also known as endospanin-1 and endospanin-2, respectively),[296] close human homologs of Vps55, both the N- and C-terminus of Vps55 are cytosolic. Hence, Pib2 remains in the cytosol in this targeting

construct. The Vps55-yEGFP-Pib2 construct localized primarily to perivacuolar puncta with less vacuolar presence (Figure 4.3B,C). Like the Mvp1-yEGFP-Pib2 construct, the endosomal Vps55-yEGFP-Pib2 construct was unable to rescue growth in the rapamycin exposure assays (Figure 4.3D). The wild-type-like Vps21-yEGFP-Pib2 construct however, was able to rescue growth in these assays, demonstrating that the N-terminal addition of this protein does not affect Pib2 activity (Figure 4.3D). Together, these data suggest that vacuolar Pib2 is necessary for the reactivation of TORC1 and resumed cell growth following rapamycin exposure.

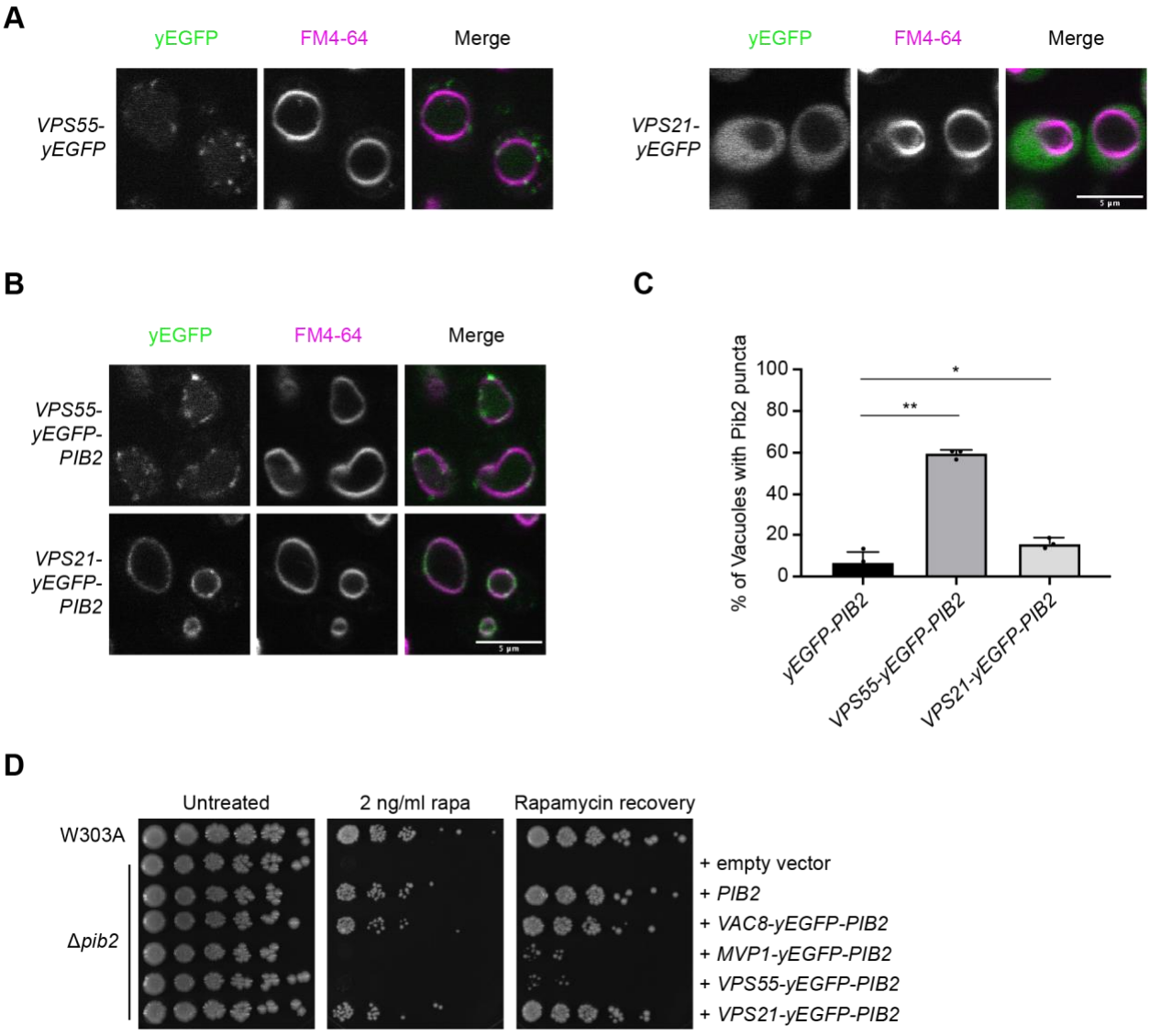

Figure 4.3 Second generation targeting constructs A) Localization of indicated yEGFP-tagged proteins. Vacuoles were stained with FM4-64. B) Localization of the indicated targeting constructs. Vacuoles were stained with FM4-64. C) Quantification (mean±s.d.), from z-stack images, of the percentage of vacuoles containing Pib2 puncta in Δ*pib2* cells expressing the indicated constructs. Data for yEGFP-Pib2 is the same as in **Figure 4.2**. Differences were assessed by one-way ANOVA ($F=168.5$, $P < 0.0001$). Significant differences from yEGFP-Pib2 as determined by Tukey post-hoc multiple comparisons are noted (*$p=0.0351$, **$p<0.0001$). D) Rapamycin exposure and recovery assays of Δ*pib2* cells expressing the indicated targeting constructs. These were performed as in **Figure 3.1**.

4.2.4 Pib2 vacuolar localization is essential for TORC1 reactivation and cell growth

To determine whether vacuolar localization of Pib2 was sufficient for TORC1 reactivation, we incorporated two of the previously described Pib2 mutations, Pib2 VLR and Pib2 WD, into the Vac8-yEGFP-Pib2 construct. As expected, due to the presence of Vac8, these mutants localized to the vacuole (Figure 4.4A,B). The Vac8-yEGFP-Pib2 WD mutant was able to rescue growth under rapamycin exposure conditions just as well as the wild-type Vac8-yEGFP-Pib2 construct (Figure 4.4C). As vacuolar localization of the Pib2 WD mutant with this targeting construct was able to rescue growth rate, this suggests that vacuolar localization of Pib2 is necessary for TORC1 reactivation in these conditions. The Vac8-yEGFP-Pib2 VLR mutant, however, was still unable to rescue growth (Figure 4.4C). These results support the hypothesis that these VLR residues within the helE region of Pib2 are essential for TORC1 reactivation and might be involved in glutamine sensing[238] and/or direct interactions with TORC1 components. Overall, these results demonstrate that vacuolar localization of Pib2 is necessary but not sufficient for TORC1 reactivation following rapamycin exposure in vivo.

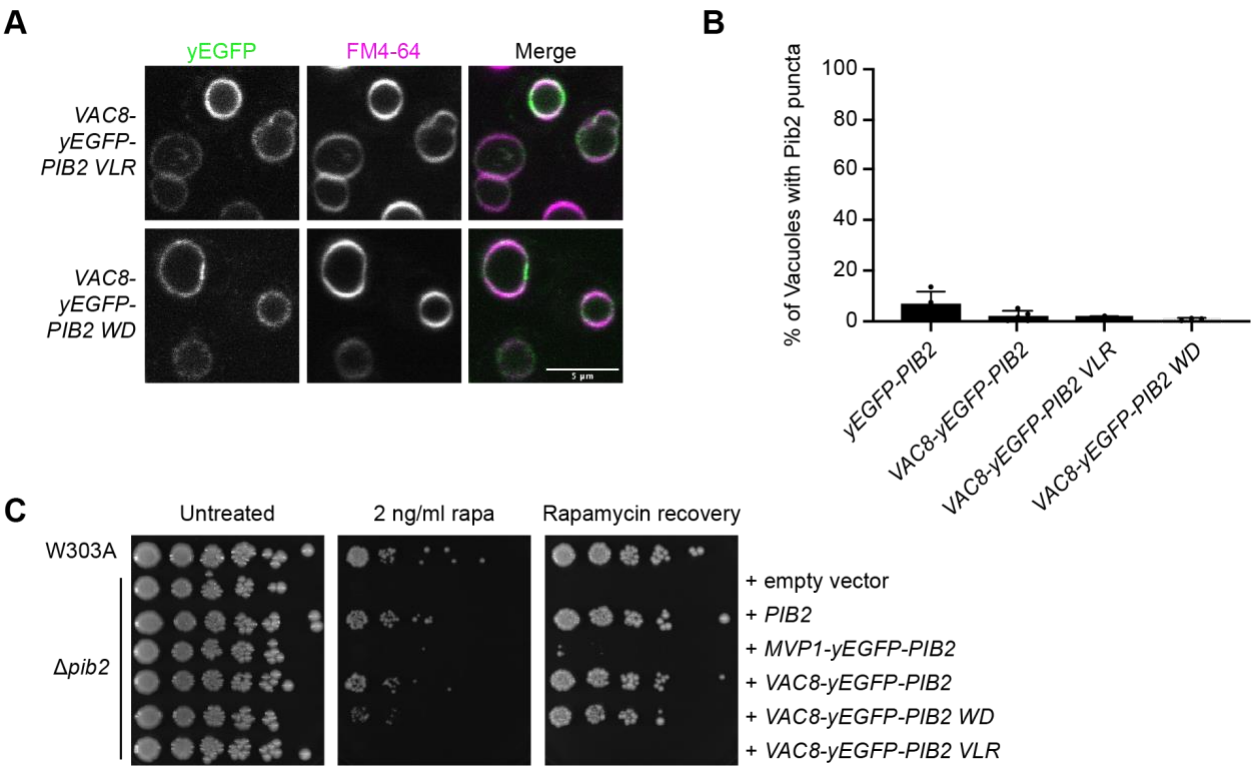

Figure 4.4 Vacuolar localization of Pib2 is essential for TORC1 reactivation A) Localization of the indicated targeting constructs. Vacuoles were stained with FM4-64. B) Quantification (mean±s.d.), from z-stack images, of the percentage of vacuoles containing Pib2 puncta in Δ*pib2* cells expressing the indicated constructs. Differences were assessed by one-way ANOVA (F=2.911, P=0.0822). Data for yEGFP-Pib2 and Vac8-yEGFP-Pib2 are the same as in **Figure 4.2**. There were no significant differences from yEGFP-Pib2 as determined by Tukey post-hoc multiple comparisons. C) Rapamycin exposure and recovery assays of Δ*pib2* cells expressing the indicated targeting constructs. These were performed as in **Figure 3.1**.

4.3 Discussion

Subcellular localization is a key aspect of TORC1 regulation and activity.[28,218,219] Here, we used endosomal and vacuolar targeting constructs to identify the role of Pib2 in TORC1 reactivation at these subcellular localizations. The Mvp1-yEGFP-Pib2 and Vps55-yEGFP-Pib2

constructs, which have an endosomal distribution, showed that endosomal Pib2 is not sufficient for TORC1 reactivation and cell growth. Furthermore, vacuolar targeting with the Vac8-yEGFP-Pib2 WD construct rescued the growth deficit seen with the largely cytosolic Pib2 WD mutant. This suggests vacuolar localization of Pib2 is essential for cell growth and recovery following rapamycin exposure. This proposed role of vacuolar Pib2 in reactivating TORC1 and promoting cell growth is in keeping with the role of vacuolar TORC1 in promoting cell growth through phosphorylation of Sch9.[26,28] Although vacuolar localization of Pib2 appears to be essential for cell growth following rapamycin exposure, it is not sufficient to promote TORC1 activity. The helE region PLY and VLR mutants, which maintain vacuolar localization of Pib2, still did not support TORC1 reactivation (Figure 4.4C). This implies that other interactions at the vacuolar membrane are necessary for Pib2 to reactivate TORC1. As previously noted, the helE region is part of the putative binding region for interactions with Kog1 and Tor1.[231,232,235,237] Thus, these helE residues, PLY and VLR, might be involved in interactions with TORC1 components that are required for TORC1 activation at the vacuole.

As endosomal Pib2 is not sufficient for TORC1 reactivation and cell growth, and Pib2 does not seem to influence autophagy regulation, its role remains unclear. One possibility, which was briefly mentioned earlier, is that endosomal localization may serve as an additional aspect of TORC1 regulation. The sequestration of Pib2 at endosomes may be a method of reducing TORC1 activity in certain conditions. In log phase cells, Pib2 endosomal puncta do not appear in every cell. Future experiments could investigate the dynamics of endosomal Pib2 and how different growth conditions (i.e., log phase, stationary phase, starvation, etc.) affect the number of Pib2 puncta and flux of Pib2 between the vacuole and endosomes.

5.0 Discussion and Perspectives

5.1 Study Synopses

In this work we describe how different conserved regions within the Pib2 sequence contribute to its function in TORC1 regulation with emphasis on the following:

1. N-terminal regions of Pib2 inhibit TORC1 activity
2. C-terminal regions of Pib2 control Pib2 localization and activation of TORC1
3. Pib2 vacuolar localization is essential for TORC1 reactivation and cell growth

5.1.1 N-terminal regions of Pib2 inhibit TORC1 activity

N-terminal regions of Pib2 have previously been shown to be involved in the TORC1 inhibitory function of Pib2. Large truncations of the protein, varying from removal of residues 1-50 to residues 1-164 have displayed an improved ability to activate TORC1.[231,237] In this work, we have highlighted two essential regions, and key residues within them, that are responsible for this inhibitory action of Pib2. Pib2 regions A (residues 54-81) and B (residues 109-118) have shown to be crucial to the inhibitory mechanism. The lysine residues in region A (lysines 59-61) and the positive charge that they provide is a major aspect of the ability of Pib2 to inhibit TORC1 activity. Within region B, serines 113 and 118, and their phosphorylation status, also play a decisive role in coordinating the inhibitory function of Pib2. While more work needs to be done to determine the precise mechanism as to how Pib2 inhibits TORC1, it is clear that these residues contribute to this function of Pib2.

5.1.2 C-terminal regions of Pib2 control Pib2 localization and activation of TORC1

C-terminal regions of Pib2 have been demonstrated to be involved in the localization and reactivation of TORC1. We demonstrate here that the Pib2 helical E region (residues 298-418) and FYVE domain (residues 442-533) are essential for the vacuolar localization of Pib2 (Figure 2.2). It has been shown previously that the FYVE domain is necessary for vacuolar localization and this localization is dependent on PI3P and the kinase, Vps34.[240] Here, we show that both the Pib2 FYVE domain and helE region are needed for vacuolar localization (Figure 2.2, Figure 2.3). Pib2 FYVE domain targeting to the vacuole is dependent on an interaction with PI3P as demonstrated by the cytosolic distribution of Pib2 mutants with PI3P binding-motif mutations (Figure 2.3) and ITC binding experiments between the purified Pib2 FYVE domain and a short chain PI3P or lipid head group (Figure 2.4, Table 2.1). The Pib2 FYVE domain also influences TORC1 reactivation, although less so than other C-terminal regions. We hypothesize that the reduced concentration of Pib2 at the vacuole in the Pib2 ΔFYVE mutant results in the decreased rate of growth observed with this mutant compared to wild-type Pib2 in the rapamycin exposure assays.

It has previously been demonstrated that the E region and tail motif are vital for TORC1 reactivation following rapamycin exposure.[231,237,240] The helE region is the predicted Kog1-binding region[231,232] and its deletion results in the cytosolic distribution of Pib2. We identified several conserved residues in this region that show sensitivity to rapamycin. We demonstrated that Pib2 residues 339VLR341 and 333PLY335 are essential for TORC1 reactivation and cell growth (Figure 3.6A). In a recent study, R341 was demonstrated to be involved in the glutamine dependent interaction with TORC1.[238] We hypothesize that the other residues in this region are also involved in this proposed interaction that is necessary for Pib2-dependent TORC1 reactivation. While the investigated helE mutations showed increased rapamycin sensitivity, none of them were coupled

with the Pib2 mislocalization that we see with the helE deletion strain (Figure 2.3). Thus, the mechanism by which the Pib2 helE region mediates vacuolar localization remains unclear.

5.1.3 Pib2 vacuolar localization is essential for TORC1 reactivation and cell growth

Proper subcellular localization is essential for the appropriate function of proteins throughout the cell. Here, we explored the role of vacuolar Pib2 on the reactivation of TORC1. Using chimeric vacuolar and endosomal targeting constructs, we found that endosomal Pib2 is not able to promote TORC1 reactivation and cell growth (Figure 4.2, Figure 4.3), which is consistent with recent work showing that vacuolar TORC1 is the point of cell growth activity.[28] We also demonstrate that vacuolar localization of Pib2 is necessary but not sufficient for reactivating TORC1 in these cell growth assays (Figure 4.4). A vacuolar targeting construct containing the Pib2 VLR mutation, is still sensitive to rapamycin, whereas a vacuolar targeting construct containing the Pib2 WD mutation is able to rescue both the cytosolic distribution and slow TORC1 reactivation and cell growth rate of that mutant alone (Figure 4.4). Combined, these data suggest that vacuolar localization of Pib2 is essential, however, other interactions at the vacuole need to occur for TORC1 reactivation and cell growth.

5.2 Limitations

There are some limitations to the scope of the conclusions from this work that provide avenues for further experimentation and should be considered. Limitations related to the yeast strain and growth conditions need to be accounted for. The experiments in this work were done

with haploid cells. Based on our results, no conclusions can be drawn on how diploid cells would respond in these experiments; starvation of diploid cells could just trigger sporulation. We also grew our cells in a glucose rich media, so they were not forced to use their mitochondria for respiration. Thus, we cannot draw conclusions about how respiration might affect these experiments. Temperature variations can also affect cell growth; as most of these experiments were performed at 30°C, it remains unclear how Pib2 regulation of TORC1 may be affected by temperature. In this work, we used the *Saccharomyces cerevisiae* strain, W303, which is derived from the strain, S288c.[297] W303 is the primary strain used in studying membrane trafficking and has the following auxotrophies: adenine, tryptophan, leucine, and histidine. These auxotrophies can result in confounding effects due to the need of amino acid supplementation for growth. While many plasmids convert strains to prototrophic, there are still differences in the expression of the complementing gene, and this can affect the details of signaling pathways. The additional use of prototrophic strains would be beneficial in validating these results. There are several lab strains of *S. cerevisiae* which each have several differences. A lot of signaling work has been done using the Σ1287b strain, which has established differences in detail for some signaling pathways compared to W303 or S288c due to genetic and epigenetic differences between strains.[298] A recent example depicting differences between lab strains is in the characterization of the VINE complex.[299] In this work, the authors characterized a protein, Vlr1, that is mutated and non-functional in many lab strains of yeast that have been used for trafficking studies, including W303.[299] They identify Vlr1 as a SNX-BAR protein which forms a complex that plays an important role in forming endosomal coats and sorting cargo proteins that they suggest may work alongside other similar pathways.[299]

5.3 Future Directions

There are several questions that remain surrounding Pib2 and its mechanism of action. I will discuss some of these questions and additional avenues of experimentation below.

1. How does the Pib2 helical E region mediate vacuolar localization?

   The Pib2 helical E region plays a role in both vacuolar localization of Pib2 and the reactivation of TORC1. However, it remains unclear what aspect of the helE region promotes its localization to the vacuole. One possibility is that the Pib2 interaction with TORC1 components help to anchor it to the vacuole. A potential way to investigate this would be to assess Pib2 localization in cells lacking TORC1 components, particularly Kog1. There are other possibilities to consider, including the presence of a lipid binding motif or interactions with a vacuolar membrane-associated protein. A further investigation of Pib2 binding partners could help to define this.

2. What proteins does Pib2 interact with?

   Pib2 has been shown to interact with Tor1, Kog1, and Gtr1 via the helical E region;[231,232,235–237] however, these interactions were shown by pull-downs and yeast two-hybrid experiments, thus they may have missed some weaker interactions. Transient interaction partners could be determined using BioID or similar methods which biotinylate nearby proteins.[300,301] In addition, the Pib2 tail motif has been demonstrated to interact with TORC1 and has been suggested to do so after the helical E region, and in a glutamine dependent manner, to complete Pib2-mediated TORC1 activation.[238] Several hyperactive tail mutants have been described[238] and a further investigation of these could help to define the interaction sites and binding partners, as well as the dependence on other interactions. These tail mutations may result in conformational changes of the TORC1 complex that

result in hyperactivation. There are several known hyperactive Tor1 mutants, such as L2134M, that affect the Tor1 kinase domain.[302,303] It is possible that these Pib2 tail motif mutations may interact with Tor1 near the kinase domain to similarly cause hyperactivation.

3. What is Pib2 doing at the endosome?

   As previously shown[28,240] and as described here (Figure 2.2), Pib2 localizes to both vacuolar and endosomal membranes. We show here that vacuolar Pib2 is needed for the reactivation of TORC1 after rapamycin exposure (Figure 4.4), however, it is still unclear what the role of Pib2 is at endosomes. Pib2 does not influence autophagy (Figure 3.2A,B), so it seems unlikely that endosomal Pib2 regulates autophagy at this pool of TORC1. However, this altered localization could be a regulatory mechanism in which, under certain conditions, Pib2 is moved away from the vacuole to provide fine-tuning of TORC1 activity. Assessing the dynamics of Pib2 at the endosomal membrane could provide some insight into what it is doing there. Different growth conditions, such as log phase, stationary phase, or starvation, could affect the number of Pib2 puncta and flux of Pib2 between the vacuole and endosomes. Live-cell imaging using FRAP (fluorescence recovery after photobleaching)[304] or a photo-switchable fluorophore, like mOrange,[305] could be used to determine Pib2 dynamics under varying conditions.

4. How do Pib2 and the EGO complex coordinate to regulate TORC1?

   Whether Pib2 activates TORC1 via an EGO-dependent or EGO-independent process has been debated. Deletion of Pib2 in combination with EGO complex genes results in synthetic lethality, however, it is possible to generate both Δ*pib2* and Δ*gtr1*/*gtr2* strains independently.[240] This implies that under nutrient replete, unstressed conditions either

pathway is sufficient for TORC1 activity. However, neither Δ*pib2* or Δ*gtr1*/*gtr2* cells are able to recover from stressors like rapamycin, which suggests that both the Pib2 and Gtr pathways are required for TORC1 reactivation. This supports a model of dual-phase activation that has been suggested in which Pib2 and the Gtrs work cooperatively in some instances and independently in others to promote TORC1 activity.[280] Of note, amino acid-induced TORC1 activation has been shown to occur in two stages.[244] The first of these stages, acute activation, is a quick, transient activation of TORC1 that lasts for only a few minutes.[244] The second is a sustained activation which is slower to begin but is continuously maintained.[244] Future experiments could further investigate the timing of these events to further elucidate how Pib2 and the Gtrs work together.

Additional avenues of experimentation:

a. Pib2 structure:

A structural determination of Pib2 in complex with TORC1 would be beneficial to further understanding the mechanisms by which it regulates TORC1. Since the protein is predicted to be mostly unstructured, as shown in the AlphaFold2 model,[241] it would likely be difficult to determine a structure of Pib2 in isolation. However, a low-resolution structure of the partial TORC1 complex containing Tor1 and Kog1, the presumed Pib2 binding partner, has been previously determined using cryogenic electron microscopy (cryo-EM) (EMD-1361).[306] As Pib2 has been pulled down with the TORC1 complex, it is likely that the recombinant proteins could be purified for use in cryo-EM to determine the structure of the Pib2-Tor1-Kog1 complex. Determining the interaction sites between these proteins could provide further insights into binding regions and crucial residues. These conclusions could

then be validated by introducing mutations into these regions to confirm their importance in cells.

b. Pib2 in aging

Another interesting avenue to explore would be the role of Pib2 and other TORC1 regulators in the modulation of yeast lifespan. Yeast aging studies examine two aging processes: replicative life span (RLS) and chronological life span (CLS). RLS is defined by how many times a mother cell can divide before it dies[217,307] and CLS describes how long cells remain viable after they stop dividing.[217] Many mechanisms of aging that are evolutionarily conserved have been observed in both RLS and CLS assays.[217] These mechanisms implicate roles in aging for a wide range of proteins and pathways, including Tor1 and Sch9.[217] Inhibition of TORC1 and/or its downstream effector Sch9, has been shown to increase both RLS and CLS in yeast.[217,308–311] Due to its role in nutrient sensing, TORC1 inhibition is part of the mechanism which results in lifespan extension through caloric restriction, a method of reducing nutrient intake without malnutrition.[217] Changes in amino acid levels have also been shown to affect aging processes.[312] Glutamine[311] and Leucine,[313–315] which are important in TORC1 signaling, have both been shown to affect yeast lifespan in different ways. While it is clear that TORC1 itself and many of its downstream effectors play a variety of roles in modulating lifespan, it is unknown how TORC1 regulators and nutrient sensing play into these lifespan extension processes. As Pib2 is a glutamine sensor with a role in both activation and inhibition of TORC1, this could provide insights into how nutrient integration affects lifespan modulation.

5.4 Implications for mammals

TORC1 dysregulation is implicated in a variety of diseases including cancer, diabetes, and neurodegeneration. Understanding the regulation of this pathway is crucial for identifying therapeutics or bioengineering treatments for these diseases. While Pib2 plays a vital role in controlling TORC1 activity in *S. cerevisiae*, it does not have a true mammalian homolog. Pib2 shares some similarity with the mammalian proteins phafin1 and phafin2 and while they have been shown to be involved in processes at the lysosome,[240,316,317] neither of these proteins have been directly implicated in mTORC1 regulation. Phafin1 more closely resembles Pib2, as it has a similar tail motif,[240] however, expression of phafin1 in Δ*pib2* cells does not rescue the rapamycin sensitivity of the strain (See Appendix 3 for more detail). Even without the direct conservation of Pib2, learning how yeast integrate nutrient levels and stress signals will provide insight into these mechanisms in any system. Evolutionary divergence and the need of multicellular organisms to integrate extracellular signals, like growth factors, likely resulted in differences in TORC1 regulation mechanisms in yeast and mammals. In mammalian organisms, cell-to-cell signaling plays an important role in mTORC1 regulation. As Pib2 has two separable functions it is possible that in mammalian cells, two distinct proteins evolved to fulfill those roles. Further, in mammals, yeast can cause infections and disease. Thus, highlighting differences in the mechanisms of nutrient sensing and integration can provide unique targets for the treatment of yeast-caused ailments.

6.0 Materials and Methods

6.1 Multiple Sequence Alignments

Sequence alignments were made using MUSCLE[318] and Clustal Omega.[319] Alignments shown were formatted using the output of ESPRIPT 3.0[320] using the AlphaFold2 Pib2 prediction (PDB AF-P53191-F1-model_v1)[241] as an input for secondary structure assignments.

6.2 Protein Structure Images

All protein structure images were rendered using PyMOL.[321] The PDB IDs used are as follows: yeast TORC1 (5FYM),[39] mTORC1 (5H64),[40] Snf1 (2QLV),[96] AMPK (4CFH),[97] yeast GCN2 (1ZYC),[127] mammalian GCN2 (7QQ6),[128] PIB2 (AF-P53191-F1-model_v1),[241] EEA1 1287-1411 (1JOC),[268] and EEA1 1347-1411 (1HYI).[277]

6.3 Yeast Media

YPD (1% yeast extract, 2% peptone, 2% glucose, supplemented with L-tryptophan and adenine) was used for routine growth. Synthetic complete (SC; yeast nitrogen base, ammonium sulfate, 2% glucose, amino acids) or synthetic defined (SD; yeast nitrogen base, ammonium sulfate, 2% glucose, appropriate amino acid dropout) media were used as indicated prior to microscopy or to maintain plasmid selection. For sporulation, cells were successively cultured in

YPA (1% yeast extract, 2% peptone, 2% potassium acetate) and SPO (1% potassium acetate, 0.1% yeast extract, 0.05% glucose). For nitrogen starvation, cells were grown in SD–N (0.17% yeast nitrogen base without amino acids and ammonium sulfate, 2% glucose).

6.4 Genetic Methods

6.4.1 Yeast genetic manipulation

Yeast strains used in this work are listed in Table 6.1. W303A GFP-N10-*PIB2*::HIS3 (PY_262) was generated by complete replacement of the kanMX cassette in W303A Δ*pib2*::KAN (PY_126).[234] The replacement cassette, which includes ~40 nucleotide regions from the *PIB2* promoter and terminator sequences immediately upstream and downstream of the *PIB2* ATG and STOP codons to enable site-specific reintegration, was generated by splicing by overlap extension PCR using a GFP-N10-*PIB2* fragment amplified from pRS316 yEGFP-N10-*PIB2* + UTRs[234] and an ADH1 terminator-His3MX6 fragment, amplified from pFA6a-link-yEGFP-SpHIS5 (pKT0128).[200] The full-length replacement cassette was gel purified and transformed into PY_126. Cells were plated onto SD -HIS and incubated for 3 days at 30 °C. A mixture of recombinants was expected: replacement of the kan resistance gene by conversion into HIS prototrophy, without integration of GFP-N10-*PIB2* (due to recombination between the *Ashbya gossipii* TEF promoter and terminators sequences flanking the kanamycin resistance gene in Δ*pib2*::KAN and the *S pombe* his5 gene in the replacement cassette) and complete replacement of kanMX6 with the GFP-N10-*PIB2*::HIS replacement cassette, by recombination in the *PIB2* promoter and terminator regions. Colony PCR indicated about one-third of the resulting HIS prototrophs contained the GFP-N10-

PIB2 coding sequence at the correct genomic locus. Loss of kanamycin resistance was also verified. Candidate colonies were backcrossed to W303α and re-sporulated to ensure the expected pattern of segregation. The knock-in strain was further verified by sequencing, imaging, and functional assays.

W303A *PIB2*::KAN, W303A *PIB2* ΔA::KAN, W303A *PIB2* ΔB::KAN, and W303A *PIB2* ΔhelE::KAN were generated using a similar approach, but by complete replacement of the His3MX6 cassette in the Δ*pib2*::HIS3 strain (PY_128). The replacement cassettes were generated by splicing by overlap extension using the appropriate *PIB2* construct amplified from pRS316 *S cer*. *PIB2* + UTRs[234], pRS316 *S cer*. *PIB2* ΔA + UTRs, pRS316 *S cer*. *PIB2* ΔB + UTRs, pRS316 *S cer*. *PIB2* ΔhelE + UTRs and a ADH1 terminator-kanMX6 fragment amplified from pFA6a-link-yEGFP-KanR (pKT0127).[200] After verification of correct reintroduction of the appropriate *PIB2* sequence by sequencing and loss of HIS prototrophy, the strains were further validated after backcrossing to W303α and resporulation.

Table 6.1: Yeast strains used in this work

Strain	Genotype	Reference
W303A	*MAT***a**; *ade2-1; leu2-3, 112; his3-11,15; trp1-1; ura3-1; can1-100*	Thomas and Rothstein, 1989
W303α	*MAT*α; *ade2-1*; *leu2-3,112*; *his3-11,15*; *trp1-1*; *ura3-1*; *can1-100*	Thomas and Rothstein, 1989
PY_126	*MAT***a**; *ade2-1*; *leu2-3,112*; *his3-11,15*; *trp1-1*; *ura3-1*; *can1-100*; Δ*pib2*::KAN	Varlakhanova et al., 2017
PY_128	*MAT***a**; *ade2-1*; *leu2-3,112*; *his3-11,15*; *trp1-1*; *ura3-1*; *can1-100*; Δ*pib2*::*HIS3*	Troutman et al., 2022
PY_104	*MAT***a**; *ade2-1*; *leu2-3,112*; *his3-11,15*; *trp1-1*; *ura3-1*; *can1-100*; Δ*gtr1*::*HIS3*; Δ*gtr2*::KAN	Varlakhanova et al., 2017
PY_262	*MAT***a**; *ade2-1*; *leu2-3,112*; *his3-11,15*; *trp1-1*; *ura3-1*; *can1-100*; yEGFP-N10-*PIB2*::*HIS3*	Troutman et al., 2022
PY_270	*MAT***a**; *ade2-1*; *leu2-3,112*; *his3-11,15*; *trp1-1*; *ura3-1*; *can1-100*; *PIB2*::KAN	Troutman et al., 2022
PY_272	*MAT***a**; *ade2-1*; *leu2-3,112*; *his3-11,15*; *trp1-1*; *ura3-1*; *can1-100*; *PIB2* ΔB::KAN	Troutman et al., 2022

Strain	Genotype	Reference
PY_274	*MAT***a**; *ade2-1*; *leu2-3,112*; *his3-11,15*; *trp1-1*; *ura3-1*; *can1-100*; *PIB2* ΔA::KAN	Troutman et al., 2022
PY_282	*MAT***a**; *ade2-1*; *leu2-3,112*; *his3-11,15*; *trp1-1*; *ura3-1*; *can1-100*; Δ*pib2*::*HIS3; Δvps4*::KAN	Troutman et al., 2022
PY_284	*MAT***a**; *ade2-1*; *leu2-3,112*; *his3-11,15*; *trp1-1*; *ura3-1*; *can1-100*; *PIB2* ΔhelE::KAN	Troutman et al., 2022

6.4.2 Cloning

Plasmids used in this work are listed in Table 6.2. Pib2 mutant constructs were cloned by splicing by overlap extension (SOE) PCR at the site of the mutation using appropriate primers followed by Gibson assembly into the target vector. For Pib2 deletion constructs, the deleted regions were replaced with an AGAGA linker. N-terminal yEGFP-Pib2 constructs were generated with an N10 linker (NSSSNNNNNNNNNNLGIE). Targeting constructs were generated by amplification of the targeting protein from genomic DNA isolated from W303A/α diploids using the Yeast DNA Extraction kit (Thermo Scientific) or an existing plasmid. The targeting protein was then fused to the appropriate yEGFP-*PIB2* construct by SOE with a short linker between the targeting protein and yEGFP (GRRIPGLIN for *MVP1*-yEGFP constructs or GDGAGLIN for all others). These constructs also contain both the *PIB2* promoter (175 bp) and terminator (150 bp) and were fully assembled using Gibson assembly. All plasmids were verified by sanger and/or nanopore sequencing.

Table 6.2: Plasmds used in this study

Plasmid		Reference
S *cer*. *PIB2*	pRS316 S *cer*. *PIB2* + UTRs	Troutman et al., 2022
PIB2 ΔA	pRS316 *S cer*. *PIB2* del A (del 54-81) + UTRs	Troutman et al., 2022

Plasmid		Reference
PIB2 ΔB	pRS316 *S cer*. *PIB2* del B (del 109-118) + UTRs	Troutman et al., 2022
PIB2 ΔC	pRS316 *S cer*. *PIB2* del C (del 152-162) + UTRs	Troutman et al., 2022
PIB2 ΔD	pRS316 *S cer*. *PIB2* del D (del 205-219) + UTRs	Troutman et al., 2022
PIB2 ΔhelE	pRS316 *S cer*. *PIB2* del helE (del 298-418) + UTRs	Troutman et al., 2022
PIB2 ΔFYVE	pRS316 *S cer*. *PIB2* del FYVE (del 442-533) + UTRs	Troutman et al., 2022
PIB2 ΔTail	pRS316 *S cer*. *PIB2* del Tail (del 626-635) + UTRs	Troutman et al., 2022
yEGFP-*PIB2*	pRS316 yEGFP-N10-*S cer*. *PIB2* + UTRs	Varlakhanova et al., 2017
yEGFP-*PIB2* ΔA	pRS316 yEGFP-N10-*S cer*. *PIB2* del A (del 54-81) + UTRs	Troutman et al., 2022
yEGFP-*PIB2* ΔB	pRS316 yEGFP-N10-*S cer*. *PIB2* del B (del 109-118) + UTRs	Troutman et al., 2022
yEGFP-*PIB2* ΔC	pRS316 yEGFP-N10-*S cer*. *PIB2* del C (del 152-162) + UTRs	Troutman et al., 2022
yEGFP-*PIB2* ΔD	pRS316 yEGFP-N10-*S cer*. *PIB2* del D (del 205-219) + UTRs	Troutman et al., 2022
yEGFP-*PIB2* ΔhelE	pRS316 yEGFP-N10-*S cer*. *PIB2* del helE (del 298-418) + UTRs	Troutman et al., 2022
yEGFP-*PIB2* ΔFYVE	pRS316 yEGFP-N10-*S cer*. *PIB2* del FYVE (del 442-533) + UTRs	Troutman et al., 2022
yEGFP-*PIB2* ΔTail	pRS316 yEGFP-N10-*S cer*. *PIB2* del Tail (del 626-635) + UTRs	Troutman et al., 2022
PIB2 VLR	pRS316 *S cer*. *PIB2* 339VLR341->AAA + UTRs	Troutman et al., 2022
yEGFP-*PIB2* VLR	pRS316 yEGFP-N10-*S cer*. *PIB2* 339VLR341->AAA + UTRs	Troutman et al., 2022
PIB2 RQI	pRS316 S *cer*. *PIB2* 325RQI327->AAA + UTRs	Troutman et al., 2022
yEGFP-*PIB2 RQI*	pRS316 yEGFP-N10-S *cer*. *PIB2* 325RQI327->AAA + UTRs	Troutman et al., 2022
PIB2 PKK	pRS316 S *cer*. *PIB2* 330PKK332->AAA + UTRs	Troutman et al., 2022
yEGFP-*PIB2 PKK*	pRS316 yEGFP-N10-S *cer*. *PIB2* 330PKK332->AAA + UTRs	Troutman et al., 2022
PIB2 PLY	pRS316 S *cer*. *PIB2* 333PLY335->AAA + UTRs	Troutman et al., 2022
yEGFP-*PIB2 PLY*	pRS316 yEGFP-N10-S *cer*. *PIB2* 333PLY335->AAA + UTRs	Troutman et al., 2022
PIB2 PA	pRS316 S *cer*. *PIB2* P337A + UTRs	This work

Plasmid		Reference
yEGFP-*PIB2* PA	pRS316 yEGFP-N10-S *cer*. *PIB2* P337A + UTRs	This work
PIB2 PS	pRS316 S *cer*. *PIB2* P337S + UTRs	This work
yEGFP-PIB2 PS	pRS316 yEGFP-N10-S *cer*. *PIB2* P337S + UTRs	This work
PIB2 WD	pRS316 *S cer*. *PIB2* W449A, D452A + UTRs	Troutman et al., 2022
yEGFP-*PIB2* WD	pRS316 yEGFP-N10-*S cer*. *PIB2* W449A, D452A + UTRs	Troutman et al., 2022
PIB2 RHH	pRS316 *S cer*. *PIB2* R470A, H472A, H473A + UTRs	Troutman et al., 2022
yEGFP-*PIB2* RHH	pRS316 yEGFP-N10-*S cer*. *PIB2* R470A, H472A, H473A + UTRs	Troutman et al., 2022
yEGFP-*PIB2* ΔhelE ΔFYVE	pRS316 yEGFP-N10-*S cer*. *PIB2* del helE del FYVE + UTRs	Troutman et al., 2022
PIB2 KA	pRS316 *S cer*. *PIB2* 59KKK61->AAA + UTRs	Troutman et al., 2022
yEGFP-*PIB2* KA	pRS316 yEGFP-N10-*S cer*. *PIB2* 59KKK61->AAA + UTRs	Troutman et al., 2022
PIB2 KE	pRS316 *S cer*. *PIB2* 59KKK61->EEE + UTRs	Troutman et al., 2022
PIB2 KR	pRS316 *S cer*. *PIB2* 59KKK61->RRR + UTRs	Troutman et al., 2022
PIB2 4SA	pRS316 *S cer*. *PIB2* S73A, S76A, S77A, S79A + UTRs	This work
yEGFP-*PIB2* 4SA	pRS316 yEGFP-N10-*S cer*. *PIB2* S73A, S76A, S77A, S79A + UTRs	This work
PIB2 SA	pRS316 *S cer*. *PIB2* S113A, S118A + UTRs	Troutman et al., 2022
yEGFP-*PIB2* SA	pRS316 yEGFP-N10-*S cer*. *PIB2* S113A, S118A + UTRs	Troutman et al., 2022
PIB2 SE	pRS316 *S cer*. *PIB2* S113E, S118E + UTRs	Troutman et al., 2022
PIB2 QA	pRS316 *S cer*. *PIB2* Q109A, Q110A, Q112A + UTRs	This work
yEGFP-*PIB2* QA	pRS316 yEGFP-N10-*S cer*. *PIB2* Q109A, Q110A, Q112A + UTRs	This work
PIB2 PA	pRS316 *S cer*. *PIB2* P114A + UTRs	This work
yEGFP-*PIB2* PA	pRS316 yEGFP-N10-*S cer*. *PIB2* P114A + UTRs	This work
PIB2 KA SA	pRS316 *S cer*. *PIB2* 59KKK61->AAA, S113A, S118A + UTRs	Troutman et al., 2022
PIB2 KA SE	pRS316 *S cer*. *PIB2* 59KKK61->AAA, S113E, S118E + UTRs	Troutman et al., 2022

Plasmid		Reference
PIB2 KE SA	pRS316 *S cer*. *PIB2* 59KKK61->EEE, S113A, S118A + UTRs	Troutman et al., 2022
PIB2 KE SE	pRS316 *S cer*. *PIB2* 59KKK61->EEE, S113E, S118E + UTRs	Troutman et al., 2022
PIB2 ΔA ΔB	pRS316 *S cer*. *PIB2* del A (del 54-81) del B (del 109-118) + UTRs	This work
PIB2 ΔA-B	pRS316 *S cer*. *PIB2* del A-B (del 54-118) + UTRs	This work
PIB2 ΔA ΔhelE	pRS316 *S cer*. *PIB2* del A del helE + UTRs	Troutman et al., 2022
PIB2 KA ΔhelE	pRS316 *S cer*. *PIB2* 59KKK61->AAA, del helE + UTRs	This work
PIB2 ΔA VLR	pRS316 *S cer*. *PIB2* del A, 339VLR341->AAA + UTRs	This work
PIB2 ΔA ΔFYVE	pRS316 *S cer*. PIB2 del A del FYVE + UTRs	Troutman et al., 2022
PIB2 ΔA ΔTail	pRS316 *S c*er. *PIB2* del A del Tail + UTRs	Troutman et al., 2022
VAC8-yEGFP-*PIB2*	pRS316 *VAC8*-yEGFP-N10-*S cer*. *PIB2* + *PIB2* UTRs	Troutman et al., 2022
MVP1-yEGFP-*PIB2* + *PIB2* UTRs	pRS316 *S cer*. *MVP1*-yEGFP-N10-*S cer*. *PIB2* + *PIB2* UTRs	Troutman et al., 2022
MVP1(mut1)-yEGFP-*PIB2* + *PIB2* UTRs	pRS316 *S cer*. *MVP1*(198KRI200-AAA)-yEGFP-N10-*S cer*. *PIB2* + *PIB2* UTRs	Troutman et al., 2022
MVP1-yEGFP-PIB2 + *MVP1* UTRs	pRS316 *S cer*. *MVP1*-yEGFP-N10-*S cer*. *PIB2* + *MVP1* UTRs	Troutman et al., 2022
MVP1(mut1)-yEGFP-PIB2 + *MVP1* UTRs	pRS316 *S cer*. *MVP1*(198KRI200-AAA)-yEGFP-N10-*S cer*. *PIB2* + *MVP1* UTRs	Troutman et al., 2022
VAC8-MVP1(mut1)-yEGFP-*PIB2* + *PIB2* UTR*s*	pRS316 *S cer*. *VAC8-MVP1*(198KRI200-AAA)-yEGFP-N10-*S cer*. *PIB2* + *PIB2* UTRs	This work
VAC8-yEGFP-*PIB2* VLR	pRS316 *VAC8*-yEGFP-N10-*S cer*. *PIB2* 339VLR341->AAA + *PIB2* UTRs	Troutman et al., 2022
VAC8-yEGFP-*PIB2* WD	pRS316 *VAC8*-yEGFP-N10-*S cer*. *PIB2* W449A, D452A + *PIB2* UTRs	Troutman et al., 2022
VPS55-yEGFP-*PIB2*	pRS316 *S cer*. *VPS55*-yEGFP-10-*S cer*. *PIB2* + *PIB2* UTRs	Troutman et al., 2022
VPS21-yEGFP-*PIB2*	pRS316 *S cer*. *VPS21*-yEGFP-10-*S cer*. *PIB2* + *PIB2* UTRs	Troutman et al., 2022
PIB2 442-625	pET-15b *S cer*. *PIB2* 442-625	Troutman et al., 2022
PIB2 437-542	pET-15b *S cer*. *PIB2* 437-542	Troutman et al., 2022
PIB2 419-625	pET-15b S *cer*. *PIB2 419-625*	Troutman et al., 2022

Plasmid		Reference
EEA1 1287-1411	pET-15b His6-EEA1(FYVE) 1287-1411	Modified from Addgene #36096 (Burd and Emr, 1998)
EEA1 1347-1411	pET-15b His6-EEA1(FYVE) 1347-1411	Modified from Addgene #36096 (Burd and Emr, 1998)
GFP-*ATG8*	pRS314 GFP-*ATG8*	Modified from Addgene #49425 (Guan et al., 2001)

6.5 Growth analysis

Cells were grown overnight in YPD, SC, or SD with the appropriate dropout for plasmid maintenance. Cells were then diluted and regrown to mid-logarithmic phase [optical density at 600 nm (OD_{600}) of 0.5-0.8] in YPD at 30°C. Cells were diluted to 0.5 OD_{600}/ml and 1:5 serial dilutions were made in water. For each dilution, 2 µl was spotted onto the indicated plates. Where relevant, cells were incubated with 200 ng/ml of rapamycin (MP Biomedicals) in YPD at 30°C for the indicated times. After several washes the cells were resuspended in fresh YPD and plated on YPD. All plates were incubated at 30°C and imaged on days 2 and 3.

6.6 Microscopy

6.6.1 Preparation

Cells were grown overnight in YPD, SC, or the appropriate SD medium. Cells were diluted in YPD and grown to mid-logarithmic phase. Vacuolar membranes were stained with 10 µM FM4-64 (Thermo Fisher Scientific) in YPD for 1 hour, followed by washing and incubation in SC medium without dye for 1 hour. Cells were plated on No. 1.5 glass-bottomed cover dishes (MatTek Corporation, Ashland) treated with 15 µl 2 mg/ml concanavalin-A (Sigma-Aldrich).

6.6.2 Image acquisition and analysis

Confocal images were acquired on a Nikon (Melville, NY) A1 confocal microscope, with a 100x Plan Apo oil objective. NIS Elements imaging software was used to control image acquisition. Images were further process using the Fiji distribution of ImageJ.[322] GraphPad Prism was used for statistical analyses.

Vacuolar localization yEGFP-Pib2 constructs was quantified using Fiji. For each cell, vacuolar membrane and cytosolic ROIs of equal area were determined and the fluorescence within those ROIs was measured. FM4-64 fluorescence was used to determine the location of the vacuolar membrane ROIs. Within each image, an average background fluorescence was determined and subtracted from the vacuolar and cytosolic intensity measurements. The localization was then expressed as a ratio of vacuolar membrane fluorescence to cytosolic fluorescence. For statistical analyses, a ROUT outliers test (Q = 0.1%) was used and data were further assessed by one-way ANOVA with Tukey multiple comparisons.

To determine expression levels of targeting constructs, cells were imaged in widefield using a Nikon Ti Microscope with an S Plan Fluor ELWD 20x objective. NIS Elements imaging software was used to control image acquisition. Images were processed in NIS Elements imaging software using a custom macro. GraphPad Prism was used for statistical analyses.

6.7 Western Blotting

Yeast protein extracts were prepared as previously described.[323] Briefly, cells were lysed on ice by resuspension in 1 ml cold H_2O supplemented with 150 µl 1.85 M NaOH and 7.5% (v/v) β-mercaptoethanol. After a 10-minute incubation on ice, the protein was precipitated by addition of 150 µl 50% (w/v) trichloroacetic acid. Pellets were washed twice with acetone, resuspended in 100 µl 2x SDS-PAGE buffer, and boiled for 5 minutes at 95°C. Primary antibodies were incubated overnight at 4°C and were as follows: anti-GFP (1:1000, ab290, Abcam), anti-PGK1 (1:1000, ab113687, Abcam), anti-Rps6 (1:1000, ab40820, Abcam), anti-phosph-Rps6 (1:1000, 4858, Cell Signaling Technology, Danvers). Secondary antibodies were incubated for 1 hour at room temperature and were as follows: IRDye 680RD goat anti-rabbit-IgG antibody (926-68171, Li-Cor, Lincoln) and IRDye 680RD goat anti-mouse-IgG antibody (926-68070, Li-Cor). These were detected using the ChemiDoc MP Imaging System (Bio-Rad). Bands were integrated and quantified using Fiji.

6.8 SEC-MALS

After filtration through a 0.22 µm cellulose acetate membrane, the Pib2 FYVE constructs and mutants were subjected to size-exclusion chromatography using a Superdex 75 10/300 equilibrated in SEC-MALS buffer (20 mM Tris-HCl, pH 7.4, 150 mM NaCl, and 1.93 mM β-mercaptoethanol) at room temperature. 500 µl of each protein was loaded onto the column, at a concentration of 50 or 100 µM as indicated. The column was coupled to a static 18-angle light scattering detector (DAWN HELEOS-II) and a refractive index detector (Optilab T-rEX) (Wyatt Technology). Data were collected continuously at a flow rate of 0.3 ml/min, with the flow cells in the scattering and refractive index detectors set to 25°C. Data analysis was performed using the program Astra VII. Monomeric BSA (2.0 mg/ml) (Sigma) was used for data quality control.

6.9 ITC

ITC was used to determine the thermodynamics of the interaction of the Pib2 FYVE domain (using Pib2 442-625) with inositol 1,3 bisphosphate (Ins(1,3)P2) or short-chain PI3P. The titrations were performed at 25°C using a PEAQ-ITC instrument (Malvern Analytical), in 20 mM Tris-HCl pH 7.4, 150 mM NaCl, 1.93 mM β-mercaptoethanol. 4 mM Ins(1,3)P2 or 2 mM diC4 PI3P was titrated into 100-150 µM protein. Integrated peaks for each titration were fit to a single site binding model using the MicroCal PEAQ-ITC software provided by the manufacturer.

6.10 FYVE domain binding to PIP strip

PIP strips (Echelon Biosciences) were used to assess binding of purified FYVE domains to indicated lipids. Membrane was incubated for 1 hour at room temperature in Tris-buffered saline with 0.1% Tween 20 (TBST) plus 3% fatty-acid (FA) free BSA (Akron Biotechnology). The indicated concentration of protein in TBST plus 3% FA free BSA was incubated at room temperature for 1 hour. Membrane was washed three times in TBST plus 3% FA-free BSA for 10 minutes each between protein and antibody incubations. The primary antibody was incubated at 4°C overnight: rabbit anti-His6 (1:1000, ab137839, Abcam). The secondary antibody was incubated for 1 hour at room temperature: IRDye 680RD goat ant-rabbit-IgG antibody (926-68171, Li-Cor, Lincoln). Membranes were imaged using the ChemiDoc MP Imaging System (Bio-Rad).

Appendix A Supplemental Figures

Appendix A.1 Pib2 Sequences and Conservation

A

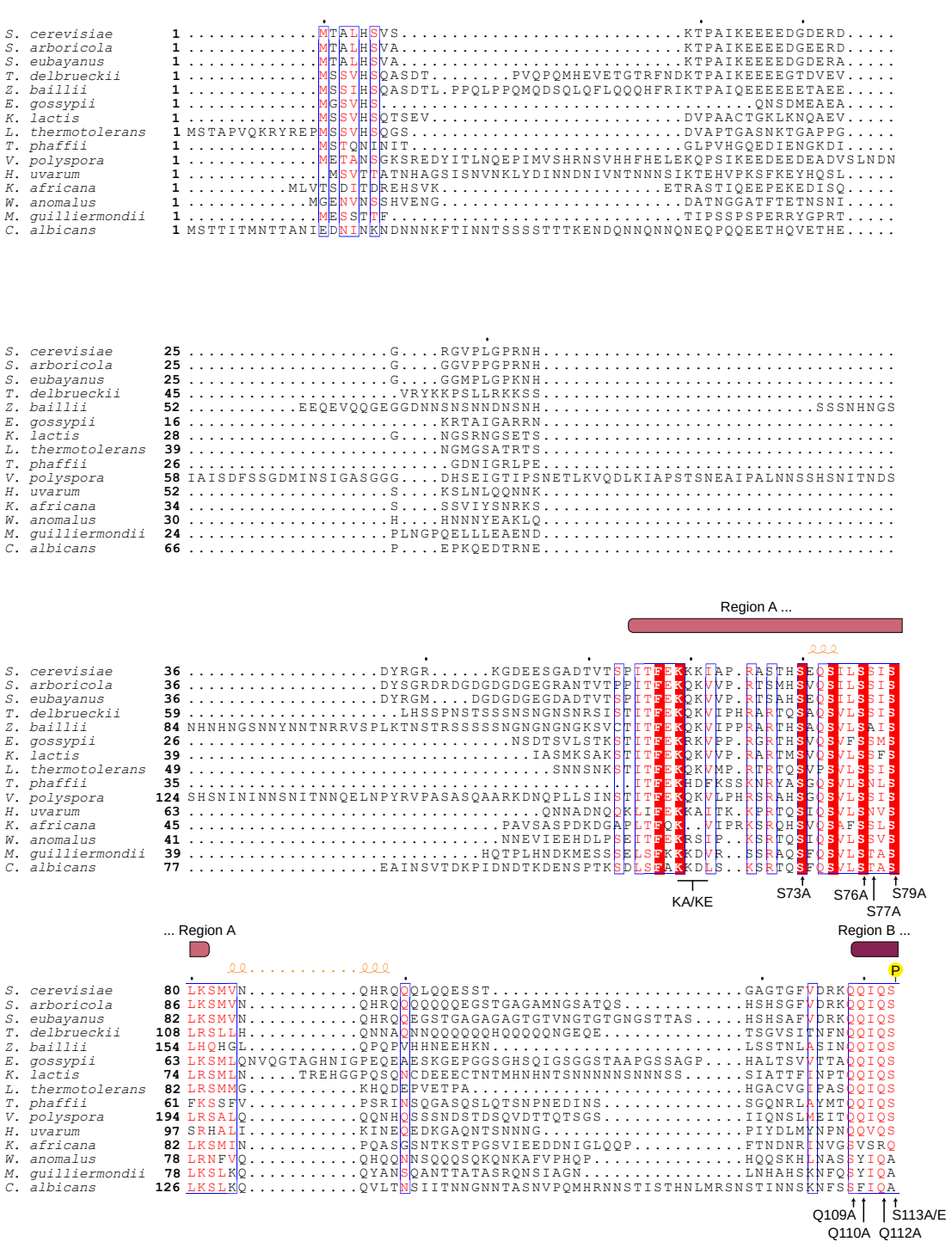
S. cerevisiae
S. arboricola
S. eubayanus
T. delbrueckii
Z. baillii
E. gossypii
K. lactis
L. thermotolerans
T. phaffii
V. polyspora
H. uvarum
K. africana
W. anomalus
M. guilliermondii
C. albicans
Region A ...
KA/KE
S73A
S76A
S77A
S79A
... Region A
Region B ...
P
Q109A
Q110A
Q112A
S113A/E


... Region B
Region C
P114A
S118A/E

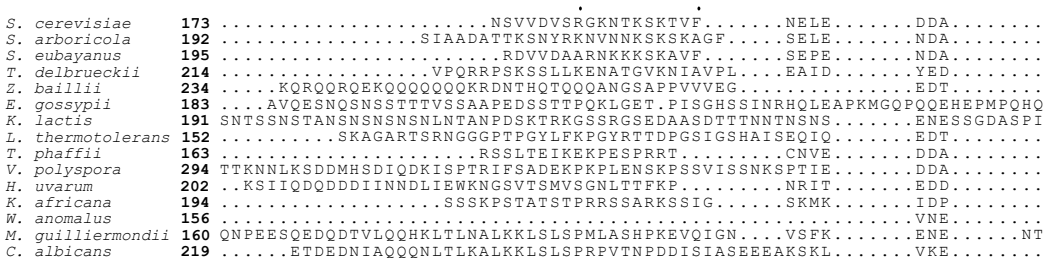

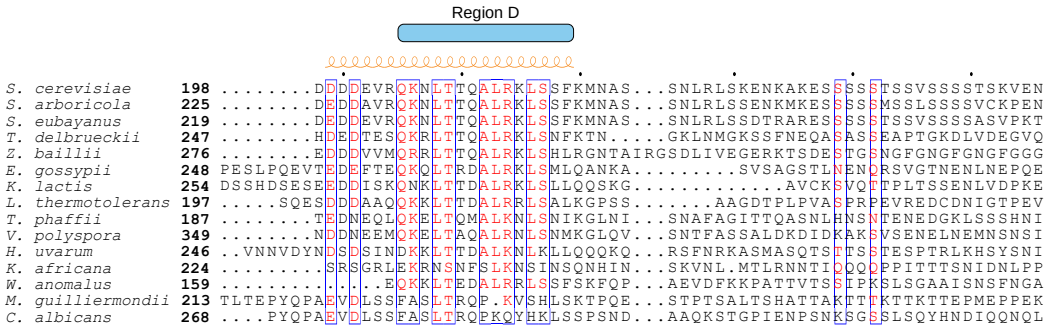
Region D

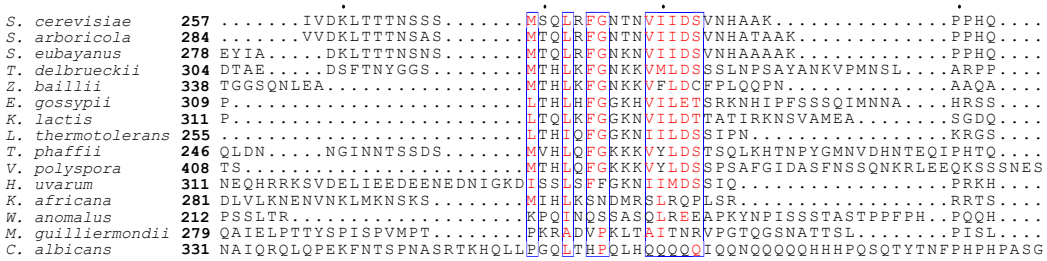

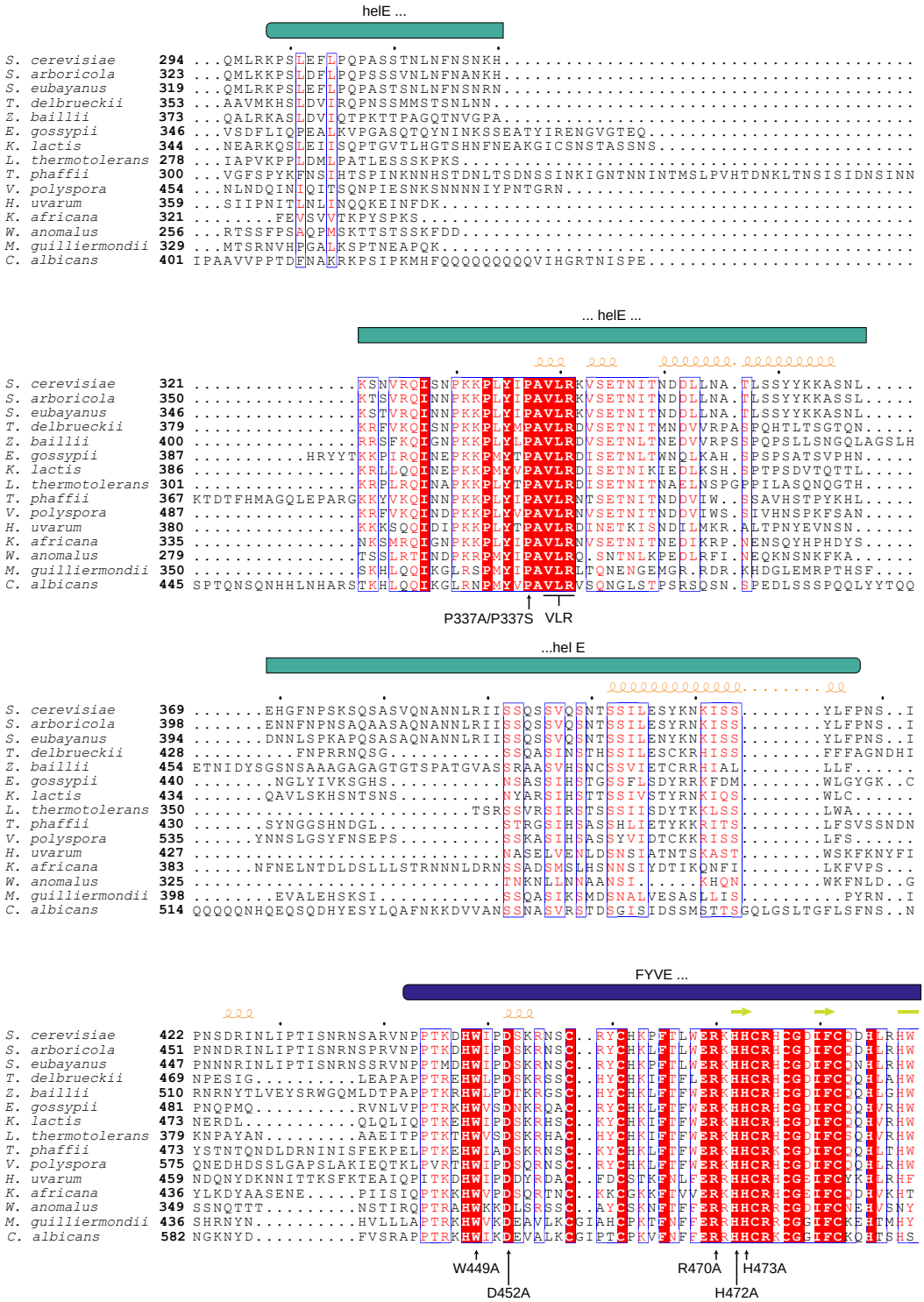
helE ...
... helE ...
P337A/P337S
VLR
...hel E
FYVE ...
W449A
D452A
R470A
H473A
H472A

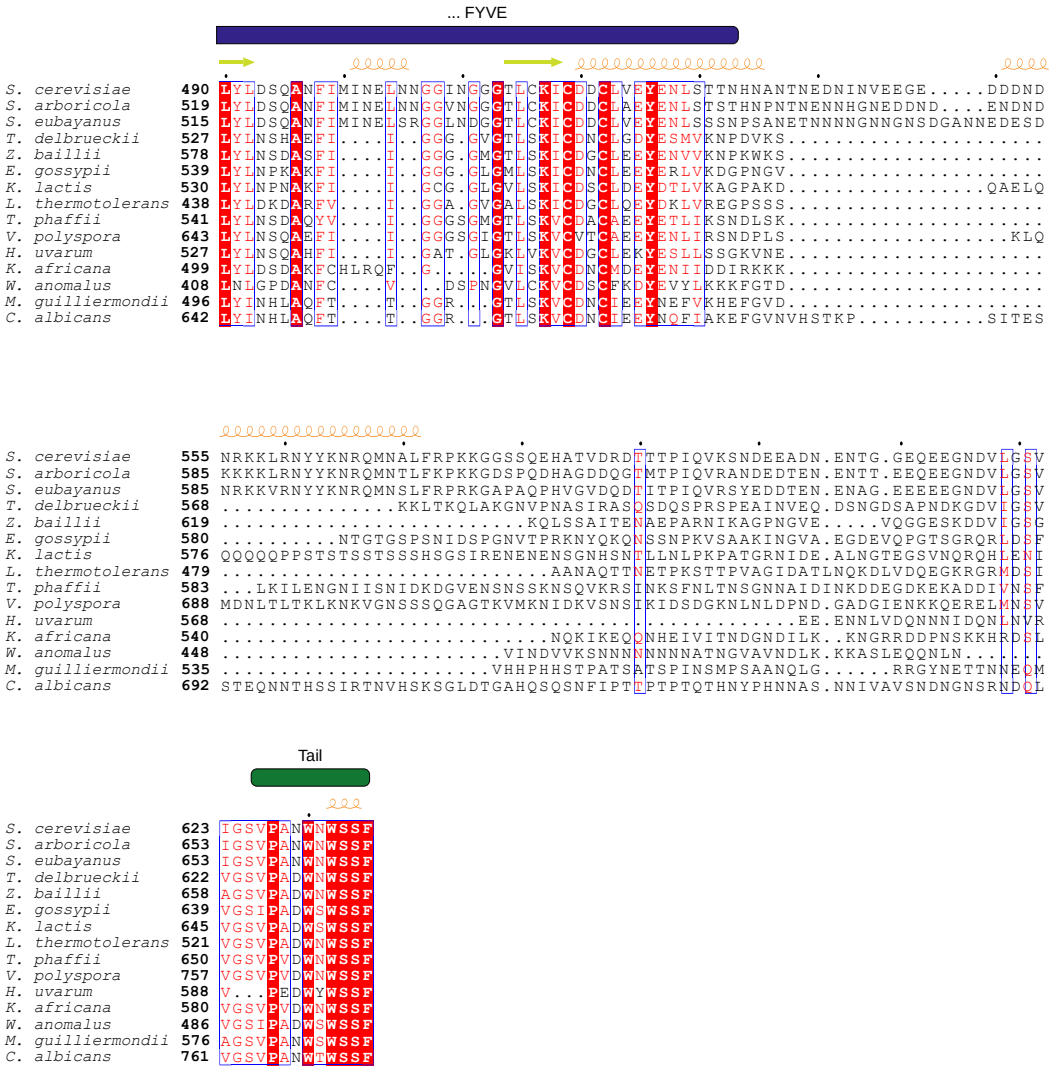
... FYVE
S. cerevisiae 490 LYLDSQANFIMINELNNGGINGGGTLCKLGDDCLVEYENLSTTNHNANTNEDNINVEEGE.....DDDND
S. arboricola 519 LYLDSQANFIMINELNNGGVNGGGTLCKIGDDCLAEYENLSTSTHNPNTNENNHGNEDDND....ENDND
S. eubayanus 515 LYLDSQANFIMINELSRGGLNDGGTLCKIGDDCLVEYENLSSSNPSANETNNNNGNNGNSDGANNEDESD
T. delbrueckii 527 LYLNSHAEFI....I..GGG.GVGTLSKIGDNCLGDYESMVKNPDVKS.....
Z. baillii 578 LYLNSDASFI....I..GGG.GMGTLSKLGDGCLEEYENVVKNPKWKS.....
E. gossypii 539 LYLNPKAKFI....I..GGG.GLGMLSKIGDNCLEEYERLVKDGPNGV.....
K. lactis 530 LYLNPNAKFI....I..GCG.GLGVLSKIGDSCLDEYDTLVKAGPAKD.....QAELQ
L. thermotolerans 438 LYLDKDARFV....I..GGA.GVGALSKIGDGCLQEWDKLVREGPSSS.....
T. phaffii 541 LYLNSDAQYV....I..GGGSGMGTLSKVGDACAEEYETLIKSNDLSK.....
V. polyspora 643 LYLNSQAEFI....I..GGGSGIGTLSKVGVTCAEEYENLIRSNDPLS.....KLQ
H. uvarum 527 LYLNSQAHFI....I..GAT.GLGKLVKVGDGCLEKYESLLSSGKVNE.....
K. africana 499 LYLDSDAKFCHLRQF..G.....GVISKVGDNCMDEYENIIDDIRKKK.....
W. anomalus 408 LNLGPDANFC....V....DSPNGVLCKVGDSCFKDYEVYLKKKFGTD.....
M. guilliermondii 496 LYINHLAQFT....T..GGR.....GTLSKVGDNCIEEYNEFVKHEFGVD.....
C. albicans 642 LYINHLAQFT....T..GGR.....GTLSKVGDNCIEEYNQFIAKEFGVNVHSTKP.....SITES
S. cerevisiae 555 NRKKLRNYYKNRQMNALFRPKKGGSSQEHATVDRDTTTPIQVKSNDEEADN.ENTG.GEQEEGNDVLGSV
S. arboricola 585 KKKKLRNYYKNRQMNTLFKPKKGDSPQDHAGDDQGTMTPIQVRANDEDTEN.ENTT.EEQEEGNDVLGSV
S. eubayanus 585 NRKKVRNYYKNRQMNSLFRPRKGAPAQPHVGVDQDTITPIQVRSYEDDTEN.ENAG.EEEEEGNDVLGSV
T. delbrueckii 568 .....KKLTKQLAKGNVPNASIRASQSDQSPRSPEAINVEQ.DSNGDSAPNDKGDVIGSV
Z. baillii 619 .....KQLSSAITENAEPARNIKAGPNGVE.....VQGGESKDDVIGSG
E. gossypii 580 .....NTGTGSPSNIDSPGNVTPRKNYQKQNSSNPKVSAAKINGVA.EGDEVQPGTSGRQRLDSF
K. lactis 576 QQQQQPPSTSTSSTSSSHSGSIRENENENSGNHSNTLLNLPKPATGRNIDE.ALNGTEGSVNQRQHLENI
L. thermotolerans 479 .....AANAQTTNETPKSTTPVAGIDATLNQKDLVDQEGKRGRMDSI
T. phaffii 583 ...LKILENGNIISNIDKDGVENSNSSKNSQVKRSINKSFNLTNSGNNAIDINKDDEGDKEKADDIVNSF
V. polyspora 688 MDNLTLTKLKNKVGNSSSQGAGTKVMKNIDKVSNSIKIDSDGKNLNLDPND.GADGIENKKQERELMNSV
H. uvarum 568 .....EE.ENNLVDQNNNIDQNLNVR
K. africana 540 .....NQKIKEQQNHEIVITNDGNDILK..KNGRRDDPNSKKHRDSL
W. anomalus 448 .....VINDVVKSNNNNNNNNATNGVAVNDLK.KKASLEQQNLN.....
M. guilliermondii 535 .....VHHPHHSTPATSATSPINSMPSAANQLG.....RRGYNETTNNEQM
C. albicans 692 STEQNNTHSSIRTNVHSKSGLDTGAHQSQSNFIPTTPTPTQTHNYPHNNAS.NNIVAVSNDNGNSRNDQL
Tail
S. cerevisiae 623 IGSVPANWNWSSF
S. arboricola 653 IGSVPANWNWSSF
S. eubayanus 653 IGSVPANWNWSSF
T. delbrueckii 622 VGSVPADWNWSSF
Z. baillii 658 AGSVPADWNWSSF
E. gossypii 639 VGSIPADWSWSSF
K. lactis 645 VGSVPADWSWSSF
L. thermotolerans 521 VGSVPADWNWSSF
T. phaffii 650 VGSVPVDWNWSSF
V. polyspora 757 VGSVPVDWNWSSF
H. uvarum 588 V...PEDWYWSSF
K. africana 580 VGSVPVDWNWSSF
W. anomalus 486 VGSIPADWSWSSF
M. guilliermondii 576 AGSVPANWSWSSF
C. albicans 761 VGSVPANWTWSSF

B

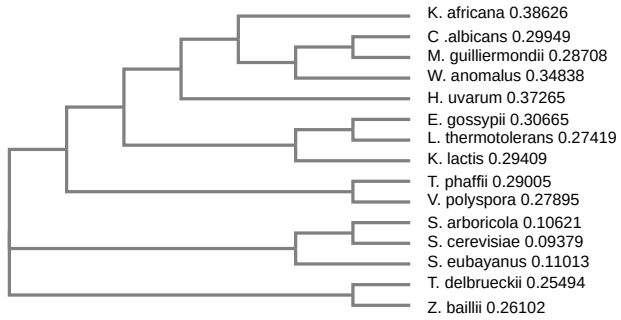
K. africana 0.38626
C .albicans 0.29949
M. guilliermondii 0.28708
W. anomalus 0.34838
H. uvarum 0.37265
E. gossypii 0.30665
L. thermotolerans 0.27419
K. lactis 0.29409
T. phaffii 0.29005
V. polyspora 0.27895
S. arboricola 0.10621
S. cerevisiae 0.09379
S. eubayanus 0.11013
T. delbrueckii 0.25494
Z. baillii 0.26102

Appendix Figure 1 - Pib2 Sequences A) Sequence alignment of ascomycete fungi Pib2 sequences. Conserved Pib2 regions are labeled as per the *S. cerevisiae* sequence. Identical residues are highlighted in red boxes. Residues with > 70% conservation are denoted by red font. AlphaFold2 predicted structural elements are indicated above the sequence with alpha-helices represented by orange loops and beta-sheets represented by green arrows. Key conserved residues are shown with arrows below the sequence. Predicted PTMs are shown above the sequence. The sequences used in this alignment are: *Kazachstania africana* (XP_003958048.1), *Hanseniaspora uvarum* (KKA03925.1), *Candida albicans* (KGU35957.1), *Meyerozyma guilliermondii* (XP_001484326.1), *Wickerhamomyces anomalus* (XP_019038326.1), *Tetrapisispora phaffii* (XP_003687734.1), *Vanderwaltozyma polyspora* (XP_001644984.1), *Eremothecium gossypii* (NP_986037.1), *Kluyveromyces lactis* (XP_452960.1), *Lachancea thermotolerans* (XP_002553804.1), *Saccharomyces arboricola* (EJS43738.1), *Saccharomyces cerevisiae* (NP_011492.3), *Saccharomyces eubayanus* (XP_018222201.1), *Torulaspora delbrueckii* (XP_003682272.1), *Zygosacharomyces bailli* (SJM87752.1). B) Cladogram of ascomycete species in A generated with sequence alignment. Scores shown to the right of the species name represent the evolutionary sequence distances.

Appendix B Technical Theory

Appendix B.1 Microscopy

Appendix B.1.1 Fluorescence microscopy and fluorophores

Fluorescence microscopy is dependent on the ability of a sample to absorb light of one wavelength and emit light of a longer wavelength. Molecules that are able to do this are termed fluorophores. When a fluorophore is hit with a photon of the right wavelength, the photon's energy is transferred to the fluorophore and the molecules exhibit changes in vibration and rotation.[324] If the energy is sufficient, it will move the electrons to an excited state.[324] To release the energy and return to the ground state, the molecules emit a photon with a longer wavelength.[324] This emitted photon is then sensed by the cameras used in fluorescent microscopy techniques.[324]

Fluorophores can be excited by and emit light over a range of wavelengths, these ranges are called the excitation and emission spectra, respectively.[324] Each of these spectra have a peak where the excitation and emission are most efficient and the difference between these peaks is called Stoke's shift.[324] Generally, a good fluorophore has a large Stoke's shift and narrow excitation and emission spectra.[324] These attributes are especially useful when imaging with multiple fluorophores. In this work we primarily used EGFP and FM4-64 for imaging experiments. The excitation and emission wavelengths of these fluorophores are shown in Appendix Table 1.

There are several nuances to consider when using fluorescence microscopy. When using multiple fluorophores in one sample, they need to be carefully selected to avoid overlap in their excitation and emission spectra which can result in bleed-through between the channels in the

resulting image.[324] Autofluorescence should also be considered when imaging certain samples. When imaging yeast, for example, the cells themselves and certain media can have autofluorescence which blur the signal from fluorophores. The standard nutrient replete yeast media, YPD, is highly autofluorescent, which is why in our experiments we imaged yeast cells in SC media. Further, while imaging, extended exposure of the sample to light can cause photobleaching which results in the fluorophores inability to produce fluorescence.[324,325]

Appendix Table 1: Exciation and emission wavelengths of select fluorophores

Fluorophore	Excitation Wavelength (nm)	Emission Wavelength (nm)
EGFP	488	507
FM4-64	515	640

Appendix B.1.2 - Confocal microscopy

In this work we used a Nikon A1 confocal microscope to collect live-cell images of yeast. Confocal microscopy is a light rejection fluorescence technique that demonstrates improved resolution over techniques like widefield microscopy. To accomplish the improved resolution, confocal microscopy makes use of point illumination, typically from a laser, and a pinhole that removes out of focus light. The excitation laser (of appropriate wavelength for the fluorophore in use) is directed to a dichroic mirror and then redirected by scanning mirrors to the objective lens and then to the sample.[326] The use of a laser as a light source is beneficial in that it only exposes a select portion of the sample to the light, limiting photobleaching damage to a small area.[326] The scanning mirrors adjust to redirect the laser to scan across the x,y-plane.[326] The emitted light from

the sample is directed back through the lens and mirrors to the pinhole aperture.[326] The pinhole allows light from the plane of focus to reach the photodetector and rejects light from outside of the plane of focus, resulting in a sharper image.[326] The photodetector then converts the detected light into electrical signals which are used to produce the image. The light path in a typical confocal is depicted in Appendix Figure 2.

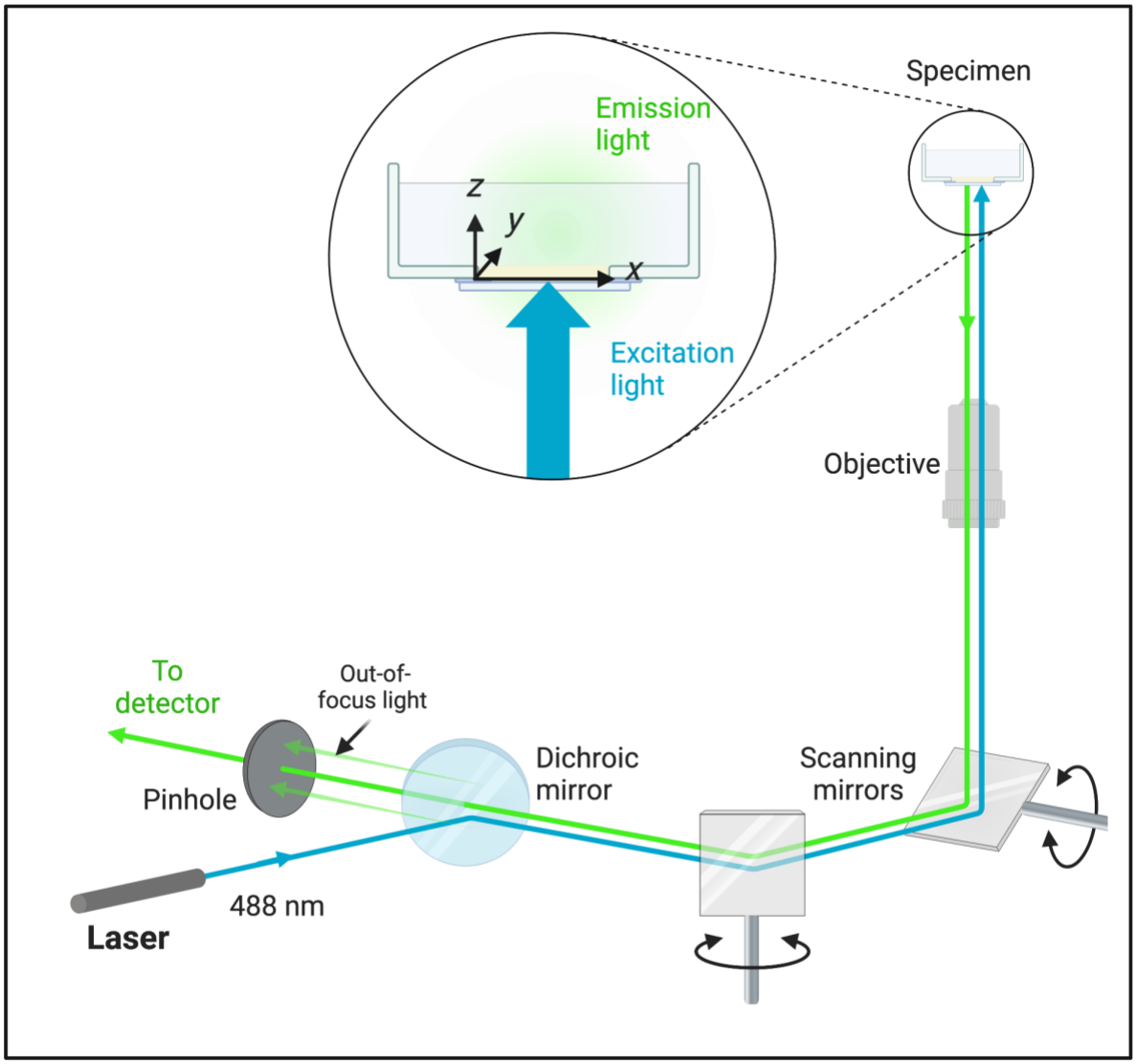

Appendix Figure 2 - Confocal Microscopy Diagram of confocal microscopy light path. Blue line represents the laser light used for exciation and the green line represents the emitted light. Out-of-focus light is represented by the

translucent green arrows blocked by the pinhole. Image adapted from "Laser Scanning Confocal Microscopy", by BioRender.com (2022). Retrieved from https://app.biorender.com/biorender-templates.

The resolution of a microscope can be determined using the properties of the point spread function. The point spread function is the diffraction pattern of light emitted from a point in the sample.[327] The constructive and destructive interference of the light waves result in a pattern of concentric rings around a central point called the Airy disk.[327] The size of the Airy disk is dependent on the wavelength of light and the numerical aperture (NA) of the objective lens.[327] The NA is critical in determining resolution; a large NA objective produces a smaller, more defined Airy disk which results better resolution.[327] The lateral and axial resolutions of a confocal system can be determined by the following equations:[326]

$$R_{lateral} = \frac{0.4\,\lambda}{NA}$$

$$R_{axial} = \frac{1.4\,\lambda\,\eta}{NA^2}$$

Lateral resolution ($R_{lateral}$) is related to the emission light wavelength (λ) and the numerical aperture (NA). Axial resolution (R_{axial}) is limited in confocal microscopy and in addition to dependency on λ and NA, it is further dependent on the refractive index (η).[326] Since emission wavelength influences resolution, resolution will vary depending on the fluorophore that is used. For our experiments we used a 100x plan apo oil objective lens with an NA of 1.4 and the immersion oil used has a refractive index of 1.51. So, using EGFP with this setup, the lateral resolution would be 145 nm and the axial resolution would be 545 nm, as shown below.

$$R_{lateral\_GFP} = \frac{0.4 \times 507}{1.4} \approx 145\,nm$$

$$R_{axial\_GFP} = \frac{1.4 \times 507 \times 1.51}{1.4^2} \approx 545\,nm$$

Appendix C Preliminary Results - Phafins

Appendix C.1 Introduction

Pib2 has been investigated as a relative of the mammalian proteins LAPF and EAPF (lysosome-associated apoptosis-inducing protein containing PH and FYVE domains and endoplasmic reticulum-associated apoptosis-involved protein containing PH and FYVE domains), also known as phafin1 and phafin2, respectively (Appendix Figure 3). Phafin1 has been found to promote lysosomal membrane permeabilization (LMP) in mammalian cell lines.[240] Phafin1 has also been shown to promote autophagy.[328] Phafin1 and phafin2 contain a PH-domain and FYVE domain, and phafin1 also has a C-terminal tail motif which is similar to that of Pib2.[240] Pib2 has shown to utilize its FYVE domain and tail motif to promote LMP through TORC1 activation in yeast exposed to ER stressors.[240] Due to these similarities, we sought to determine if phafin1 could rescue rapamycin sensitivity in Δ*pib2* cells.

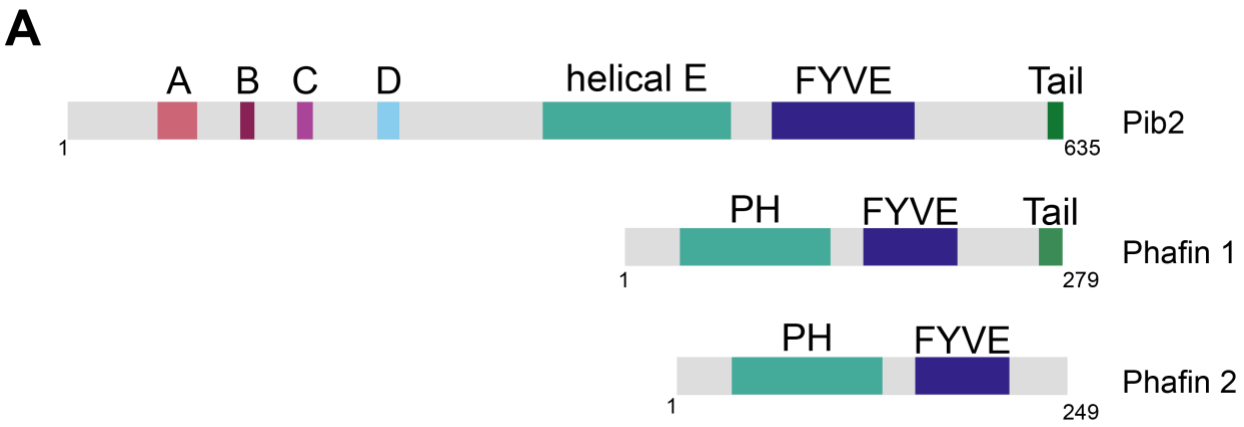

Appendix Figure 3 - Pib2 and the mammalian phafin proteins A) Comparison of Pib2 and the mammalian phafin proteins. Note all proteins contain a C-terminal FYVE domain and Pib2 and phafin1 share a similar tail motif.

Appendix C.2 Results

To investigate whether phafin1 can rescue the rapamycin sensitivity of Δ*pib2* cells, we expressed phafin1 in Δ*pib2* cells with the native *PIB2* promoter. Cells expressing phafin1 were not able to rescue the rapamycin sensitivity phenotype (Appendix Figure 4A). Since Pib2 does not have a PH domain like phafin1, we created a chimeric phafin1 protein which contained the helical E region of Pib2 in place of the phafin1 PH domain (Pib2 residues 298-418 in place of phafin1 residues 7-131). This chimeric protein localized to the vacuole but was still unable to rescue the rapamycin sensitivity phenotype (Appendix Figure 4).

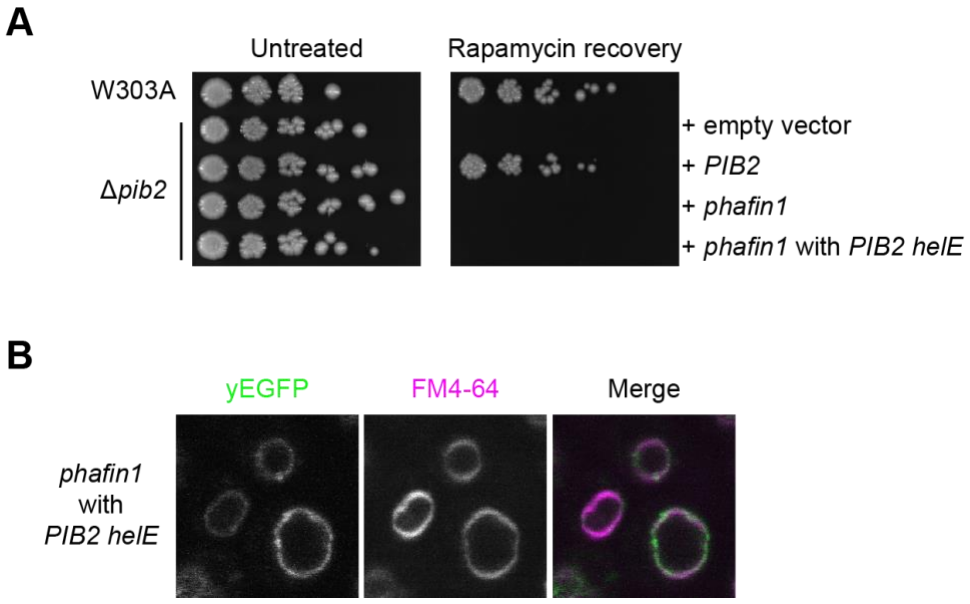

Appendix Figure 4 - Phafin1 does not rescue Pib2 deletion A) Representative rapamycin recovery assay of Δ*pib2* cells expressing the indicated constructs. These were performed as in **Figure 3.1**. B) Localization of the indicated phafin1 construct. Vacuoles were stained with FM4-64.

Appendix C.3 Discussion

Here we used chimeric proteins to explore whether the mammalian phafin1 protein can rescue the rapamycin phenotype of Δ*pib2* cells. Rapamycin exposure assays showed that phafin1 is unable to rescue the rapamycin sensitive phenotype of Δ*pib2* cells. Using the Pib2 helical E region in place of the phafin1 PH region also did not rescue the phenotype. Phafin1 has not been implicated in the regulation of mammalian TORC1 activity, however it has shown to be involved in LMP like Pib2. Beyond this, the role of Phafin proteins in mammals is not well defined and thus its similarity to Pib2 may be related to a function other than TORC1 regulation. It is also possible that the phafin1 tail motif is not similar enough to Pib2 to promote TORC1 reactivation in yeast.

Appendix C.4 Methods

Appendix C.4.1 Yeast media

YPD (1% yeast extract, 2% peptone, 2% glucose, supplemented with L-tryptophan and adenine) was used for routine growth. Synthetic complete (SC; yeast nitrogen base, ammonium sulfate, 2% glucose, amino acids) or synthetic defined (SD; yeast nitrogen base, ammonium sulfate, 2% glucose, appropriate amino acid dropout) media were used as indicated prior to microscopy or to maintain plasmid selection.

Appendix C.4.2 Cloning

Pib2/Phafin1 chimeric constructs were cloned by splicing by overlap extension (SOE) PCR using appropriate primers followed by Gibson assembly into the target vector. These constructs also contain both the *PIB2* promoter (175 bp) and terminator (150 bp) and were fully assembled using Gibson assembly. All plasmids were verified by sanger sequencing.

Appendix C.4.3 Growth assays

Cells were grown overnight in YPD, SC, or SD with the appropriate dropout for plasmid maintenance. Cells were then diluted and regrown to mid-logarithmic phase [optical density at 600 nm (OD_{600}) of 0.5-0.8] in YPD at 30°C. Cells were diluted to 0.5 OD_{600}/ml and 1:5 serial dilutions were made in water. For each dilution, 2 µl was spotted onto the indicated plates. Where relevant, cells were incubated with 200 ng/ml of rapamycin (MP Biomedicals) in YPD at 30°C for the indicated times. After several washes the cells were resuspended in fresh YPD and plated on YPD. All plates were incubated at 30°C and imaged on days 2 and 3.

Appendix C.4.4 Microscopy

Cells were grown overnight in YPD, SC, or the appropriate SD medium. Cells were diluted in YPD and grown to mid-logarithmic phase. Vacuolar membranes were stained with 10 µM FM4-64 (Thermo Fisher Scientific) in YPD for 1 hour, followed by washing and incubation in SC medium without dye for 1 hour. Cells were plated on No. 1.5 glass-bottomed cover dishes (MatTek Corporation, Ashland) treated with 15 µl 2 mg/ml concanavalin-A (Sigma-Aldrich). Confocal

images were acquired on a Nikon (Melville, NY) A1 confocal microscope, with a 100x Plan Apo oil objective. NIS Elements imaging software was used to control image acquisition. Images were further process using the Fiji distribution of ImageJ.[322]

Appendix D Aridor Lab Experiments

In addition to my work on Pib2, I have performed some experiments for the Aridor Lab to help investigate the relationship between lipid homeostasis and protein degradation pathways. A brief introduction and summary of my results, independently of the other data the Aridor Lab has collected, is discussed below.

Appendix D.1 Introduction & Results

Proteostasis is the maintenance of protein biosynthesis, folding, and degradation processes necessary for proper cell function. When these processes are dysregulated, it can cause a variety of issues in the cell. Proteostasis dysregulation is implicated in a number of diseases, particularly in neurodegeneration. The Aridor Lab is investigating how lipid homeostasis and protein degradation pathways, such as ERAD (endoplasmic reticulum-associated degradation) and UPR (unfolded protein response), are related. The accumulation of cholesterol in the lysosome and late endosomes has been shown to occur in response to the accumulation of misfolded proteins in the ER.[329–333] In yeast, the accumulation of vacuolar sterols supports μ-lipophagy of lipid droplets.[334,335]

Some proteins of interest in assessing the links between μ-lipophagy and protein degradation are the yeast VAP (vesicle-associated membrane protein (VAMP) – associated proteins) proteins, Scs2 and Scs22, an Scs2 interacting protein, Yet1, and UPR associated proteins, Ire1 and Hac1. VAP proteins are involved in membrane contact sites and lipid exchange between

the ER and organellar membranes and have been demonstrated to couple cholesterol homeostasis with ER protein degradation.[329,336] Yet1 interacts with Scs2 and helps control lipid synthesis.[337] Ire1 and Hac1 are involved in UPR.[338–341] These proteins were knocked-out to develop the following strains: Δ*scs2*Δ*scs22*, Δ*yet1*, Δ*ire1*, and Δ*hac1*. To assess how ER protein misfolding regulates lipid homeostasis, we overexpressed a well characterized ERAD substrate, Ste6*.[342] As a control for previous experiments, I assessed growth of these strains on YPD plates and the expression of Ste6* in these knock out strains does not influence their growth on nutrient replete media (Appendix Figure 5).

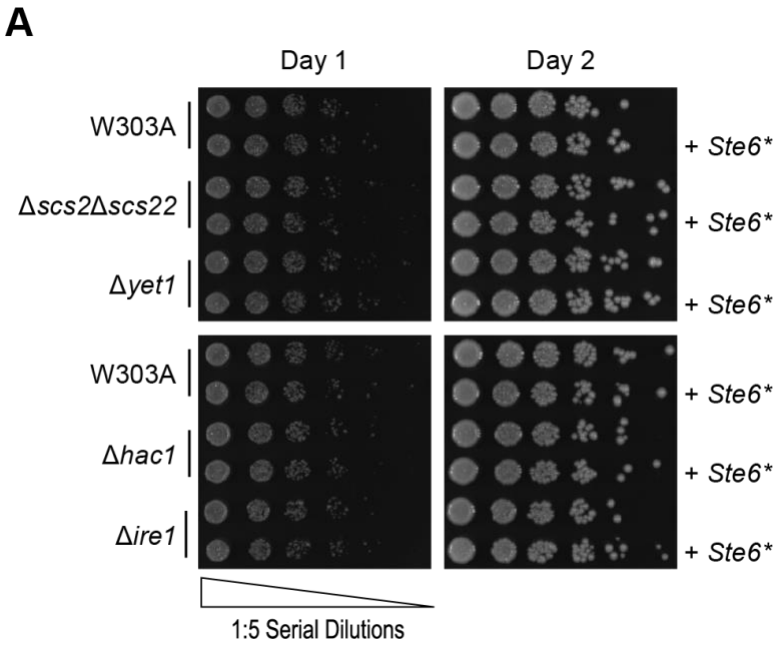

Appendix Figure 5 - Effects of Ste6* Expression in various strains grown on YPD A) Growth of indicated yeast strains on YPD with and without Ste6* expression. The left-most spots correspond to 2 µl of a OD_{600}=0.5 culture, followed by 2 µl of sequential 1:5 diliutions.

I also assessed the chronological lifespan (CLS) of these strains with and without Ste6* expression and using gradual or acute glucose starvation. For gradual glucose starvation, cells were grown in media containing 2% glucose and for acute glucose starvation cells were grown in media

containing 0.4% glucose. In both cases, nutrients were not replenished over the course of the assay. Cell viability of the strains in these conditions was monitored over the course of approximately 30 days. Acute glucose starvation (0.4% glucose) resulted in a significant increase in lifespan compared to cells grown in the standard 2% glucose media (Appendix Figure 6). Acute glucose starvation has been previously shown to extend yeast lifespan[334] and this trend was consistent for all strains in this assay regardless of Ste6* expression (Appendix Figure 6).

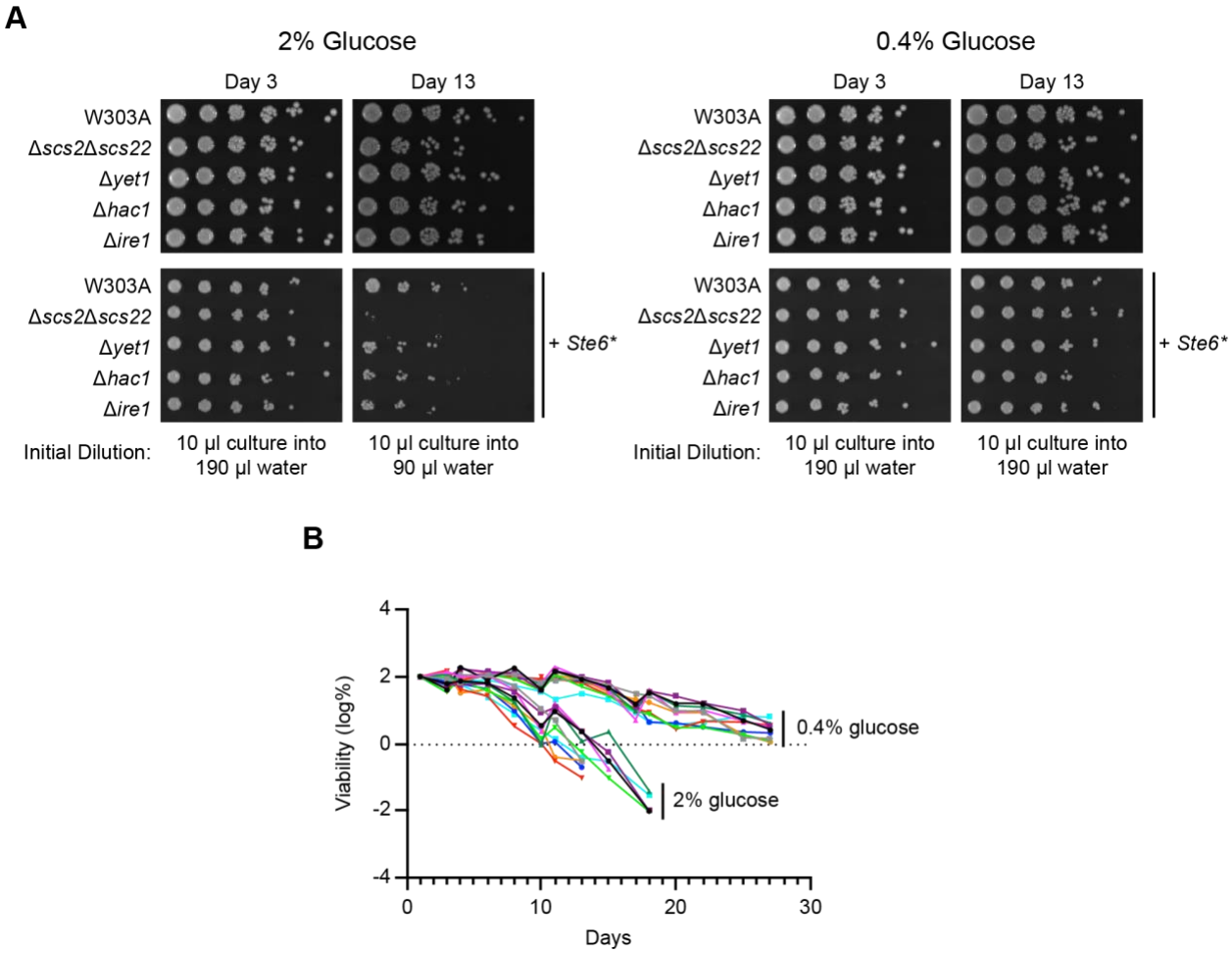

Appendix Figure 6 – Effects of glucose restriction on CLS A) Plates showing cell viability at the indicated day of a CLS assay. Cells grown in SC media with 2% or 0.4% glucose. The left-most spots correspond to 2 µl of the culture diluted as indicated, followed by 2 µl of sequenctial 1:5 dilutions. Initial culture dilutions are as indicated below each plate. B) Long-term survival of cells grown in 2% or 0.4% glucose. Cell viability at Day 3 (panel A) is set at 100% and plotted here as Day 1. Viability is plotted as the log of the percentage of viable cells on Day 1.

Further analysis of the CLS assays demonstrate that during gradual glucose starvation Ste6* expression has an effect on the lifespan of some of these strains. In wild-type cells (W303A), Ste6* expression does not influence lifespan (Appendix Figure 7). However, when comparing results between Ste6* expressing and non-Ste6* expressing Δ*scs2*Δ*scs22* cells, Ste6* expression resulted in a marked decrease in lifespan (Appendix Figure 7). The other strains, Δ*yet1*, Δ*ire1*, and Δ*hac1*, also showed a decreased lifespan with Ste6* expression, however, to a lesser extent which is particularly noticeable on the growth assay plates shown in Appendix Figure 6A.

A

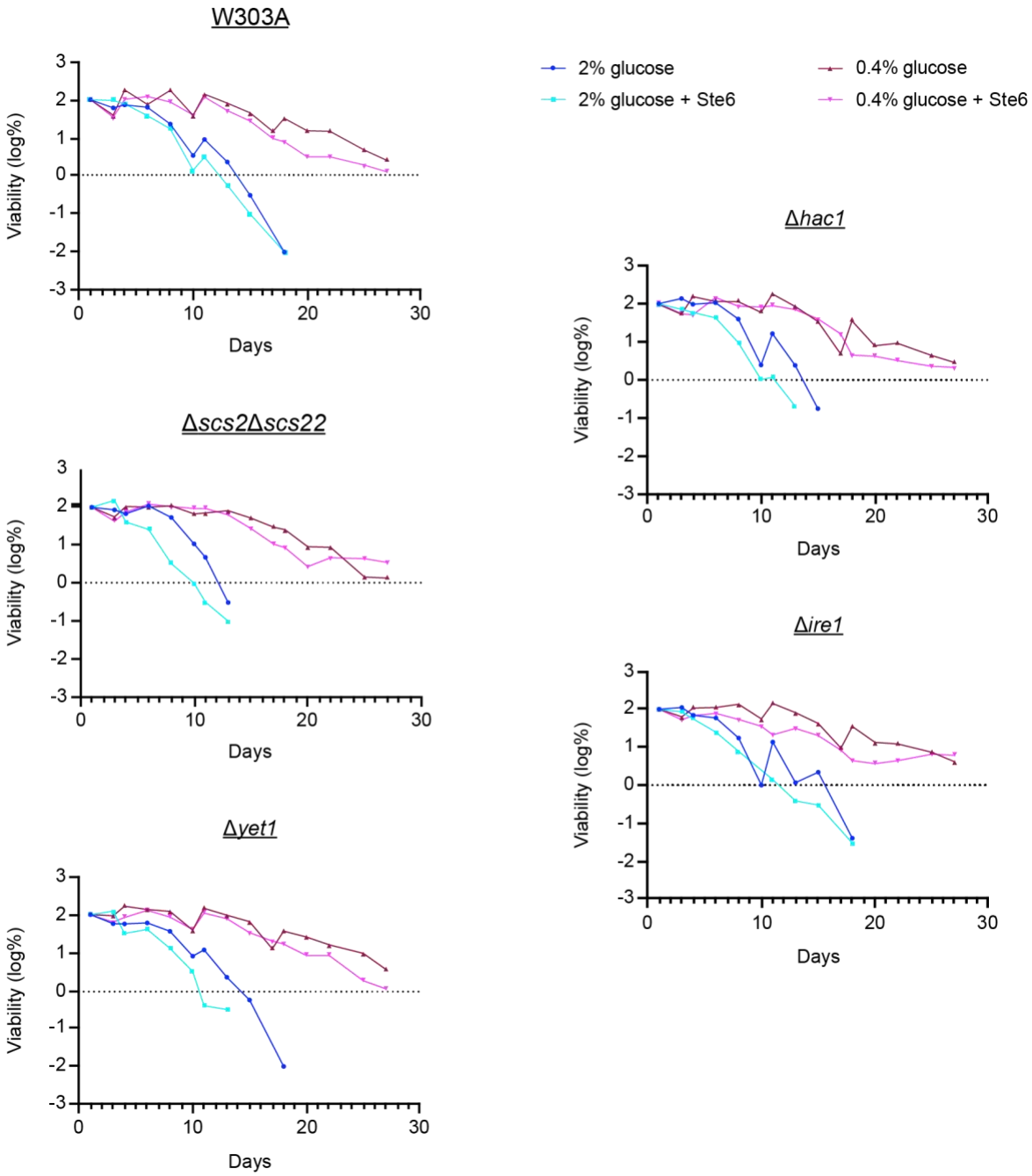

Appendix Figure 7 - CLS cell viability for individual strains A) Cell viability for each indicated knock-out strain with and without Ste6* expression grown in 2% or 0.4% glucose as indicated in the legend. Viability is plotted as the log of the percentage of viable cells on Day 1.

Appendix D.2 Methods

Appendix D.2.1 Yeast media

YPD (1% yeast extract, 2% peptone, 2% glucose, supplemented with L-tryptophan and adenine) was used for routine growth. Synthetic complete (SC; yeast nitrogen base, ammonium sulfate, 2% glucose, amino acids) or synthetic defined (SD; yeast nitrogen base, ammonium sulfate, 2% glucose, appropriate amino acid dropout) media were used as indicated and to maintain plasmid selection. For glucose restriction, cells were grown in SC or SD -Ura with 0.4% glucose.

Appendix D.2.2 Growth analysis

Cells were grown overnight in SC or SD with the appropriate dropout for plasmid maintenance. Cells were then diluted and regrown to mid-logarithmic phase (OD_{600} = 0.5-0.8) in YPD at 30°C. Cells were diluted to 0.5 OD_{600}/ml and 1:5 serial dilutions were made in water. For each dilution, 2 µl was spotted onto the indicated plates. Plates were incubated at the indicated temperatures and imaged starting on day 1.

Appendix D.2.3 Chronological lifespan and glucose restriction

Chronological lifespan and glucose restriction experiments were performed as in Seo et al., 2017[334] and Alvers et al., 2009.[313] Briefly, cells were streaked from -80°C and transformations were done within 3 days of the start of the experiment. Cells were grown in SC or SD media with appropriate drop out (2% glucose) at 30°C. After ~24 hours, cells were diluted 1/100 into 5 ml of

2% glucose SC or SD media. After ~24 hours, cells were diluted to OD_{600} = 0.1 into 5 ml of either 2% glucose SC or SD media for gradual glucose restriction or 0.4% glucose SC or SD media for acute glucose restriction. This was considered Day 0, and cells were returned to rotate at 30°C. The OD_{600} was measured over the first 3-5 days to confirm saturation of the culture. Starting on Day 3 and continuing every 2-3 days after, cells were serially diluted 1:5 and 2 µl were plated on YPD or SD -Ura to maintain plasmid selection. Dilutions were adjusted as cell viability declined and near the end of the experiment 25-100 µl of culture were directly plated. Plates were grown at 30°C for 2 days and CFUs were determined for the two highest dilutions and averaged. Viability results are presented as a percentage of the initial cell count normalized to the first day of culture saturation. Throughout the experiment, removed volume was closely tracked and water was added back to the cultures to compensate for evaporation. The addition of water was factored into the dilution factors when calculating CFUs.

Bibliography

1. Jorgensen, P. & Tyers, M. How Cells Coordinate Growth and Division. *Curr Biol* 14, R1014–R1027 (2004).

2. Chantranupong, L., Wolfson, R. L. & Sabatini, D. M. Nutrient-Sensing Mechanisms across Evolution. *Cell* 161, 67–83 (2015).

3. Saxton, R. A. & Sabatini, D. M. mTOR Signaling in Growth, Metabolism, and Disease. *Cell* 168, 960–976 (2017).

4. Johnson, S. C., Rabinovitch, P. S. & Kaeberlein, M. mTOR is a key modulator of ageing and age-related disease. *Nature* 493, 338–345 (2013).

5. Loewith, R. *et al.* Two TOR Complexes, Only One of which Is Rapamycin Sensitive, Have Distinct Roles in Cell Growth Control. *Mol Cell* 10, 457–468 (2002).

6. Wedaman, K. P. *et al.* Tor Kinases Are in Distinct Membrane-associated Protein Complexes in Saccharomyces cerevisiae. *Mol Biol Cell* 14, 1204–1220 (2003).

7. Reinke, A. *et al.* TOR Complex 1 Includes a Novel Component, Tco89p (YPL180w), and Cooperates with Ssd1p to Maintain Cellular Integrity in Saccharomyces cerevisiae. *J Biol Chem* 279, 14752–14762 (2004).

8. Kim, D.-H. *et al.* mTOR Interacts with Raptor to Form a Nutrient-Sensitive Complex that Signals to the Cell Growth Machinery. *Cell* 110, 163–175 (2002).

9. Kim, D.-H. *et al.* GβL, a Positive Regulator of the Rapamycin-Sensitive Pathway Required for the Nutrient-Sensitive Interaction between Raptor and mTOR. *Mol Cell* 11, 895–904 (2003).

10. Hara, K. *et al.* Raptor, a Binding Partner of Target of Rapamycin (TOR), Mediates TOR Action. *Cell* 110, 177–189 (2002).

11. Binda, M. *et al.* The Vam6 GEF Controls TORC1 by Activating the EGO Complex. *Mol Cell* 35, 563–573 (2009).

12. Nojima, H. *et al.* The Mammalian Target of Rapamycin (mTOR) Partner, Raptor, Binds the mTOR Substrates p70 S6 Kinase and 4E-BP1 through Their TOR Signaling (TOS) Motif. *J Biol Chem* 278, 15461–15464 (2003).

13. Schalm, S. S., Fingar, D. C., Sabatini, D. M. & Blenis, J. TOS Motif-Mediated Raptor Binding Regulates 4E-BP1 Multisite Phosphorylation and Function. *Curr Biol* 13, 797–806 (2003).

14. Wullschleger, S., Loewith, R. & Hall, M. N. TOR Signaling in Growth and Metabolism. *Cell* 124, 471–484 (2006).

15. Yonezawa, K., Tokunaga, C., Oshiro, N. & Yoshino, K. Raptor, a binding partner of target of rapamycin. *Biochem Bioph Res Co* 313, 437–441 (2004).

16. Chen, E. J. & Kaiser, C. A. LST8 negatively regulates amino acid biosynthesis as a component of the TOR pathway. *J Cell Biology* 161, 333–347 (2003).

17. Crespo, J. L., Powers, T., Fowler, B. & Hall, M. N. The TOR-controlled transcription activators GLN3, RTG1, and RTG3 are regulated in response to intracellular levels of glutamine. *Proc National Acad Sci* 99, 6784–6789 (2002).

18. Cohen, A. & Hall, M. N. An Amino Acid Shuffle Activates mTORC1. *Cell* 136, 399–400 (2009).

19. Inoki, K., Zhu, T. & Guan, K.-L. TSC2 Mediates Cellular Energy Response to Control Cell Growth and Survival. *Cell* 115, 577–590 (2003).

20. Manning, B. D., Tee, A. R., Logsdon, M. N., Blenis, J. & Cantley, L. C. Identification of the Tuberous Sclerosis Complex-2 Tumor Suppressor Gene Product Tuberin as a Target of the Phosphoinositide 3-Kinase/Akt Pathway. *Mol Cell* 10, 151–162 (2002).

21. Cai, S.-L. *et al.* Activity of TSC2 is inhibited by AKT-mediated phosphorylation and membrane partitioning. *J Cell Biology* 173, 279–289 (2006).

22. Deng, L. *et al.* Ubiquitination of Rheb governs growth factor-induced mTORC1 activation. *Cell Res* 29, 136–150 (2019).

23. Long, X., Lin, Y., Ortiz-Vega, S., Yonezawa, K. & Avruch, J. Rheb Binds and Regulates the mTOR Kinase. *Curr Biol* 15, 702–713 (2005).

24. Loewith, R. & Hall, M. N. Target of Rapamycin (TOR) in Nutrient Signaling and Growth Control. *Genetics* 189, 1177–1201 (2011).

25. González, A. & Hall, M. N. Nutrient sensing and TOR signaling in yeast and mammals. *Embo J* 36, 397–408 (2017).

26. Urban, J. *et al.* Sch9 Is a Major Target of TORC1 in Saccharomyces cerevisiae. *Mol Cell* 26, 663–674 (2007).

27. Kamada, Y. *et al.* Tor Directly Controls the Atg1 Kinase Complex To Regulate Autophagy. *Mol Cell Biol* 30, 1049–1058 (2009).

28. Hatakeyama, R. *et al.* Spatially Distinct Pools of TORC1 Balance Protein Homeostasis. *Mol Cell* 73, 325-338.e8 (2019).

29. Powers, T. TOR Signaling and S6 Kinase 1: Yeast Catches Up. *Cell Metab* 6, 1–2 (2007).

30. Pearce, L. R., Komander, D. & Alessi, D. R. The nuts and bolts of AGC protein kinases. *Nat Rev Mol Cell Bio* 11, 9–22 (2010).

31. Jorgensen, P. *et al.* A dynamic transcriptional network communicates growth potential to ribosome synthesis and critical cell size. *Gene Dev* 18, 2491–2505 (2004).

32. Jefferies, H. B., Reinhard, C., Kozma, S. C. & Thomas, G. Rapamycin selectively represses translation of the "polypyrimidine tract" mRNA family. *Proc National Acad Sci* 91, 4441–4445 (1994).

33. Terada, N. *et al.* Rapamycin selectively inhibits translation of mRNAs encoding elongation factors and ribosomal proteins. *Proc National Acad Sci* 91, 11477–11481 (1994).

34. Kim, J., Kundu, M., Viollet, B. & Guan, K.-L. AMPK and mTOR regulate autophagy through direct phosphorylation of Ulk1. *Nat Cell Biol* 13, 132–141 (2011).

35. Jung, C. H. *et al.* ULK-Atg13-FIP200 Complexes Mediate mTOR Signaling to the Autophagy Machinery. *Mol Biol Cell* 20, 1992–2003 (2009).

36. Ganley, I. G. *et al.* ULK1·ATG13·FIP200 Complex Mediates mTOR Signaling and Is Essential for Autophagy. *J Biol Chem* 284, 12297–12305 (2009).

37. Hosokawa, N. *et al.* Nutrient-dependent mTORC1 Association with the ULK1–Atg13–FIP200 Complex Required for Autophagy. *Mol Biol Cell* 20, 1981–1991 (2009).

38. Guerra, P., Vuillemenot, L.-A. P. E., Oppen, Y. B. van, Been, M. & Milias-Argeitis, A. TORC1 and PKA activity towards ribosome biogenesis oscillates in synchrony with the budding yeast cell cycle. *J Cell Sci* (2022) doi:10.1242/jcs.260378.

39. Baretić, D., Berndt, A., Ohashi, Y., Johnson, C. M. & Williams, R. L. Tor forms a dimer through an N-terminal helical solenoid with a complex topology. *Nat Commun* 7, 11016 (2016).

40. Yang, H. *et al.* 4.4 Å Resolution Cryo-EM structure of human mTOR Complex 1. *Protein Cell* 7, 878–887 (2016).

41. Mihaylova, M. M. & Shaw, R. J. The AMPK signalling pathway coordinates cell growth, autophagy and metabolism. *Nat Cell Biol* 13, 1016–1023 (2011).

42. Carling, D., Clarke, P. R., Zammit, V. A. & Hardie, D. G. Purification and characterization of the AMP-activated protein kinase. *Eur J Biochem* 186, 129–136 (1989).

43. Carling, D. *et al.* Mammalian AMP-activated protein kinase is homologous to yeast and plant protein kinases involved in the regulation of carbon metabolism. *J Biol Chem* 269, 11442–11448 (1994).

44. Mitchelhill, K. I. *et al.* Mammalian AMP-activated protein kinase shares structural and functional homology with the catalytic domain of yeast Snf1 protein kinase. *J Biol Chem* 269, 2361–2364 (1994).

45. Woods, A. *et al.* Yeast SNF1 is functionally related to mammalian AMP-activated protein kinase and regulates acetyl-CoA carboxylase in vivo. *J Biol Chem* 269, 19509–19515 (1994).

46. Carlson, M., Osmond, B. C. & Botstein, D. Mutants of yeast defective in sucrose utilization. *Genetics* 98, 25–40 (1981).

47. Jeon, S.-M. Regulation and function of AMPK in physiology and diseases. *Exp Mol Medicine* 48, e245–e245 (2016).

48. Hardie, D. G. AMP-activated/SNF1 protein kinases: conserved guardians of cellular energy. *Nat Rev Mol Cell Bio* 8, 774–785 (2007).

49. Yang, X., Hubbard, E. J. A. & Carlson, M. A Protein Kinase Substrate Identified by the Two-Hybrid System. *Science* 257, 680–682 (1992).

50. Yang, X., Jiang, R. & Carlson, M. A family of proteins containing a conserved domain that mediates interaction with the yeast SNF1 protein kinase complex. *Embo J* 13, 5878–5886 (1994).

51. Erickson, J. R. & Johnston, M. Genetic and molecular characterization of GAL83: its interaction and similarities with other genes involved in glucose repression in Saccharomyces cerevisiae. *Genetics* 135, 655–664 (1993).

52. Celenza, J. L. & Carlson, M. Mutational analysis of the Saccharomyces cerevisiae SNF1 protein kinase and evidence for functional interaction with the SNF4 protein. *Mol Cell Biol* 9, 5034–5044 (1989).

53. Celenza, J. L., Eng, F. J. & Carlson, M. Molecular analysis of the SNF4 gene of Saccharomyces cerevisiae: evidence for physical association of the SNF4 protein with the SNF1 protein kinase. *Mol Cell Biol* 9, 5045–5054 (1989).

54. Vincent, O., Townley, R., Kuchin, S. & Carlson, M. Subcellular localization of the Snf1 kinase is regulated by specific β subunits and a novel glucose signaling mechanism. *Gene Dev* 15, 1104–1114 (2001).

55. Hedbacker, K., Townley, R. & Carlson, M. Cyclic AMP-Dependent Protein Kinase Regulates the Subcellular Localization of Snf1-Sip1 Protein Kinase. *Mol Cell Biol* 24, 1836–1843 (2004).

56. Hedbacker, K., Hong, S.-P. & Carlson, M. Pak1 Protein Kinase Regulates Activation and Nuclear Localization of Snf1-Gal83 Protein Kinase. *Mol Cell Biol* 24, 8255–8263 (2004).

57. Scott, J. W. *et al.* CBS domains form energy-sensing modules whose binding of adenosine ligands is disrupted by disease mutations. *J Clin Invest* 113, 274–284 (2004).

58. Kemp, B. E. Bateman domains and adenosine derivatives form a binding contract. *J Clin Invest* 113, 182–184 (2004).

59. Corton, J. M., Gillespie, J. G. & Hardie, D. G. Role of the AMP-activated protein kinase in the cellular stress response. *Curr Biol* 4, 315–324 (1994).

60. Hawley, S. A. *et al.* 5′-AMP Activates the AMP-activated Protein Kinase Cascade, and Ca2+/Calmodulin Activates the Calmodulin-dependent Protein Kinase I Cascade, via Three Independent Mechanisms. *J Biol Chem* 270, 27186–27191 (1995).

61. Gowans, G. J., Hawley, S. A., Ross, F. A. & Hardie, D. G. AMP Is a True Physiological Regulator of AMP-Activated Protein Kinase by Both Allosteric Activation and Enhancing Net Phosphorylation. *Cell Metab* 18, 556–566 (2013).

62. Chen, L. *et al.* AMP-activated protein kinase undergoes nucleotide-dependent conformational changes. *Nat Struct Mol Biol* 19, 716–718 (2012).

63. Woods, A. *et al.* LKB1 Is the Upstream Kinase in the AMP-Activated Protein Kinase Cascade. *Curr Biol* 13, 2004–2008 (2003).

64. Hawley, S. A. *et al.* Complexes between the LKB1 tumor suppressor, STRADα/β and MO25α/β are upstream kinases in the AMP-activated protein kinase cascade. *J Biology* 2, 28 (2003).

65. Shaw, R. J. *et al.* The tumor suppressor LKB1 kinase directly activates AMP-activated kinase and regulates apoptosis in response to energy stress. *Proc National Acad Sci* 101, 3329–3335 (2004).

66. Woods, A. *et al.* Ca2+/calmodulin-dependent protein kinase kinase-β acts upstream of AMP-activated protein kinase in mammalian cells. *Cell Metab* 2, 21–33 (2005).

67. Hawley, S. A. *et al.* Calmodulin-dependent protein kinase kinase-β is an alternative upstream kinase for AMP-activated protein kinase. *Cell Metab* 2, 9–19 (2005).

68. Hurley, R. L. *et al.* The Ca2+/Calmodulin-dependent Protein Kinase Kinases Are AMP-activated Protein Kinase Kinases. *J Biol Chem* 280, 29060–29066 (2005).

69. Momcilovic, M., Hong, S.-P. & Carlson, M. Mammalian TAK1 Activates Snf1 Protein Kinase in Yeast and Phosphorylates AMP-activated Protein Kinase in Vitro. *J Biol Chem* 281, 25336–25343 (2006).

70. Xie, M. *et al.* A pivotal role for endogenous TGF-β-activated kinase-1 in the LKB1/AMP-activated protein kinase energy-sensor pathway. *Proc National Acad Sci* 103, 17378–17383 (2006).

71. Kim, M.-D., Hong, S.-P. & Carlson, M. Role of Tos3, a Snf1 Protein Kinase Kinase, during Growth of Saccharomyces cerevisiae on Nonfermentable Carbon Sources. *Eukaryot Cell* 4, 861–866 (2005).

72. Hong, S.-P., Leiper, F. C., Woods, A., Carling, D. & Carlson, M. Activation of yeast Snf1 and mammalian AMP-activated protein kinase by upstream kinases. *Proc National Acad Sci* 100, 8839–8843 (2003).

73. Nath, N., McCartney, R. R. & Schmidt, M. C. Yeast Pak1 Kinase Associates with and Activates Snf1. *Mol Cell Biol* 23, 3909–3917 (2003).

74. Sutherland, C. M. *et al.* Elm1p Is One of Three Upstream Kinases for the Saccharomyces cerevisiae SNF1 Complex. *Curr Biol* 13, 1299–1305 (2003).

75. Gowans, G. J. & Hardie, D. G. AMPK: a cellular energy sensor primarily regulated by AMP. *Biochem Soc T* 42, 71–75 (2014).

76. Davies, S. P., Helps, N. R., Cohen, P. T. & Hardie, D. G. 5′-AMP inhibits dephosphorylation, as well as promoting phosphorylation, of the AMP-activated protein kinase. Studies using bacterially expressed human protein phosphatase-2Cα and native bovine protein phosphatase-2Ac. *Febs Lett* 377, 421–425 (1995).

77. Tu, J. & Carlson, M. The GLC7 type 1 protein phosphatase is required for glucose repression in Saccharomyces cerevisiae. *Mol Cell Biol* 14, 6789–6796 (1994).

78. Tu, J. & Carlson, M. REG1 binds to protein phosphatase type 1 and regulates glucose repression in Saccharomyces cerevisiae. *Embo J* 14, 5939–5946 (1995).

79. Ludin, K., Jiang, R. & Carlson, M. Glucose-regulated interaction of a regulatory subunit of protein phosphatase 1 with the Snf1 protein kinase in Saccharomyces cerevisiae. *Proc National Acad Sci* 95, 6245–6250 (1998).

80. Sanz, P., Alms, G. R., Haystead, T. A. J. & Carlson, M. Regulatory Interactions between the Reg1-Glc7 Protein Phosphatase and the Snf1 Protein Kinase. *Mol Cell Biol* 20, 1321–1328 (2000).

81. Voss, M. *et al.* Ppm1E is an in cellulo AMP-activated protein kinase phosphatase. *Cell Signal* 23, 114–124 (2011).

82. Joseph, B. K. *et al.* Inhibition of AMP Kinase by the Protein Phosphatase 2A Heterotrimer, PP2APpp2r2d. *J Biol Chem* 290, 10588–10598 (2015).

83. Adams, J. *et al.* Intrasteric control of AMPK via the γ1 subunit AMP allosteric regulatory site. *Protein Sci* 13, 155–165 (2004).

84. Mayer, F. V. *et al.* ADP Regulates SNF1, the Saccharomyces cerevisiae Homolog of AMP-Activated Protein Kinase. *Cell Metab* 14, 707–714 (2011).

85. Andersson, U. *et al.* AMP-activated Protein Kinase Plays a Role in the Control of Food Intake. *J Biol Chem* 279, 12005–12008 (2004).

86. Minokoshi, Y. *et al.* AMP-kinase regulates food intake by responding to hormonal and nutrient signals in the hypothalamus. *Nature* 428, 569–574 (2004).

87. Pinto, S. *et al.* Rapid Rewiring of Arcuate Nucleus Feeding Circuits by Leptin. *Science* 304, 110–115 (2004).

88. Dietrich, M. O. & Horvath, T. L. Synaptic Plasticity of Feeding Circuits: Hormones and Hysteresis. *Cell* 146, 863–865 (2011).

89. Yang, Y., Atasoy, D., Su, H. H. & Sternson, S. M. Hunger States Switch a Flip-Flop Memory Circuit via a Synaptic AMPK-Dependent Positive Feedback Loop. *Cell* 146, 992–1003 (2011).

90. Hardie, D. G., Ross, F. A. & Hawley, S. A. AMPK: a nutrient and energy sensor that maintains energy homeostasis. *Nat Rev Mol Cell Bio* 13, 251–262 (2012).

91. Carling, D., Zammit, V. A. & Hardie, D. G. A common bicyclic protein kinase cascade inactivates the regulatory enzymes of fatty acid and cholesterol biosynthesis. *Febs Lett* 223, 217–222 (1987).

92. Sato, R., Goldstein, J. L. & Brown, M. S. Replacement of serine-871 of hamster 3-hydroxy-3-methylglutaryl-CoA reductase prevents phosphorylation by AMP-activated kinase and blocks inhibition of sterol synthesis induced by ATP depletion. *Proc National Acad Sci* 90, 9261–9265 (1993).

93. Gwinn, D. M. *et al.* AMPK Phosphorylation of Raptor Mediates a Metabolic Checkpoint. *Mol Cell* 30, 214–226 (2008).

94. Braun, K. A. *et al.* Phosphoproteomic analysis identifies proteins involved in transcription-coupled mRNA decay as targets of Snf1 signaling. *Sci Signal* 7, ra64 (2014).

95. Rashida, Z., Srinivasan, R., Cyanam, M. & Laxman, S. Kog1/Raptor mediates metabolic rewiring during nutrient limitation by controlling SNF1/AMPK activity. *Sci Adv* 7, eabe5544 (2021).

96. Amodeo, G. A., Rudolph, M. J. & Tong, L. Crystal structure of the heterotrimer core of Saccharomyces cerevisiae AMPK homologue SNF1. *Nature* 449, 492–495 (2007).

97. Xiao, B. *et al.* Structure of mammalian AMPK and its regulation by ADP. *Nature* 472, 230–233 (2011).

98. Hinnebusch, A. G. Evidence for translational regulation of the activator of general amino acid control in yeast. *Proc National Acad Sci* 81, 6442–6446 (1984).

99. Diallinas, G. & Thireos, G. Genetic and biochemical evidence for yeast GCN2 protein kinase polymerization. *Gene* 143, 21–27 (1994).

100. Narasimhan, J., Staschke, K. A. & Wek, R. C. Dimerization Is Required for Activation of eIF2 Kinase Gcn2 in Response to Diverse Environmental Stress Conditions. *J Biol Chem* 279, 22820–22832 (2004).

101. Marton, M. J., Aldana, C. R. V. de, Qiu, H., Chakraburtty, K. & Hinnebusch, A. G. Evidence that GCN1 and GCN20, translational regulators of GCN4, function on elongating ribosomes in activation of eIF2alpha kinase GCN2. *Mol Cell Biol* 17, 4474–4489 (1997).

102. Garcia-Barrio, M., Dong, J., Ufano, S. & Hinnebusch, A. G. Association of GCN1–GCN20 regulatory complex with the N-terminus of eIF2α kinase GCN2 is required for GCN2 activation. *Embo J* 19, 1887–1899 (2000).

103. Dever, T. E. *et al.* Phosphorylation of initiation factor 2α by protein kinase GCN2 mediates gene-specific translational control of GCN4 in yeast. *Cell* 68, 585–596 (1992).

104. Costa-Mattioli, M. & Walter, P. The integrated stress response: From mechanism to disease. *Science* 368, (2020).

105. Abastado, J. P., Miller, P. F., Jackson, B. M. & Hinnebusch, A. G. Suppression of ribosomal reinitiation at upstream open reading frames in amino acid-starved cells forms the basis for GCN4 translational control. *Mol Cell Biol* 11, 486–496 (1991).

106. Hinnebusch, A. G. Gene-specific translational control of the yeast GCN4 gene by phosphorylation of eukaryotic initiation factor 2. *Mol Microbiol* 10, 215–223 (1993).

107. Berlanga, J. J., Santoyo, J. & Haro, C. de. Characterization of a mammalian homolog of the GCN2 eukaryotic initiation factor 2α kinase. *Eur J Biochem* 265, 754–762 (1999).

108. Sood, R., Porter, A. C., Olsen, D., Cavener, D. R. & Wek, R. C. A Mammalian Homologue of GCN2 Protein Kinase Important for Translational Control by Phosphorylation of Eukaryotic Initiation Factor-2α. *Genetics* 154, 787–801 (2000).

109. Hinnebusch, A. G. Translational Regulation of GCN4 and the General Amino Acid Control of Yeast. *Microbiology+* 59, 407–450 (2005).

110. Vattem, K. M. & Wek, R. C. Reinitiation involving upstream ORFs regulates ATF4 mRNA translation in mammalian cells. *Proc National Acad Sci* 101, 11269–11274 (2004).

111. B'chir, W. *et al.* The eIF2α/ATF4 pathway is essential for stress-induced autophagy gene expression. *Nucleic Acids Res* 41, 7683–7699 (2013).

112. Bunpo, P. *et al.* GCN2 Protein Kinase Is Required to Activate Amino Acid Deprivation Responses in Mice Treated with the Anti-cancer Agent l-Asparaginase. *J Biol Chem* 284, 32742–32749 (2009).

113. Harding, H. P. *et al.* Regulated Translation Initiation Controls Stress-Induced Gene Expression in Mammalian Cells. *Mol Cell* 6, 1099–1108 (2000).

114. Harding, H. P. *et al.* An Integrated Stress Response Regulates Amino Acid Metabolism and Resistance to Oxidative Stress. *Mol Cell* 11, 619–633 (2003).

115. Krokowski, D. *et al.* A Self-defeating Anabolic Program Leads to β-Cell Apoptosis in Endoplasmic Reticulum Stress-induced Diabetes via Regulation of Amino Acid Flux. *J Biol Chem* 288, 17202–17213 (2013).

116. Dokládal, L. *et al.* Global phosphoproteomics pinpoints uncharted Gcn2-mediated mechanisms of translational control. *Mol Cell* (2021) doi:10.1016/j.molcel.2021.02.037.

117. Cherkasova, V. A. & Hinnebusch, A. G. Translational control by TOR and TAP42 through dephosphorylation of eIF2α kinase GCN2. *Gene Dev* 17, 859–872 (2003).

118. Yuan, W. *et al.* General Control Nonderepressible 2 (GCN2) Kinase Inhibits Target of Rapamycin Complex 1 in Response to Amino Acid Starvation in Saccharomyces cerevisiae. *J Biol Chem* 292, 2660–2669 (2017).

119. Kubota, H., Obata, T., Ota, K., Sasaki, T. & Ito, T. Rapamycin-induced Translational Derepression of GCN4 mRNA Involves a Novel Mechanism for Activation of the eIF2α Kinase GCN2. *J Biol Chem* 278, 20457–20460 (2003).

120. Staschke, K. A. *et al.* Integration of General Amino Acid Control and Target of Rapamycin (TOR) Regulatory Pathways in Nitrogen Assimilation in Yeast. *J Biol Chem* 285, 16893–16911 (2010).

121. Anthony, T. G. *et al.* Preservation of Liver Protein Synthesis during Dietary Leucine Deprivation Occurs at the Expense of Skeletal Muscle Mass in Mice Deleted for eIF2 Kinase GCN2. *J Biol Chem* 279, 36553–36561 (2004).

122. Bjordal, M., Arquier, N., Kniazeff, J., Pin, J. P. & Léopold, P. Sensing of Amino Acids in a Dopaminergic Circuitry Promotes Rejection of an Incomplete Diet in Drosophila. *Cell* 156, 510–521 (2014).

123. Koehnle, T. J., Russell, M. C. & Gietzen, D. W. Rats Rapidly Reject Diets Deficient in Essential Amino Acids. *J Nutrition* 133, 2331–2335 (2003).

124. Ribeiro, C. & Dickson, B. J. Sex Peptide Receptor and Neuronal TOR/S6K Signaling Modulate Nutrient Balancing in Drosophila. *Curr Biol* 20, 1000–1005 (2010).

125. Toshima, N. & Tanimura, T. Taste preference for amino acids is dependent on internal nutritional state in Drosophila melanogaster. *J Exp Biol* 215, 2827–2832 (2012).

126. Vargas, M. A., Luo, N., Yamaguchi, A. & Kapahi, P. A Role for S6 Kinase and Serotonin in Postmating Dietary Switch and Balance of Nutrients in D. melanogaster. *Curr Biol* 20, 1006–1011 (2010).

127. Padyana, A. K., Qiu, H., Roll-Mecak, A., Hinnebusch, A. G. & Burley, S. K. Structural Basis for Autoinhibition and Mutational Activation of Eukaryotic Initiation Factor 2α Protein Kinase GCN2. *J Biol Chem* 280, 29289–29299 (2005).

128. Oliveira, T. M. de *et al.* The structure of human GCN2 reveals a parallel, back-to-back kinase dimer with a plastic DFG activation loop motif. *Biochem J* 477, 275–284 (2020).

129. Yin, Z., Pascual, C. & Klionsky, D. Autophagy: machinery and regulation. *Microb Cell* 3, 588–596 (2016).

130. Lamb, C. A., Yoshimori, T. & Tooze, S. A. The autophagosome: origins unknown, biogenesis complex. *Nat Rev Mol Cell Bio* 14, 759–774 (2013).

131. Kamada, Y. *et al.* Tor-Mediated Induction of Autophagy via an Apg1 Protein Kinase Complex. *J Cell Biol* 150, 1507–1513 (2000).

132. Suzuki, K., Kubota, Y., Sekito, T. & Ohsumi, Y. Hierarchy of Atg proteins in pre-autophagosomal structure organization. *Genes Cells* 12, 209–218 (2007).

133. Papinski, D. *et al.* Early Steps in Autophagy Depend on Direct Phosphorylation of Atg9 by the Atg1 Kinase. *Mol Cell* 53, 471–483 (2014).

134. Schu, P. V. *et al.* Phosphatidylinositol 3-Kinase Encoded by Yeast VPS34 Gene Essential for Protein Sorting. *Science* 260, 88–91 (1993).

135. Kihara, A., Noda, T., Ishihara, N. & Ohsumi, Y. Two Distinct Vps34 Phosphatidylinositol 3–Kinase Complexes Function in Autophagy and Carboxypeptidase Y Sorting in Saccharomyces cerevisiae. *J Cell Biology* 152, 519–530 (2001).

136. Alers, S., Löffler, A. S., Wesselborg, S. & Stork, B. Role of AMPK-mTOR-Ulk1/2 in the Regulation of Autophagy: Cross Talk, Shortcuts, and Feedbacks. *Mol Cell Biol* 32, 2–11 (2012).

137. Burman, C. & Ktistakis, N. T. Regulation of autophagy by phosphatidylinositol 3-phosphate. *Febs Lett* 584, 1302–1312 (2010).

138. Russell, R. C. *et al.* ULK1 induces autophagy by phosphorylating Beclin-1 and activating VPS34 lipid kinase. *Nat Cell Biol* 15, 741–750 (2013).

139. Obara, K., Sekito, T., Niimi, K. & Ohsumi, Y. The Atg18-Atg2 Complex Is Recruited to Autophagic Membranes via Phosphatidylinositol 3-Phosphate and Exerts an Essential Function. *J Biol Chem* 283, 23972–23980 (2008).

140. Ohsumi, Y. Molecular dissection of autophagy: two ubiquitin-like systems. *Nat Rev Mol Cell Bio* 2, 211–216 (2001).

141. Cao, Y., Cheong, H., Song, H. & Klionsky, D. J. In vivo reconstitution of autophagy in Saccharomyces cerevisiae. *J Cell Biology* 182, 703–713 (2008).

142. Kobayashi, T., Suzuki, K. & Ohsumi, Y. Autophagosome formation can be achieved in the absence of Atg18 by expressing engineered PAS-targeted Atg2. *Febs Lett* 586, 2473–2478 (2012).

143. Kirisako, T. *et al.* The Reversible Modification Regulates the Membrane-Binding State of Apg8/Aut7 Essential for Autophagy and the Cytoplasm to Vacuole Targeting Pathway. *J Cell Biology* 151, 263–276 (2000).

144. Nair, U. *et al.* A role for Atg8–PE deconjugation in autophagosome biogenesis. *Autophagy* 8, 780–793 (2012).

145. Mizushima, N., Yoshimori, T. & Ohsumi, Y. The Role of Atg Proteins in Autophagosome Formation. *Cell Dev Biology* 27, 107–132 (2011).

146. Klionsky, D. J. The molecular machinery of autophagy: unanswered questions. *J Cell Sci* 118, 7–18 (2004).

147. Fujita, N. *et al.* An Atg4B Mutant Hampers the Lipidation of LC3 Paralogues and Causes Defects in Autophagosome Closure. *Mol Biol Cell* 19, 4651–4659 (2008).

148. Weidberg, H. *et al.* LC3 and GATE-16 N Termini Mediate Membrane Fusion Processes Required for Autophagosome Biogenesis. *Dev Cell* 20, 444–454 (2011).

149. Kirisako, T. *et al.* Formation Process of Autophagosome Is Traced with Apg8/Aut7p in Yeast. *J Cell Biology* 147, 435–446 (1999).

150. Kabeya, Y. *et al.* LC3, a mammalian homologue of yeast Apg8p, is localized in autophagosome membranes after processing. *Embo J* 19, 5720–5728 (2000).

151. Huang, W.-P., Scott, S. V., Kim, J. & Klionsky, D. J. The Itinerary of a Vesicle Component, Aut7p/Cvt5p, Terminates in the Yeast Vacuole via the Autophagy/Cvt Pathways. *J Biol Chem* 275, 5845–5851 (2000).

152. Epple, U. D., Suriapranata, I., Eskelinen, E.-L. & Thumm, M. Aut5/Cvt17p, a Putative Lipase Essential for Disintegration of Autophagic Bodies inside the Vacuole. *J Bacteriol* 183, 5942–5955 (2001).

153. Teter, S. A. *et al.* Degradation of Lipid Vesicles in the Yeast Vacuole Requires Function of Cvt17, a Putative Lipase. *J Biol Chem* 276, 2083–2087 (2001).

154. Yang, Z., Huang, J., Geng, J., Nair, U. & Klionsky, D. J. Atg22 Recycles Amino Acids to Link the Degradative and Recycling Functions of Autophagy. *Mol Biol Cell* 17, 5094–5104 (2006).

155. Yuan, H.-X., Russell, R. C. & Guan, K.-L. Regulation of PIK3C3/VPS34 complexes by MTOR in nutrient stress-induced autophagy. *Autophagy* 9, 1983–1995 (2013).

156. Stephan, J. S., Yeh, Y.-Y., Ramachandran, V., Deminoff, S. J. & Herman, P. K. The Tor and PKA signaling pathways independently target the Atg1/Atg13 protein kinase complex to control autophagy. *Proc National Acad Sci* 106, 17049–17054 (2009).

157. Zurita-Martinez, S. A. & Cardenas, M. E. Tor and Cyclic AMP-Protein Kinase A: Two Parallel Pathways Regulating Expression of Genes Required for Cell Growth. *Eukaryot Cell* 4, 63–71 (2005).

158. Russell, R. C., Yuan, H.-X. & Guan, K.-L. Autophagy regulation by nutrient signaling. *Cell Res* 24, 42–57 (2014).

159. Vermeulen, K., Bockstaele, D. R. V. & Berneman, Z. N. The cell cycle: a review of regulation, deregulation and therapeutic targets in cancer. *Cell Proliferat* 36, 131–149 (2003).

160. Matthews, H. K., Bertoli, C. & Bruin, R. A. M. de. Cell cycle control in cancer. *Nat Rev Mol Cell Bio* 23, 74–88 (2022).

161. Malumbres, M. & Barbacid, M. Mammalian cyclin-dependent kinases. *Trends Biochem Sci* 30, 630–641 (2005).

162. Malumbres, M. Cyclin-dependent kinases. *Genome Biol* 15, 122 (2014).

163. Kovacs, L. A. S., Orlando, D. A. & Haase, S. B. Transcription network and cyclin/CDKs: The yin and yang of cell cycle oscillators. *Cell Cycle* 7, 2626–2629 (2008).

164. Schachter, M. M. & Fisher, R. P. The CDK-activating kinase Cdk7. *Cell Cycle* 12, 3239–3240 (2013).

165. Panagopoulos, A. & Altmeyer, M. The Hammer and the Dance of Cell Cycle Control. *Trends Biochem Sci* 46, 301–314 (2020).

166. Cookson, N. A., Cookson, S. W., Tsimring, L. S. & Hasty, J. Cell cycle-dependent variations in protein concentration. *Nucleic Acids Res* 38, 2676–2681 (2010).

167. Ferrezuelo, F. *et al.* The critical size is set at a single-cell level by growth rate to attain homeostasis and adaptation. *Nat Commun* 3, 1012 (2012).

168. Liu, X., Oh, S., Peshkin, L. & Kirschner, M. W. Computationally enhanced quantitative phase microscopy reveals autonomous oscillations in mammalian cell growth. *Proc National Acad Sci* 117, 27388–27399 (2020).

169. Lippman, S. I. & Broach, J. R. Protein kinase A and TORC1 activate genes for ribosomal biogenesis by inactivating repressors encoded by Dot6 and its homolog Tod6. *Proc National Acad Sci* 106, 19928–19933 (2009).

170. Martin, D. E., Soulard, A. & Hall, M. N. TOR Regulates Ribosomal Protein Gene Expression via PKA and the Forkhead Transcription Factor FHL1. *Cell* 119, 969–979 (2004).

171. Powers, T. & Walter, P. Regulation of Ribosome Biogenesis by the Rapamycin-sensitive TOR-signaling Pathway in Saccharomyces cerevisiae. *Mol Biol Cell* 10, 987–1000 (1999).

172. Yerlikaya, S. *et al.* TORC1 and TORC2 work together to regulate ribosomal protein S6 phosphorylation in Saccharomyces cerevisiae. *Mol Biol Cell* 27, 397–409 (2016).

173. Barbet, N. C. *et al.* TOR controls translation initiation and early G1 progression in yeast. *Mol Biol Cell* 7, 25–42 (1996).

174. Hall, D. D., Markwardt, D. D., Parviz, F. & Heideman, W. Regulation of the Cln3–Cdc28 kinase by cAMP in Saccharomyces cerevisiae. *Embo J* 17, 4370–4378 (1998).

175. Mizunuma, M. *et al.* Ras/cAMP-dependent Protein Kinase (PKA) Regulates Multiple Aspects of Cellular Events by Phosphorylating the Whi3 Cell Cycle Regulator in Budding Yeast. *J Biol Chem* 288, 10558–10566 (2013).

176. Polymenis, M. & Schmidt, E. V. Coupling of cell division to cell growth by translational control of the G1 cyclin CLN3 in yeast. *Gene Dev* 11, 2522–2531 (1997).

177. Pedruzzi, I. *et al.* TOR and PKA Signaling Pathways Converge on the Protein Kinase Rim15 to Control Entry into G0. *Mol Cell* 12, 1607–1613 (2003).

178. Reinders, A., Bürckert, N., Boller, T., Wiemken, A. & Virgilio, C. D. Saccharomyces cerevisiae cAMP-dependent protein kinase controls entry into stationary phase through the Rim15p protein kinase. *Gene Dev* 12, 2943–2955 (1998).

179. Schneper, L., Düvel, K. & Broach, J. R. Sense and sensibility: nutritional response and signal integration in yeast. *Curr Opin Microbiol* 7, 624–630 (2004).

180. Wanke, V., Pedruzzi, I., Cameroni, E., Dubouloz, F. & Virgilio, C. D. Regulation of G0 entry by the Pho80–Pho85 cyclin–CDK complex. *Embo J* 24, 4271–4278 (2005).

181. Moreno-Torres, M., Jaquenoud, M. & Virgilio, C. D. TORC1 controls G1–S cell cycle transition in yeast via Mpk1 and the greatwall kinase pathway. *Nat Commun* 6, 8256 (2015).

182. Moreno-Torres, M., Jaquenoud, M., Péli-Gulli, M.-P., Nicastro, R. & Virgilio, C. D. TORC1 coordinates the conversion of Sic1 from a target to an inhibitor of cyclin-CDK-Cks1. *Cell Discov* 3, 17012 (2017).

183. Zinzalla, V., Graziola, M., Mastriani, A., Vanoni, M. & Alberghina, L. Rapamycin-mediated G1 arrest involves regulation of the Cdk inhibitor Sic1 in Saccharomyces cerevisiae. *Mol Microbiol* 63, 1482–1494 (2007).

184. Nakashima, A. *et al.* The Yeast Tor Signaling Pathway Is Involved in G2/M Transition via Polo-Kinase. *Plos One* 3, e2223 (2008).

185. Tran, L. T. *et al.* TORC1 kinase and the S-phase cyclin Clb5 collaborate to promote mitotic spindle assembly and DNA replication in S. cerevisiae. *Curr Genet* 56, 479–493 (2010).

186. Tsukada, M. & Ohsumi, Y. Isolation and characterization of autophagy-defective mutants of Saccharomyces cerevisiae. *Febs Lett* 333, 169–174 (1993).

187. Goffeau, A. *et al.* Life with 6000 Genes. *Science* 274, 546–567 (1996).

188. Haber, J. E. Mating-Type Genes and MAT Switching in Saccharomyces cerevisiae. *Genetics* 191, 33–64 (2012).

189. Strathern, J. N. *et al.* Homothallic switching of yeast mating type cassettes is initiated by a double-stranded cut in the MAT locus. *Cell* 31, 183–192 (1982).

190. Kostriken, R., Strathern, J. N., Klar, A. J. S., Hicks, J. B. & Heffron, F. A site-specific endonuclease essential for mating-type switching in Saccharomyces cerevisiae. *Cell* 35, 167–174 (1983).

191. Meiron, H., Nahon, E. & Raveh, D. Identification of the heterothallic mutation in HO-endonuclease of S. cerevisiae using HO/ho chimeric genes. *Curr Genet* 28, 367–373 (1995).

192. Pronk, J. T. Auxotrophic Yeast Strains in Fundamental and Applied Research. *Appl Environ Microb* 68, 2095–2100 (2002).

193. Gietz, R. D. & Woods, R. A. Transformation of yeast by lithium acetate/single-stranded carrier DNA/polyethylene glycol method. *Methods Enzymol* 350, 87–96 (2002).

194. Gietz, R. D. & Schiestl, R. H. High-efficiency yeast transformation using the LiAc/SS carrier DNA/PEG method. *Nat Protoc* 2, 31–34 (2007).

195. Rothstein, R. J. One-step gene disruption in yeast. *Methods Enzymol* 101, 202–211 (1983).

196. Baudin, A., Ozier-Kalogeropoulos, O., Denouel, A., Lacroute, F. & Cullin, C. A simple and efficient method for direct gene deletion in Saccharomyces cerevisiae. *Nucleic Acids Res* 21, 3329–3330 (1993).

197. Wach, A., Brachat, A., Pöhlmann, R. & Philippsen, P. New heterologous modules for classical or PCR-based gene disruptions in Saccharomyces cerevisiae. *Yeast* 10, 1793–1808 (1994).

198. Goldstein, A. L., Pan, X. & McCusker, J. H. Heterologous URA3MX cassettes for gene replacement in Saccharomyces cerevisiae. *Yeast* 15, 507–511 (1999).

199. Petracek, M. E. & Longtine, M. S. PCR-based engineering of yeast genome. *Methods Enzymol* 350, 445–469 (2002).

200. Sheff, M. A. & Thorn, K. S. Optimized cassettes for fluorescent protein tagging in Saccharomyces cerevisiae. *Yeast* 21, 661–670 (2004).

201. Giaever, G. & Nislow, C. The Yeast Deletion Collection: A Decade of Functional Genomics. *Genetics* 197, 451–465 (2014).

202. Kofoed, M. *et al.* An Updated Collection of Sequence Barcoded Temperature-Sensitive Alleles of Yeast Essential Genes. *G3 Genes Genomes Genetics* 5, 1879–1887 (2015).

203. Li, Z. *et al.* Systematic exploration of essential yeast gene function with temperature-sensitive mutants. *Nat Biotechnol* 29, 361–367 (2011).

204. Breslow, D. K. *et al.* A comprehensive strategy enabling high-resolution functional analysis of the yeast genome. *Nat Methods* 5, 711–718 (2008).

205. Tong, A. H. Y. *et al.* Systematic Genetic Analysis with Ordered Arrays of Yeast Deletion Mutants. *Science* 294, 2364–2368 (2001).

206. Costanzo, M. *et al.* A global genetic interaction network maps a wiring diagram of cellular function. *Science* 353, aaf1420–aaf1420 (2016).

207. Usaj, M. *et al.* TheCellMap.org: A Web-Accessible Database for Visualizing and Mining the Global Yeast Genetic Interaction Network. *G3 Genes Genomes Genetics* 7, 1539–1549 (2017).

208. Klionsky, D. J. *et al.* A Unified Nomenclature for Yeast Autophagy-Related Genes. *Dev Cell* 5, 539–545 (2003).

209. Heitman, J., Movva, N. & Hall, M. Targets for cell cycle arrest by the immunosuppressant rapamycin in yeast. *Science* 253, 905–909 (1991).

210. Kunz, J. *et al.* Target of rapamycin in yeast, TOR2, is an essential phosphatidylinositol kinase homolog required for G1 progression. *Cell* 73, 585–596 (1993).

211. Cafferkey, R. *et al.* Dominant missense mutations in a novel yeast protein related to mammalian phosphatidylinositol 3-kinase and VPS34 abrogate rapamycin cytotoxicity. *Mol Cell Biol* 13, 6012–6023 (1993).

212. Brown, E. J. *et al.* A mammalian protein targeted by G1-arresting rapamycin–receptor complex. *Nature* 369, 756–758 (1994).

213. Feyder, S., Craene, J.-O. D., Bär, S., Bertazzi, D. L. & Friant, S. Membrane Trafficking in the Yeast Saccharomyces cerevisiae Model. *Int J Mol Sci* 16, 1509–1525 (2015).

214. Novick, P., Field, C. & Schekman, R. Identification of 23 complementation groups required for post-translational events in the yeast secretory pathway. *Cell* 21, 205–215 (1980).

215. Novick, P., Ferro, S. & Schekman, R. Order of events in the yeast secretory pathway. *Cell* 25, 461–469 (1981).

216. Bonifacino, J. S. & Glick, B. S. The Mechanisms of Vesicle Budding and Fusion. *Cell* 116, 153–166 (2004).

217. Longo, V. D., Shadel, G. S., Kaeberlein, M. & Kennedy, B. Replicative and Chronological Aging in Saccharomyces cerevisiae. *Cell Metab* 16, 18–31 (2012).

218. Prouteau, M. *et al.* TORC1 organized in inhibited domains (TOROIDs) regulate TORC1 activity. *Nature* 550, 265–269 (2017).

219. Chen, Z. *et al.* TORC1 Determines Fab1 Lipid Kinase Function at Signaling Endosomes and Vacuoles. *Curr Biol* 31, 297-309.e8 (2021).

220. Vézina, C., Kudelski, A. & Sehgal, S. N. Rapamycin (AY-22, 989), A New Antifungal Anitbiotic. *J Antibiotics* 28, 721–726 (1975).

221. Banaszynski, L. A., Liu, C. W. & Wandless, T. J. Characterization of the FKBP·Rapamycin·FRB Ternary Complex. *J Am Chem Soc* 127, 4715–4721 (2005).

222. Yoo, Y. J., Kim, H., Park, S. R. & Yoon, Y. J. An overview of rapamycin: from discovery to future perspectives. *J Ind Microbiol Biot* 44, 537–553 (2017).

223. Dubouloz, F., Deloche, O., Wanke, V., Cameroni, E. & Virgilio, C. D. The TOR and EGO Protein Complexes Orchestrate Microautophagy in Yeast. *Mol Cell* 19, 15–26 (2005).

224. Powis, K. *et al.* Crystal structure of the Ego1-Ego2-Ego3 complex and its role in promoting Rag GTPase-dependent TORC1 signaling. *Cell Res* 25, 1043–1059 (2015).

225. Jeong, J.-H. *et al.* Crystal Structure of the Gtr1pGTP-Gtr2pGDP Protein Complex Reveals Large Structural Rearrangements Triggered by GTP-to-GDP Conversion. *J Biol Chem* 287, 29648–29653 (2012).

226. Nakashima, N., Noguchi, E. & Nishimoto, T. Saccharomyces cerevisiae Putative G Protein, Gtr1p, Which Forms Complexes With Itself and a Novel Protein Designated as Gtr2p, Negatively Regulates the Ran/Gsp1p G Protein Cycle Through Gtr2p. *Genetics* 152, 853–867 (1999).

227. Panchaud, N., Péli-Gulli, M.-P. & Virgilio, C. D. Amino Acid Deprivation Inhibits TORC1 Through a GTPase-Activating Protein Complex for the Rag Family GTPase Gtr1. *Sci Signal* 6, ra42–ra42 (2013).

228. Péli-Gulli, M.-P., Sardu, A., Panchaud, N., Raucci, S. & De Virgilio, C. Amino Acids Stimulate TORC1 through Lst4-Lst7, a GTPase-Activating Protein Complex for the Rag Family GTPase Gtr2. *Cell Reports* 13, 1–7 (2015).

229. Bonfils, G. *et al.* Leucyl-tRNA Synthetase Controls TORC1 via the EGO Complex. *Mol Cell* 46, 105–110 (2012).

230. Parsons, A. B. *et al.* Integration of chemical-genetic and genetic interaction data links bioactive compounds to cellular target pathways. *Nat Biotechnol* 22, 62–69 (2004).

231. Michel, A. H. *et al.* Functional mapping of yeast genomes by saturated transposition. *Elife* 6, e23570 (2017).

232. Sullivan, A., Wallace, R. L., Wellington, R., Luo, X. & Capaldi, A. P. Multilayered regulation of TORC1-body formation in budding yeast. *Mol Biol Cell* 30, 400–410 (2019).

233. Troutman, K. K., Varlakhanova, N. V., Tornabene, B. A., Ramachandran, R. & Ford, M. G. J. Conserved Pib2 regions have distinct roles in TORC1 regulation at the vacuole. *Biorxiv* 2022.03.04.483060 (2022) doi:https://doi.org/10.1242/jcs.259994.

234. Varlakhanova, N. V., Mihalevic, M., Bernstein, K. A. & Ford, M. G. J. Pib2 and EGO Complex are both required for activation of TORC1. *J Cell Sci* 130, jcs.207910 (2017).

235. Tanigawa, M. & Maeda, T. An In Vitro TORC1 Kinase Assay That Recapitulates the Gtr-Independent Glutamine-Responsive TORC1 Activation Mechanism on Yeast Vacuoles. *Mol Cell Biol* 37, e00075-17 (2017).

236. Tarassov, K. *et al.* An in Vivo Map of the Yeast Protein Interactome. *Science* 320, 1465–1470 (2008).

237. Ukai, H. *et al.* Gtr/Ego-independent TORC1 activation is achieved through a glutamine-sensitive interaction with Pib2 on the vacuolar membrane. *Plos Genet* 14, e1007334 (2018).

238. Tanigawa, M. *et al.* A glutamine sensor that directly activates TORC1. *Commun Biology* 4, 1093 (2021).

239. Shin, M. E., Ogburn, K. D., Varban, O. A., Gilbert, P. M. & Burd, C. G. FYVE Domain Targets Pib1p Ubiquitin Ligase to Endosome and Vacuolar Membranes. *J Biol Chem* 276, 41388–41393 (2001).

240. Kim, A. & Cunningham, K. W. A LAPF/phafin1-like protein regulates TORC1 and lysosomal membrane permeabilization in response to endoplasmic reticulum membrane stress. *Mol Biol Cell* 26, 4631–4645 (2015).

241. Jumper, J. *et al.* Highly accurate protein structure prediction with AlphaFold. *Nature* 1–11 (2021) doi:10.1038/s41586-021-03819-2.

242. Nie, C., He, T., Zhang, W., Zhang, G. & Ma, X. Branched Chain Amino Acids: Beyond Nutrition Metabolism. *Int J Mol Sci* 19, 954 (2018).

243. Wang, C. & Guo, F. Branched chain amino acids and metabolic regulation. *Chinese Sci Bull* 58, 1228–1235 (2013).

244. Stracka, D., Jozefczuk, S., Rudroff, F., Sauer, U. & Hall, M. N. Nitrogen Source Activates TOR (Target of Rapamycin) Complex 1 via Glutamine and Independently of Gtr/Rag Proteins. *J Biol Chem* 289, 25010–25020 (2014).

245. Hofman-Bang, J. Nitrogen catabolite repression in Saccharomyces cerevisiae. *Mol Biotechnol* 12, 35–71 (1999).

246. Magasanik, B. & Kaiser, C. A. Nitrogen regulation in Saccharomyces cerevisiae. *Gene* 290, 1–18 (2002).

247. Xiao, D. *et al.* The glutamine-alpha-ketoglutarate (AKG) metabolism and its nutritional implications. *Amino Acids* 48, 2067–2080 (2016).

248. Yoo, H. C., Yu, Y. C., Sung, Y. & Han, J. M. Glutamine reliance in cell metabolism. *Exp Mol Medicine* 52, 1496–1516 (2020).

249. Hallett, J. E. H., Luo, X. & Capaldi, A. P. State Transitions in the TORC1 Signaling Pathway and Information Processing in Saccharomyces cerevisiae. *Genetics* 198, 773–786 (2014).

250. Hallett, J. E. H., Luo, X. & Capaldi, A. P. Snf1/AMPK promotes the formation of Kog1/Raptor-bodies to increase the activation threshold of TORC1 in budding yeast. *Elife* 4, e09181 (2015).

251. Kira, S. *et al.* Dynamic relocation of the TORC1–Gtr1/2–Ego1/2/3 complex is regulated by Gtr1 and Gtr2. *Mol Biol Cell* 27, 382–396 (2016).

252. Bridges, D. *et al.* Rab5 Proteins Regulate Activation and Localization of Target of Rapamycin Complex 1. *J Biol Chem* 287, 20913–20921 (2012).

253. Bridges, D. *et al.* Phosphatidylinositol 3,5-bisphosphate plays a role in the activation and subcellular localization of mechanistic target of rapamycin 1. *Mol Biol Cell* 23, 2955–2962 (2012).

254. Gary, J. D., Wurmser, A. E., Bonangelino, C. J., Weisman, L. S. & Emr, S. D. Fab1p Is Essential for PtdIns(3)P 5-Kinase Activity and the Maintenance of Vacuolar Size and Membrane Homeostasis. *J Cell Biology* 143, 65–79 (1998).

255. Hatakeyama, R. & Virgilio, C. D. A spatially and functionally distinct pool of TORC1 defines signaling endosomes in yeast. *Autophagy* 15, 915–916 (2019).

256. Gao, J. *et al.* The HOPS tethering complex is required to maintain signaling endosome identity and TORC1 activity. *J Cell Biol* 221, e202109084 (2022).

257. Varlakhanova, N. V., Tornabene, B. A. & Ford, M. G. J. Feedback regulation of TORC1 by its downstream effectors Npr1 and Par32. *Mol Biol Cell* 29, 2751–2765 (2018).

258. Schmidt, A., Beck, T., Koller, A., Kunz, J. & Hall, M. N. The TOR nutrient signalling pathway phosphorylates NPR1 and inhibits turnover of the tryptophan permease. *Embo J* 17, 6924–6931 (1998).

259. MacGurn, J. A., Hsu, P.-C., Smolka, M. B. & Emr, S. D. TORC1 Regulates Endocytosis via Npr1-Mediated Phosphoinhibition of a Ubiquitin Ligase Adaptor. *Cell* 147, 1104–1117 (2011).

260. Boeckstaens, M. *et al.* Identification of a Novel Regulatory Mechanism of Nutrient Transport Controlled by TORC1-Npr1-Amu1/Par32. *Plos Genet* 11, e1005382 (2015).

261. Brito, A. S. *et al.* Pib2-dependent feedback control of the TORC1 signaling network by the Npr1 kinase. *Iscience* 20, 415–433 (2019).

262. Lempiäinen, H. *et al.* Sfp1 Interaction with TORC1 and Mrs6 Reveals Feedback Regulation on TOR Signaling. *Mol Cell* 33, 704–716 (2009).

263. Hu, Z. *et al.* Multilayered Control of Protein Turnover by TORC1 and Atg1. *Cell Reports* 28, 3486-3496.e6 (2019).

264. Stenmark, H., Aasland, R. & Driscoll, P. C. The phosphatidylinositol 3-phosphate-binding FYVE finger. *Febs Lett* 513, 77–84 (2002).

265. Stenmark, H., Aasland, R., Toh, B.-H. & D'Arrigo, A. Endosomal Localization of the Autoantigen EEA1 Is Mediated by a Zinc-binding FYVE Finger. *J Biol Chem* 271, 24048–24054 (1996).

266. Gaullier, J.-M., Rønning, E., Gillooly, D. J. & Stenmark, H. Interaction of the EEA1 FYVE Finger with Phosphatidylinositol 3-phosphate and early endosomes. Role of conserved residues. *J Biol Chem* 275, 24595–24600 (2000).

267. Kutateladze, T. G. *et al.* Phosphatidylinositol 3-Phosphate Recognition by the FYVE Domain. *Mol Cell* 3, 805–811 (1999).

268. Dumas, J. J. *et al.* Multivalent Endosome Targeting by Homodimeric EEA1. *Mol Cell* 8, 947–958 (2001).

269. Sturgill, T. W. *et al.* TOR1 and TOR2 Have Distinct Locations in Live Cells. *Eukaryot Cell* 7, 1819–1830 (2008).

270. Vida, T. A. & Emr, S. D. A new vital stain for visualizing vacuolar membrane dynamics and endocytosis in yeast. *J Cell Biology* 128, 779–792 (1995).

271. Babst, M., Sato, T. K., Banta, L. M. & Emr, S. D. Endosomal transport function in yeast requires a novel AAA-type ATPase, Vps4p. *Embo J* 16, 1820–1831 (1997).

272. Babst, M., Wendland, B., Estepa, E. J. & Emr, S. D. The Vps4p AAA ATPase regulates membrane association of a Vps protein complex required for normal endosome function. *Embo J* 17, 2982–2993 (1998).

273. Coonrod, E. M. & Stevens, T. H. The Yeast vps Class E Mutants: The Beginning of the Molecular Genetic Analysis of Multivesicular Body Biogenesis. *Mol Biol Cell* 21, 4057–4060 (2010).

274. Raymond, C. K., Howald-Stevenson, I., Vater, C. A. & Stevens, T. H. Morphological classification of the yeast vacuolar protein sorting mutants: evidence for a prevacuolar compartment in class E vps mutants. *Mol Biol Cell* 3, 1389–1402 (1992).

275. Burd, C. G. & Emr, S. D. Phosphatidylinositol(3)-Phosphate Signaling Mediated by Specific Binding to RING FYVE Domains. *Mol Cell* 2, 157–162 (1998).

276. Swamy, M. J., Sankhala, R. S. & Singh, B. P. Lipid-Protein Interactions, Methods and Protocols. *Methods Mol Biology* 2003, 71–89 (2019).

277. Kutateladze, T. & Overduin, M. Structural Mechanism of Endosome Docking by the FYVE Domain. *Science* 291, 1793–1796 (2001).

278. Ford, M. G. J. & Ramachandran, R. Membrane Trafficking, Methods and Protocols. *Methods Mol Biology* 2473, 259–284 (2022).

279. Sahin, E. & Roberts, C. J. Therapeutic Proteins, Methods and Protocols. *Methods Mol Biology* 899, 403–423 (2012).

280. Hatakeyama, R. Pib2 as an Emerging Master Regulator of Yeast TORC1. *Biomol* 11, 1489 (2021).

281. Guan, J. *et al.* Cvt18/Gsa12 Is Required for Cytoplasm-to-Vacuole Transport, Pexophagy, and Autophagy in Saccharomyces cerevisiae and Pichia pastoris. *Mol Biol Cell* 12, 3821–3838 (2001).

282. Shintani, T. & Klionsky, D. J. Cargo Proteins Facilitate the Formation of Transport Vesicles in the Cytoplasm to Vacuole Targeting Pathway. *J Biol Chem* 279, 29889–29894 (2004).

283. Ingrell, C. R., Miller, M. L., Jensen, O. N. & Blom, N. NetPhosYeast: prediction of protein phosphorylation sites in yeast. *Bioinformatics* 23, 895–897 (2007).

284. Holt, L. J. *et al.* Global Analysis of Cdk1 Substrate Phosphorylation Sites Provides Insights into Evolution. *Science* 325, 1682–1686 (2009).

285. Bauer, N. C., Doetsch, P. W. & Corbett, A. H. Mechanisms Regulating Protein Localization. *Traffic* 16, 1039–1061 (2015).

286. Subramanian, K. *et al.* Palmitoylation determines the function of Vac8 at the yeast vacuole. *J Cell Sci* 119, 2477–2485 (2006).

287. Jeong, H. *et al.* Mechanistic insight into the nucleus–vacuole junction based on the Vac8p–Nvj1p crystal structure. *Proc National Acad Sci* 114, E4539–E4548 (2017).

288. Sun, D. *et al.* The cryo-EM structure of the SNX–BAR Mvp1 tetramer. *Nat Commun* 11, 1506 (2020).

289. González, A. *et al.* TORC1 Promotes Phosphorylation of Ribosomal Protein S6 via the AGC Kinase Ypk3 in Saccharomyces cerevisiae. *Plos One* 10, e0120250 (2015).

290. Gerrard, S. R., Bryant, N. J. & Stevens, T. H. VPS21 Controls Entry of Endocytosed and Biosynthetic Proteins into the Yeast Prevacuolar Compartment. *Mol Biol Cell* 11, 613–626 (2000).

291. Horazdovsky, B. F., Busch, G. R. & Emr, S. D. VPS21 encodes a rab5-like GTP binding protein that is required for the sorting of yeast vacuolar proteins. *Embo J* 13, 1297–1309 (1994).

292. Dubreuil, B. *et al.* YeastRGB: comparing the abundance and localization of yeast proteins across cells and libraries. *Nucleic Acids Res* 47, gky941- (2019).

293. Belgareh-Touzé, N., Avaro, S., Rouillé, Y., Hoflack, B. & Haguenauer-Tsapis, R. Yeast Vps55p, a Functional Homolog of Human Obesity Receptor Gene-related Protein, Is Involved in Late Endosome to Vacuole Trafficking. *Mol Biol Cell* 13, 1694–1708 (2002).

294. Schluter, C. *et al.* Global Analysis of Yeast Endosomal Transport Identifies the Vps55/68 Sorting Complex. *Mol Biol Cell* 19, 1282–1294 (2008).

295. Suzuki, S. W. *et al.* A PX-BAR protein Mvp1/SNX8 and a dynamin-like GTPase Vps1 drive endosomal recycling. *Elife* 10, e69883 (2021).

296. Séron, K. *et al.* Endospanins Regulate a Postinternalization Step of the Leptin Receptor Endocytic Pathway. *J Biol Chem* 286, 17968–17981 (2011).

297. Thomas, B. J. & Rothstein, R. Elevated recombination rates in transcriptionally active DNA. *Cell* 56, 619–630 (1989).

298. Dowell, R. D. *et al.* Genotype to Phenotype: A Complex Problem. *Science* 328, 469–469 (2010).

299. Shortill, S. P., Frier, M. S., Wongsangaroonsri, P., Davey, M. & Conibear, E. The VINE complex is an endosomal VPS9-domain GEF and SNX-BAR coat. *Elife* 11, e77035 (2022).

300. Lundberg, E. & Borner, G. H. H. Spatial proteomics: a powerful discovery tool for cell biology. *Nat Rev Mol Cell Bio* 20, 285–302 (2019).

301. Roux, K. J., Kim, D. I., Burke, B. & May, D. G. BioID: A Screen for Protein-Protein Interactions. *Curr Protoc Protein Sci* 91, 19.23.1-19.23.15 (2018).

302. Takahara, T. & Maeda, T. Transient Sequestration of TORC1 into Stress Granules during Heat Stress. *Mol Cell* 47, 242–252 (2012).

303. Ohne, Y., Takahara, T. & Maeda, T. Evaluation of mTOR function by a gain-of-function approach. *Cell Cycle* 8, 573–579 (2009).

304. Ishikawa-Ankerhold, H. C., Ankerhold, R. & Drummen, G. P. C. Advanced Fluorescence Microscopy Techniques—FRAP, FLIP, FLAP, FRET and FLIM. *Molecules* 17, 4047–4132 (2012).

305. Subach, O. M. *et al.* A photoswitchable orange-to-far-red fluorescent protein, PSmOrange. *Nat Methods* 8, 771–777 (2011).

306. Adami, A., García-Álvarez, B., Arias-Palomo, E., Barford, D. & Llorca, O. Structure of TOR and Its Complex with KOG1. *Mol Cell* 27, 509–516 (2007).

307. Mortimer, R. K. & Johnston, J. R. Life Span of Individual Yeast Cells. *Nature* 183, 1751–1752 (1959).

308. Fabrizio, P., Pozza, F., Pletcher, S. D., Gendron, C. M. & Longo, V. D. Regulation of Longevity and Stress Resistance by Sch9 in Yeast. *Science* 292, 288–290 (2001).

309. Deprez, M.-A., Eskes, E., Winderickx, J. & Wilms, T. The TORC1-Sch9 pathway as a crucial mediator of chronological lifespan in the yeast Saccharomyces cerevisiae. *Fems Yeast Res* 18, (2018).

310. Kaeberlein, M. *et al.* Regulation of Yeast Replicative Life Span by TOR and Sch9 in Response to Nutrients. *Science* 310, 1193–1196 (2005).

311. Powers, R. W., Kaeberlein, M., Caldwell, S. D., Kennedy, B. K. & Fields, S. Extension of chronological life span in yeast by decreased TOR pathway signaling. *Gene Dev* 20, 174–184 (2006).

312. Canfield, C.-A. & Bradshaw, P. C. Amino acids in the regulation of aging and aging-related diseases. *Transl Medicine Aging* 3, 70–89 (2019).

313. Alvers, A. L. *et al.* Autophagy and amino acid homeostasis are required for chronological longevity in Saccharomyces cerevisiae. *Aging Cell* 8, 353–369 (2009).

314. Aris, J. P. *et al.* Autophagy and leucine promote chronological longevity and respiration proficiency during calorie restriction in yeast. *Exp Gerontol* 48, 1107–1119 (2013).

315. Gorospe, C. M., Yu, S.-L., Kang, M.-S. & Lee, S.-K. Chronological lifespan regulation of Saccharomyces cerevisiae by leucine biosynthesis pathway genes via TOR1 and COX2 expression regulation. *Mol Cell Toxicol* 15, 65–73 (2019).

316. Chen, W. *et al.* The Lysosome-associated Apoptosis-inducing Protein Containing the Pleckstrin Homology (PH) and FYVE Domains (LAPF), Representative of a Novel Family of PH and FYVE Domain-containing Proteins, Induces Caspase-independent Apoptosis via the Lysosomal-Mitochondrial Pathway. *J Biol Chem* 280, 40985–40995 (2005).

317. Pedersen, N. M. *et al.* The PtdIns3P-Binding Protein Phafin 2 Mediates Epidermal Growth Factor Receptor Degradation by Promoting Endosome Fusion. *Traffic* 13, 1547–1563 (2012).

318. Edgar, R. C. MUSCLE: multiple sequence alignment with high accuracy and high throughput. *Nucleic Acids Res* 32, 1792–1797 (2004).

319. Sievers, F. *et al.* Fast, scalable generation of high-quality protein multiple sequence alignments using Clustal Omega. *Mol Syst Biol* 7, 539–539 (2011).

320. Robert, X. & Gouet, P. Deciphering key features in protein structures with the new ENDscript server. *Nucleic Acids Res* 42, W320–W324 (2014).

321. *The PyMOL Molecular Graphics System, Version 1.4*. (Schrödinger, LLC, 2015).

322. Schindelin, J. *et al.* Fiji: an open-source platform for biological-image analysis. *Nat Methods* 9, 676–682 (2012).

323. Millen, J. I., Krick, R., Prick, T., Thumm, M. & Goldfarb, D. S. Measuring piecemeal microautophagy of the nucleus in Saccharomyces cerevisiae. *Autophagy* 5, 75–81 (2009).

324. Lichtman, J. W. & Conchello, J.-A. Fluorescence microscopy. *Nat Methods* 2, 910–919 (2005).

325. Jonkman, J., Brown, C. M., Wright, G. D., Anderson, K. I. & North, A. J. Tutorial: guidance for quantitative confocal microscopy. *Nat Protoc* 15, 1585–1611 (2020).

326. Elliott, A. D. Confocal Microscopy: Principles and Modern Practices. *Curr Protoc Cytom* 92, e68 (2020).

327. Cole, R. W., Jinadasa, T. & Brown, C. M. Measuring and interpreting point spread functions to determine confocal microscope resolution and ensure quality control. *Nat Protoc* 6, 1929–1941 (2011).

328. Lin, W.-J. *et al.* Lysosomal targeting of phafin1 mediated by Rab7 induces autophagosome formation. *Biochem Bioph Res Co* 417, 35–42 (2012).

329. Ernst, W. L. *et al.* VAMP-associated Proteins (VAP) as Receptors That Couple Cystic Fibrosis Transmembrane Conductance Regulator (CFTR) Proteostasis with Lipid Homeostasis. *J Biol Chem* 291, 5206–5220 (2016).

330. White, N. M. *et al.* Altered cholesterol homeostasis in cultured and in vivo models of cystic fibrosis. *Am J Physiol-lung C* 292, L476–L486 (2007).

331. Gentzsch, M., Choudhury, A., Chang, X., Pagano, R. E. & Riordan, J. R. Misassembled mutant ΔF508 CFTR in the distal secretory pathway alters cellular lipid trafficking. *J Cell Sci* 120, 447–455 (2007).

332. Cianciola, N. L., Carlin, C. R. & Kelley, T. J. Molecular pathways for intracellular cholesterol accumulation: Common pathogenic mechanisms in Niemann–Pick disease Type C and cystic fibrosis. *Arch Biochem Biophys* 515, 54–63 (2011).

333. Narita, K. *et al.* Protein transduction of Rab9 in Niemann-Pick C cells reduces cholesterol storage. *Faseb J* 19, 1558–1560 (2005).

334. Seo, A. Y. *et al.* AMPK and vacuole-associated Atg14p orchestrate μ-lipophagy for energy production and long-term survival under glucose starvation. *Elife* 6, e21690 (2017).

335. Tsuji, T. *et al.* Niemann-Pick type C proteins promote microautophagy by expanding raft-like membrane domains in the yeast vacuole. *Elife* 6, e25960 (2017).

336. James, C. & Kehlenbach, R. H. The Interactome of the VAP Family of Proteins: An Overview. *Cells* 10, 1780 (2021).

337. Wilson, J. D., Thompson, S. L. & Barlowe, C. Yet1p–Yet3p interacts with Scs2p–Opi1p to regulate ER localization of the Opi1p repressor. *Mol Biol Cell* 22, 1430–1439 (2011).

338. Cox, J. S., Shamu, C. E. & Walter, P. Transcriptional induction of genes encoding endoplasmic reticulum resident proteins requires a transmembrane protein kinase. *Cell* 73, 1197–1206 (1993).

339. Cox, J. S., Chapman, R. E. & Walter, P. The unfolded protein response coordinates the production of endoplasmic reticulum protein and endoplasmic reticulum membrane. *Mol Biol Cell* 8, 1805–1814 (1997).

340. Brickner, J. H. & Walter, P. Gene Recruitment of the Activated INO1 Locus to the Nuclear Membrane. *Plos Biol* 2, e342 (2004).

341. Kawahara, T., Yanagi, H., Yura, T. & Mori, K. Endoplasmic Reticulum Stress-induced mRNA Splicing Permits Synthesis of Transcription Factor Hac1p/Ern4p That Activates the Unfolded Protein Response. *Mol Biol Cell* 8, 1845–1862 (1997).

342. Huyer, G. *et al.* Distinct Machinery Is Required in Saccharomyces cerevisiae for the Endoplasmic Reticulum-associated Degradation of a Multispanning Membrane Protein and a Soluble Luminal Protein. *J Biol Chem* 279, 38369–38378 (2004).